

Complex Langevin and other approaches to the sign problem in quantum many-body physics

C. E. Berger^a, L. Rammelmüller^{b,c}, A. C. Loheac^a, F. Ehm^b, J. Braun^{b,e,d}, J. E. Drut^a

^a*Department of Physics and Astronomy, University of North Carolina, Chapel Hill, North Carolina 27599, USA*

^b*Institut für Kernphysik (Theoriezentrum), Technische Universität Darmstadt, D-64289 Darmstadt, Germany*

^c*GSI Helmholtzzentrum für Schwerionenforschung GmbH, Planckstraße 1, D-64291 Darmstadt, Germany*

^d*FAIR, Facility for Antiproton and Ion Research in Europe GmbH, Planckstraße 1, D-64291 Darmstadt, Germany*

^e*ExtreMe Matter Institute EMMI, GSI, Planckstraße 1, D-64291 Darmstadt, Germany*

Abstract

We review the theory and applications of complex stochastic quantization to the quantum many-body problem. Along the way, we present a brief overview of a number of ideas that either ameliorate or in some cases altogether solve the sign problem, including the classic reweighting method, alternative Hubbard-Stratonovich transformations, dual variables (for bosons and fermions), Majorana fermions, density-of-states methods, imaginary asymmetry approaches, and Lefschetz thimbles. We discuss some aspects of the mathematical underpinnings of conventional stochastic quantization, provide a few pedagogical examples, and summarize open challenges and practical solutions for the complex case. Finally, we review the recent applications of complex Langevin to quantum field theory in relativistic and nonrelativistic quantum matter, with an emphasis on the nonrelativistic case.

Keywords: Sign problem, stochastic quantization, complex Langevin

Contents

1	Introduction	3
1.1	The challenge of many-body quantum mechanics: memory and statistics	3
1.2	Path integrals and the sign problem	4
2	Approaches to the sign problem: from reweighting to complex Langevin	7
2.1	Reweighting	7
2.2	Alternative Hubbard-Stratonovich transformations	9
2.3	Density-of-states methods	10
2.4	Dual variables for bosons	13
2.5	Dual variables for fermions and fermion bags	15
2.6	Majorana fermions	18
2.7	Imaginary asymmetry	18
2.8	Lefschetz thimbles	19
3	The Langevin method for real and complex variables	21
3.1	Complex Langevin: origins and modern re-emergence	21
3.2	Stochastic quantization: path integrals and the Langevin process	22

Email addresses: cberger3@live.unc.edu (C. E. Berger), lrammelmuller@theorie.ikp.physik.tu-darmstadt.de (L. Rammelmüller), loheac@live.unc.edu (A. C. Loheac), fehmann@theorie.ikp.physik.tu-darmstadt.de (F. Ehm), jens.braun@physik.tu-darmstadt.de (J. Braun), drut@email.unc.edu (J. E. Drut)

3.3	A practical guide to real Langevin	24
3.3.1	Toy problem I: a pedagogical example of real Langevin	27
3.4	A practical guide to complex Langevin	28
3.4.1	Toy problem II: a pedagogical example of complex Langevin	29
3.5	Formal aspects and justification	31
3.6	Challenges	33
3.6.1	Mathematical aspects: convergence, correctness, boundary terms, and ergodicity	33
3.6.2	Practical aspects: numerical instabilities, gauge cooling, dynamic stabilization, and regulators	34
4	Applications in relativistic physics: non-equilibrium QFT and finite density QCD	35
4.1	QCD-inspired toy models	35
4.2	3 + 1 dimensional QCD at finite chemical potential	37
4.3	Low-dimensional QCD at non-zero chemical potential	37
4.4	Ongoing work in QCD	37
5	Applications in nonrelativistic matter: ultracold atomic gases	38
5.1	Nonrelativistic bosons	38
5.2	Nonrelativistic fermions in one dimension	39
5.2.1	1D fermions in the ground state	39
5.2.2	1D fermions at finite temperature	41
5.3	Nonrelativistic fermions in three dimensions: the polarized unitary Fermi gas	42
6	Summary and Outlook	43

1. Introduction

1.1. The challenge of many-body quantum mechanics: memory and statistics

In the early days of quantum mechanics it was quickly discovered that the Schrödinger equation could be solved analytically for hydrogen and hydrogen-like atoms in a straightforward manner [1]. However, each new particle added to the problem came with a dauntingly steep price, leaving the vast majority of the periodic table of the elements unattainable due to the complexity of the equations and the accompanying high cost of computation. Indeed, the presence of more than two interacting particles yields equations that are analytically intractable; the quantum few-body problem thus appeared to be very difficult, and the chances of solving the quantum *many-body* problem seemed dire. At the heart of the problem is the fact that, while the influence of the massive atomic nucleus on the much lighter electrons can be approximated (as a static external field à la Born-Oppenheimer), addressing the Coulomb interaction among the electrons is far more challenging. Dirac famously remarked in 1929 that, while the underlying physical laws were then completely known, “the difficulty is only that the exact application of these laws leads to equations much too complicated to be soluble” [2]. This difficulty could hardly be overemphasized then, and remains a challenge to this day. In facing that challenge, a wide variety of algorithms – and continues to be – developed by specialists around the world to fit the paradigms of their specific area of physics or chemistry.

The most common first-principles approaches to the quantum many-body problem can be roughly divided into two sets: memory intensive and statistics intensive. The former include methods such as exact diagonalization (see e.g. [3, 4]) and coupled cluster (see e.g. [5, 6]), while the latter include a set of stochastic techniques generally known as quantum Monte Carlo (QMC) methods. Within that QMC set, this review focuses on a large class of approaches for which the many-body problem is expressed in the language of second-quantization or quantum field theory, such that expectation values of operators are written as a path integral over continuous fields living on a spacetime lattice. That formulation is in fact very general – it is natural in relativistic quantum field theory as well as nuclear and condensed matter physics, either in the form of low-energy effective field theories (see e.g. [7, 8, 9]), or as a reformulation of traditional Hamiltonians like the Hubbard model (see e.g. [10, 11]). Regardless of the application, the computational cost of path-integral QMC methods scales at face value (see below) polynomially with particle number and basis size (i.e. the size of the spacetime lattice), which makes them exceptionally well-suited for the many-body problem.

An essential component of QMC techniques is that they rely on a stochastic process governed by the Metropolis accept-reject algorithm [12], which itself requires a well-defined probability measure to guarantee convergence to the correct result. Simply put, the algorithm requires that the partition function \mathcal{Z} be written as a sum of positive weights $W(C)$ (which play the role of the probability mentioned above) over some set of configurations C :

$$\mathcal{Z} = \sum_C W(C). \quad (1)$$

The Metropolis algorithm, by construction, provides samples of the configurations C distributed according to $W(C)$. Under many circumstances, however, a serious issue arises for this kind of algorithm, which has hindered computation in a wide range of situations: the infamous *sign problem*. In those cases, $W(C)$ does not have a well-defined sign or even becomes complex (as explained in further detail below). Unfortunately, by far most systems of interest suffer from such a problem: high- T_c superconductors (due to strong repulsive interaction away from half filling, see e.g. [13]), nuclear structure (strong repulsive core, finite spin-isospin polarization, see e.g. [14, 15]), and quantum chromodynamics (finite quark density see e.g. [16, 17, 18]), to name only a few.

Over the last few decades, many ideas have been proposed to overcome the sign problem in quantum many-body physics and field theory. This review covers some of them briefly and focuses on the so-called complex Langevin (CL) approach, as applied to the calculation of equilibrium properties of quantum many-body systems in relativistic and nonrelativistic physics, with an emphasis on the latter. The next section sketches out the basic path-integral formalism involved in Metropolis-based and stochastic quantization approaches, with the goal of showing where and how the sign problem arises.

1.2. Path integrals and the sign problem

The central quantity of the field theoretical approach to the quantum many-body problem is the partition function, which in the grand canonical ensemble is given by

$$\mathcal{Z} = \text{Tr} \left[e^{-\beta(\hat{H} - \mu\hat{N})} \right], \quad (2)$$

where \hat{H} is the Hamiltonian of the system, \hat{N} the particle number operator, β the inverse temperature, μ the chemical potential, and the trace is over all multiparticle states (i.e. Fock space). [Note that \mathcal{Z} is shown here for a single particle species, but is straightforwardly generalized to multiple chemical potentials, etc.] As written, \mathcal{Z} contains the thermodynamic information of the system: by differentiating with respect to β and μ one obtains expectation values of the Hamiltonian and the particle number operators. More detailed information, such as momentum distributions and other correlation functions, can be obtained by adding sources to the Hamiltonian as is common in quantum field theory.

The direct evaluation of Eq. (2) is impossible for interacting systems, as it requires *a priori* knowledge of the full energy spectrum. The path-integral approach to the many-body problem provides an alternative route. Either using an operator-based approach or coherent states, one arrives at an expression for \mathcal{Z} which is written generically as

$$\mathcal{Z} = \int \mathcal{D}\phi e^{-S[\phi]}, \quad (3)$$

where ϕ is a field living in $(d+1)$ -dimensional spacetime and represents any degrees of freedom in the system. One thus replaces the problem of evaluating Eq. (2) with that of calculating the above path integral. In practice, boundary conditions in the spatial directions can be chosen in a variety of ways, but those in the time direction, which is compact and runs in the range $\tau \in [0, \beta)$, are set by the quantum statistics of the problem: bosonic fields will obey periodic boundary conditions and fermionic fields anti-periodic.

From this point on, our discussions will focus on nonrelativistic systems unless otherwise specified. In purely bosonic theories the action $S[\phi]$ will typically take a simple local form such as

$$S[\phi] = \int d\tau d^d x \{ \phi^* (\partial_\tau + \mathcal{H}) \phi + V[\phi] \}, \quad (4)$$

where \mathcal{H} represents the noninteracting Hamiltonian (including external trapping potentials) and $V[\phi]$ represents the interactions (i.e. terms cubic and beyond in ϕ).

For real bosonic variables ϕ , the action $S[\phi]$ is also real and therefore $e^{-S[\phi]}$ can be used as a probability measure in a stochastic process. For complex ϕ , however, the fact that ∂_τ is an antisymmetric operator results in a complex $S[\phi]$, which is the source of a sign problem in this formulation (see below) and has a counterpart in relativistic bosons at finite chemical potential (see Secs. 2.4 and 4). The problem of the antisymmetry of ∂_τ can be circumvented for an even number of species with attractive interactions, which however render bosons unstable (but not fermions, see below).

To make contact with the fermionic case discussed below (see also Fig. 1), it is instructive to rewrite the interaction using a Hubbard-Stratonovich (HS) transformation, although it is not strictly needed in the bosonic case. Consider for instance the case of a complex field ϕ . Schematically, one introduces an auxiliary field σ such that

$$e^{-S_{\text{int}}[\phi]} = \int \mathcal{D}\sigma e^{-S_{\text{aux}}[\phi, \sigma] - S_0[\sigma]}, \quad (5)$$

where

$$S_{\text{int}}[\phi] = \int d\tau d^d x V[\phi], \quad (6)$$

$S_{\text{aux}}[\phi, \sigma]$ is a quadratic functional of both ϕ and σ , and $S_0[\sigma]$ is a pure- σ term; both S_{aux} and S_0 depend on the specific choice of HS transformation. Since the action is now quadratic in ϕ , the corresponding path integral can be carried out, which results in a σ -dependent determinant, i.e. the full partition function can now be expressed as

$$\mathcal{Z} = \int \mathcal{D}\sigma e^{-S_{\text{HS}}[\sigma]}, \quad (7)$$

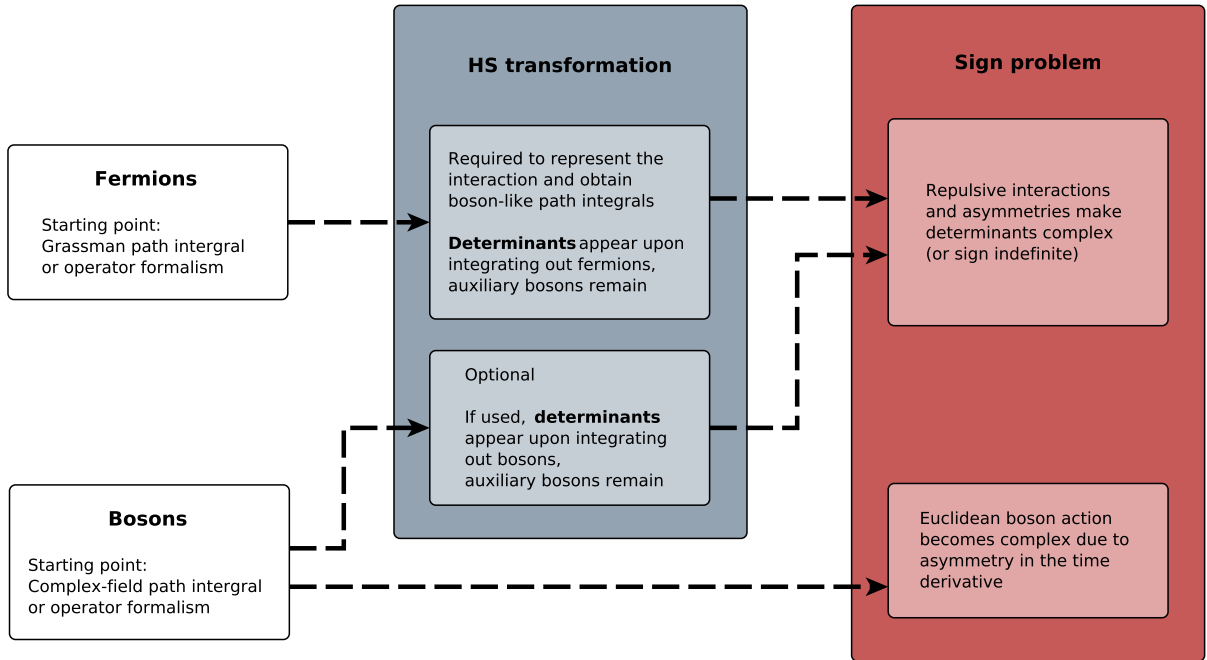


Figure 1: Pathways of the appearance of the sign problem in path-integral approaches to non-relativistic many-body systems.

where

$$e^{-S_{\text{HS}}[\sigma]} = \frac{e^{-S_0[\sigma]}}{\det M[\sigma]}. \quad (8)$$

Usually it is possible to factor the determinant into a determinant for each particle species (flavors), such that if N_f flavors are present then

$$\det M[\sigma] = \det M_1[\sigma] \det M_2[\sigma] \cdots \det M_{N_f}[\sigma]. \quad (9)$$

Naturally, calculations with bosons are not carried out using the action of Eq. (8). Indeed, the formulation based on $S[\phi]$ of Eq. (4) is considerably easier to work with as there are no determinants involved. However, the appearance of the boson determinant in Eq. (8) shows that, if $\det M$ is real and an even number of species is present, then the sign problem can be avoided if $S_0[\sigma]$ is real. Unfortunately, that situation is not relevant for bosons as it corresponds to attractive interactions, which make a many-boson system unstable. On the other hand, the determinant-based representation of Eq. (8) has a direct counterpart in the fermion case, which we discuss next.

In theories with fermions, the action will *require* the much more complicated (non-linear, non-local) form based on determinants because the fermionic analogue of Eq. (4) is written in terms of anticommuting objects, i.e. Grassmann numbers, which are not amenable to numerical computation. We therefore assume that fermionic degrees of freedom (i.e. said Grassmann variables) have been integrated out. Taking such a step *requires* a HS transformation of some kind to decouple the interaction, i.e. one introduces auxiliary fields to obtain a quadratic action in the fermion fields, which are then integrated and result in a fermion determinant. Assuming such steps have already been taken, we have the schematic form,

$$e^{-S[\phi]} = \det M[\phi] e^{-S_g[\phi]}, \quad (10)$$

where M encodes the dynamics of the fermions (quarks, electrons, atoms) in the external field ϕ , and $S_g[\phi]$ is the ‘pure HS’ part of the action (often called ‘pure gauge’ part in QED and QCD); for the latter, the form

of S_g will depend on the kind of HS transformation utilized (see Sec. 2.2). Parameters like the fermion mass and chemical potential appear in M . In particular, in many cases it is possible to choose a HS transformation that decouples N_f species (i.e. flavors) of fermions such that, as in the bosonic case described above,

$$\det M[\phi] = \det M_1[\phi] \det M_2[\phi] \cdots \det M_{N_f}[\phi]. \quad (11)$$

The above path integral formulation, being a rewriting of \mathcal{Z} , inherits the usual mechanisms to access expectation values of operators, namely differentiating \mathcal{Z} with respect to a chosen parameter. For instance, the average particle number is given by

$$\langle \hat{N} \rangle = \frac{\partial \ln \mathcal{Z}}{\partial(\beta\mu)} = \frac{1}{\mathcal{Z}} \text{Tr} \left[\hat{N} e^{-\beta(\hat{H} - \mu\hat{N})} \right], \quad (12)$$

such that in the bosonic case of Eq. (4),

$$\langle \hat{N} \rangle = \int \mathcal{D}\phi P[\phi] \left[-\frac{\partial S[\phi]}{\partial(\beta\mu)} \right], \quad (13)$$

while in the fermionic case of Eq. (10),

$$\langle \hat{N} \rangle = \int \mathcal{D}\phi P[\phi] \text{Tr} \left[M^{-1} \frac{\partial M}{\partial(\beta\mu)} \right], \quad (14)$$

where in either case

$$P[\phi] = \frac{e^{-S[\phi]}}{\mathcal{Z}}. \quad (15)$$

In evaluating Eqs. (13) or (14), the natural course of action is to sample field configurations ϕ according to the probability $P[\phi]$ and evaluate the quantities of interest that appear between square brackets. It is for that reason that the identification of $P[\phi]$ as a probability measure is a central aspect of conventional, Metropolis-based approaches to the evaluation of expectation values in quantum systems with many degrees of freedom. More specifically, in those cases where the sign (or phase) of $P[\phi]$ does not depend on ϕ , one samples ϕ according to $P[\phi]$ using the Metropolis algorithm (combined with a suitable field updating procedure, e.g. Wolff, worm, or hybrid Monte Carlo algorithms) to obtain a set of \mathcal{N}_ϕ decorrelated samples $\{\phi\}$, which in turn are used to estimate expectation values as

$$\langle \mathcal{O} \rangle = \int \mathcal{D}\phi P[\phi] \mathcal{O}[\phi] \simeq \frac{1}{\mathcal{N}_\phi} \sum_{\{\phi\}} \mathcal{O}[\phi], \quad (16)$$

for a given operator \mathcal{O} .

As mentioned above, by far for most systems of interest in physics face a sign problem, as the sign (or more generally complex phase) of $P[\phi]$ varies with ϕ . Then, $P[\phi]$ simply cannot be interpreted as a probability and the Metropolis algorithm is not applicable.

For nonrelativistic fermionic systems, the sign problem typically happens at finite polarization (i.e. chemical potential asymmetry) or when interactions contain a repulsive component. The problem therefore affects essentially all of condensed matter, nuclear physics, and quantum chemistry. There are notable exceptions such as a large class of systems in one spatial dimension and the Hubbard model at half filling, for which the sign problem can be eliminated completely. For relativistic fermions, such as quarks at finite chemical potential, the sign problem has obstructed the investigation of the phase diagram of QCD.

The case of bosons is markedly different from that of fermions. Here, the nonrelativistic case presents a sign problem even in the absence of interactions or chemical potentials: it is the asymmetry of the single time derivative, see Eq. (4), that creates the problem, as we will explain in further detail in Sec. 3. This is to be contrasted with the relativistic case, which develops a sign problem when a chemical potential is turned on (see however Sec. 2.4)

The remainder of this review is organized as follows. Sec. 2 reviews a broad (but by no means complete) set of approaches to the sign problem. Sec. 3 introduces the formal aspects of stochastic quantization and the complex Langevin method in more detail, including pedagogical examples as well as a brief discussion of the challenges and shortcomings in the mathematical underpinnings. Secs. 4 and 5 review the recent and emerging applications of CL in relativistic and nonrelativistic physics, with an emphasis on the latter. Finally, Sec. 6 concludes the review with a summary and outlook.

2. Approaches to the sign problem: from reweighting to complex Langevin

There have been multiple approaches suggested to solve or ameliorate the sign problem. Some of these methods aim at solving the problem directly, typically by rewriting the partition function in new and clever ways that remove the sign problem entirely. Other approaches involve rewriting the original problem so it can be solved stochastically but with controlled sign fluctuations. Below we present a selection of those methods in a logical sequence that starts with the simplest idea, namely reweighting, and concludes with complex-plane methods. Along the way, we present an elementary discussion of each method and comment on their advantages and shortcomings, which often result in valuable insights on the nature of the sign problem.

In Fig. 2 we propose a visual organization of the various approaches to the sign problem. Although we do not follow the proposed taxonomy in this review in a linear fashion, we do find it helpful to organize the information in this manner. On the left column of that figure we list “new-variables” methods as those that attempt to tackle the sign problem by switching from the conventional path-integral formulation to a new set of variables. We begin by reviewing a classic work that looks for sign-problem free HS transformations in Sec. 2.2. That work shows that a choice of HS transformation may not solve the problem but may help in addressing it (and certainly choosing the wrong one can be a recipe for trouble). Dual-variable and Majorana-fermion representations succeed in completely solving the sign problem in many cases, as shown in Secs. 2.4 and 2.6.

The middle column of Fig. 2 lists the set of what we call “statistical” approaches, which attempt to tackle the sign problem in a head-on manner. The simplest of those methods is by far the oldest and most commonly applied one across all areas of physics: reweighting, which we describe in Sec. 2.1. More recent statistical approaches, commonly referred to as “density-of-states” methods, proceed by probing the shape of the probability distribution at fixed action phase, and then integrating over that phase at the end; we describe those ideas in Sec. 2.3

Finally, the right column lists “complex-plane” methods, which also come in different flavors. Sec. 2.7 reviews the use of imaginary asymmetries in the parameters of a given theory (e.g. chemical potential, mass imbalance) to carry out calculations without a sign problem, necessarily followed by some kind of analytic continuation to return to the real physical values. Complex Langevin methods, the focus of this review, start in Sec. 3.1, while in Sec. 2.8 we mention ideas based on contour deformations (Lefschetz thimbles). Both of those methods rely on complexifying the integration variables; based on that idea, there exist constructive approaches (mentioned in Sec. 3.1) that aim to define a real action in such a complex space.

2.1. Reweighting

The simplest (and likely oldest [19]) idea to overcome the sign problem is that of *reweighting*, which amounts to sampling ϕ using the magnitude of $P[\phi]$ as a probability measure. In such an approach, one rewrites the expectation value of \mathcal{O} as

$$\langle \mathcal{O} \rangle = \int \mathcal{D}\phi |P[\phi]| e^{i\theta[\phi]} \mathcal{O}[\phi] = \frac{\int \mathcal{D}\phi |P[\phi]| e^{i\theta[\phi]} \mathcal{O}[\phi]}{\int \mathcal{D}\phi |P[\phi]|} = \frac{\langle \langle \mathcal{O}[\phi] e^{i\theta[\phi]} \rangle \rangle}{\langle \langle e^{i\theta[\phi]} \rangle \rangle}, \quad (17)$$

where $e^{i\theta[\phi]}$ is the phase of $P[\phi]$, and the double angle bracket denotes an expectation value taken with respect to $|P[\phi]|$.

Reweighting thus provides a way forward for systems that have sign problem: simply compute the numerator and denominator of Eq. (17) and then take their ratio. In practice, however, both the numerator

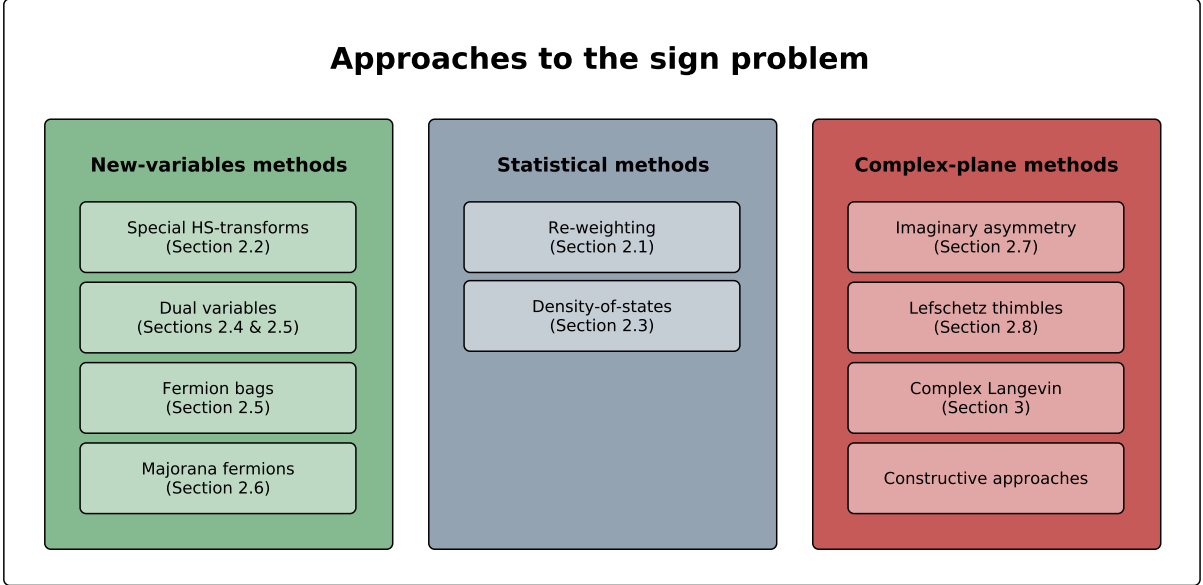


Figure 2: A proposed map of the many approaches to the sign problem.

and the denominator of Eq. (17)) vanish *exponentially* as the physical extent of the spacetime lattice is increased. The phase average is

$$\langle\langle e^{i\theta[\phi]} \rangle\rangle = \frac{\int \mathcal{D}\phi |P[\phi]| e^{i\theta[\phi]}}{\int \mathcal{D}\phi |P[\phi]|} = \frac{\mathcal{Z}}{\mathcal{Z}_{pq}} = e^{-\beta(\Omega - \Omega_{pq})}, \quad (18)$$

where \mathcal{Z}_{pq} is the partition function of the ‘phase-quenched’ theory, and Ω_{pq} and Ω are the corresponding grand thermodynamic potentials of the phase-quenched and original theory. Both \mathcal{Z} and \mathcal{Z}_{pq} are real quantities, but since \mathcal{Z}_{pq} is a sum over nonnegative real numbers, while \mathcal{Z} accounts for the phase, we necessarily have $\mathcal{Z} \leq \mathcal{Z}_{pq}$. More importantly, thermodynamic potentials are extensive quantities in the spatial volume V of the system, such that we may write the above in terms of intensive potentials ω and ω_{pq} as

$$\langle\langle e^{i\theta[\phi]} \rangle\rangle = e^{-\beta V(\omega - \omega_{pq})}, \quad (19)$$

which exposes the exponential nature of the sign problem in the thermodynamic ($V \rightarrow \infty$) and ground-state ($\beta \rightarrow \infty$) limits. This can be seen more clearly by examining the statistical uncertainty Δ , which in a Monte Carlo calculation with \mathcal{N}_s samples decreases as $\mathcal{N}_s^{-1/2}$. In the case of re-weighting, the relative statistical uncertainty on the average phase is overpowered by the exponential behavior coming from Eq. (19):

$$\frac{\Delta}{\langle\langle e^{i\theta[\phi]} \rangle\rangle} \sim \frac{e^{\beta V(\omega - \omega_{pq})}}{\sqrt{\mathcal{N}_s}}. \quad (20)$$

This last equation shows the difficulty in approaching the sign problem with a simple technique such as re-weighting: an exponentially large number of samples is needed in order to determine the average phase with any reasonable accuracy as the volume of space time is increased. Viewed through the lens of this simple idea, the sign problem may be regarded as the reappearance of an exponential type of computational wall, which affects non-stochastic methods (see Introduction) in the guise of memory requirements and statistical methods in the form of a signal-to-noise problem.

2.2. Alternative Hubbard-Stratonovich transformations

The partition function \mathcal{Z} of Eq. (2) is naturally a sum of positive quantities $e^{-\beta(E-\mu N)}$. The path-integral representation of \mathcal{Z} , while exact, introduces a large number of degrees of freedom to represent the same quantity. It therefore seems natural to expect that such a formulation would *require* massive cancellations (i.e. the sign problem) to yield correct physical answers. On the other hand, there are many ways to choose a HS representation, which may in turn yield different kinds of cancellations (i.e. more or less dramatic, by some measure). Even in the absence of a sign problem, different kinds of continuous or discrete HS transformations display varying behavior (see e.g. [20, 21]). It therefore makes sense to ask whether efficient representations exist, i.e. HS transformations which can substantially reduce the difference $\omega - \omega_{pq}$ in Eq. (19) or even eliminate it completely.

As an example, consider the fermionic Hubbard model given by

$$\hat{H} = -t \sum_{s=\uparrow,\downarrow} \sum_{\langle \mathbf{i}\mathbf{j} \rangle} \hat{c}_{s,\mathbf{i}}^\dagger \hat{c}_{s,\mathbf{j}} + U \sum_{\mathbf{i}} (\hat{n}_{\uparrow,\mathbf{i}} - 1/2)(\hat{n}_{\downarrow,\mathbf{i}} - 1/2), \quad (21)$$

where t is the nearest-neighbor hopping, $U > 0$ is the repulsive coupling, $\hat{c}_{s,\mathbf{i}}^{(\dagger)}$ is the annihilation (creation) operator for particles of spin $s = \uparrow, \downarrow$ at location \mathbf{i} , and $\hat{n}_{s,\mathbf{i}}$ is the corresponding density operator.

The work of Ref. [22] showed that a general HS transformation for the above model resulting in positive weights (i.e. a real action $S[\phi]$) does not exist. While attractive interactions – such as in the negative- U Hubbard model – feature no sign problem, repulsive interactions and in general any finite polarization (i.e. non-zero chemical potential asymmetry) do yield sign oscillations. More specifically, the problem arises because the determinant in Eq. (10) becomes a product of two determinants which are real or can be made real by choosing a proper HS transformation, but which will generally have different signs. Reference [22] showed that it is possible to isolate the origin of the signs in such a way that the determinants are real and identical, i.e. one ends up with a square of a determinant, and the signs are not eliminated but can be predicted. This remarkable property is illustrated below.

We begin by implementing a Trotter-Suzuki factorization of the Boltzmann weight with imaginary time step τ , such as

$$e^{-\tau \hat{H}} \simeq e^{-\tau \hat{T}} e^{-\tau \hat{V}}, \quad (22)$$

where \hat{T} contains the hopping terms and \hat{V} the on-site interaction, as they appear in Eq. (21). It is to address the latter that an HS transformation is used. The two most common HS representations, used in calculations of the repulsive Hubbard model, proceed by writing (omitting the spatial indices)

$$e^{-\tau U (\hat{n}_\uparrow - 1/2)(\hat{n}_\downarrow - 1/2)} = \frac{e^{-\tau U/4}}{2} \sum_{\phi=\pm 1} e^{-\lambda_d \phi (\hat{n}_\uparrow - \hat{n}_\downarrow)}, \quad (23)$$

$$e^{-\tau U (\hat{n}_\uparrow - 1/2)(\hat{n}_\downarrow - 1/2)} = \frac{e^{-\tau U/4}}{\sqrt{2\pi}} \int_{-\infty}^{\infty} d\phi e^{-\phi^2/2 - \lambda_c \phi (\hat{n}_\uparrow - \hat{n}_\downarrow)}, \quad (24)$$

where ϕ is the auxiliary field, λ_d is set by $\cosh(\lambda_d) = e^{\tau U/2}$, and $\lambda_c = \sqrt{\tau U}$. Both of these “density-channel” transformations successfully decouple the two spin species \uparrow and \downarrow , and the resulting determinants are real, but they are generally different from each other, such that

$$P[\phi] = \det M_\uparrow[\phi] \det M_\downarrow[\phi], \quad (25)$$

will generally vary in sign with ϕ . Here we omit the pure- ϕ part for the continuous case, which is real and positive anyway. [It should be pointed out that there are more general ways than the above factorized form that result in a sign-problem free situation; for an exploration of more general conditions based on time-reversal invariance, see Refs. [23, 24] and further discussion in Sec. 2.6.]

A more general transformation that aims to preserve the up-down symmetry of the Hubbard Hamiltonian, and therefore provide the square of a real determinant in $P[\phi]$, can be written as

$$e^{-\tau U (\hat{n}_\uparrow \hat{n}_\downarrow - \hat{n}_\uparrow/2 - \hat{n}_\downarrow/2)} = \int_{-\infty}^{\infty} d\phi p[\phi] e^{\phi (\hat{n}_\uparrow + \hat{n}_\downarrow)}, \quad (26)$$

where we want $p[\phi]$ to be real and positive and, evaluating both sides at the eigenvalues of the density operators (i.e. setting $\hat{n}_s \rightarrow 0, 1$), we see that

$$\int_{-\infty}^{\infty} d\phi p[\phi] = 1, \quad (27)$$

$$\int_{-\infty}^{\infty} d\phi p[\phi] e^{\phi} = e^{\tau U/2}, \quad (28)$$

$$\int_{-\infty}^{\infty} d\phi p[\phi] (e^{\phi})^2 = 1. \quad (29)$$

Unfortunately, the last two equations can only be satisfied simultaneously if $e^{\tau U/2} \leq 1$, i.e. if $U \leq 0$, which is not the case we are interested in here as there is then no sign problem.

The above shows that, at least within the rather general form proposed, it is not possible to generate the square of a determinant *and* avoid the sign problem at the same time for the repulsive Hubbard model. On the other hand, if $p[\phi]$ is allowed to vary in sign, then there is no constraint on U and we obtain the square of a real determinant. In that case, the sign problem comes not from the fermion determinant but from $p[\phi]$, which means that it is completely predictable as soon as ϕ is known, without computing determinants. Such predictability of the sign or phase of the determinant has not been exploited in the literature beyond the work of Ref. [22], but it could be of interest in the context of the density-of-states methods discussed in the next section. In those methods, the knowledge of the precise form of the imaginary part of the action as a functional of the field is essential and has been used with some success to characterize a class of relativistic field theories.

Generally speaking, the fact that there exists a family of HS transformations representing the same partition function, especially if they are non-trivially related to each other, provides in effect a variety of calculations that can be used as checks against each other. As explored in Ref. [25], the density-channel decompositions mentioned above can be replaced by their “pairing channel” counterparts (of which a new family exists, with discrete and continuous members, as above), which display different sign properties. Other kinds of useful HS transformations have been discussed in Refs. [26, 27]

Crucially, the availability of different HS transformations with different sign behavior shows that the sign problem is not an intrinsic property of a given Hamiltonian, but rather depends on the decoupling scheme. Therefore, the search for a link between the physics of a given system and the sign problem should be taken with caution, as such a link may be entirely an artifact of the formulation of the problem. An interesting example in that regard is the elimination of the sign problem by way of a fermionic reformulation of a bosonic problem in the case of a frustrated Kondo model coupled to fermions [28], followed by a HS transformation on the resulting fermionic interaction (see also [29, 30]).

It is worth pointing out, however, that there is a link between the sign problem and phase transitions. Indeed, with the path integral formulation at hand, one can reasonably argue that the sign problem can be expected to be severe close to a critical point. One way to visualize that concept is in terms of the Lee-Yang zeros of the partition function \mathcal{Z} , written as a path integral (i.e. Eq. (7)). When sampled over the relevant configurations of ϕ , the integrand $e^{-S[\phi]}$ must reflect the existence of an accumulation point of roots of \mathcal{Z} when approaching the phase transition. By itself, that property would not pose a problem. However, the natural scale of the integrand is the exponential of an extensive quantity; therefore, $e^{-S[\phi]}$ must oscillate dramatically in order to generate the large collection of zeros (in the thermodynamic limit), and the corresponding high sensitivity to the parameter values, around the transition point. For cases that do not have a sign problem, the integrand must necessarily tend to zero when approaching a phase transition (again, in the thermodynamic limit), which is often reflected in the appearance of zero modes in fermion matrices.

2.3. Density-of-states methods

The density-of-states (DoS) approaches are a class of methods that attempt to tackle the sign problem in a head-on manner, as opposed to rewriting the partition function in terms of new variables or straightforward

reweighting (although it may be argued that DoS methods are actually a kind of reweighting). The original idea of sampling the density of states as an alternative to Metropolis-based methods is due to Wang and Landau [31] and has been applied to a wide variety of systems including gauge theories [32, 33], but its generalization to systems with a sign problem was explored later on in Refs. [34, 35, 36, 37] (see also Refs. [38, 39]). The result of those explorations is now known in the literature as the logarithmic linear regression (LLR) algorithm or the functional fit approach (FFA), both of which are very closely related but differ on specific details. We will restrict ourselves here to those approaches (which have also been reviewed recently in Ref. [16]) but it is worth pointing out that DoS methods have also been applied to finite density QCD in different forms which involve histograms of the phase of the fermion determinant (see e.g. [40, 41, 42]).

The idea common to all DoS approaches is that, in the presence of a sign problem where the action can be decomposed into real and imaginary parts $S = S_R + iS_I$, the partition function can be written as

$$\mathcal{Z} = \int \mathcal{D}\phi e^{-S[\phi]} = \int ds \rho(s) e^{-is} = 2 \int ds \rho(s) \cos(s), \quad (30)$$

where we used the fact that the partition function is real and took the real part in the last step, and

$$\rho(s) = \int \mathcal{D}\phi \delta(S_I[\phi] - s) e^{-S_R[\phi]}. \quad (31)$$

The determination of $\rho(s)$ is then carried out by combining two ingredients: first, propose a functional form that can account for its variation over vast orders of magnitudes; second, carry out restricted calculations at constant or approximately constant imaginary action $S_I[\phi]$ in order to determine the coefficients in the proposed functional form for $\rho(s)$. A key aspect of the method is that, using these elements, it can deliver exponential accuracy in the calculation of $\rho(s)$.

In the approach of Refs. [35, 43], the parametrization of $\rho(s)$ is done in a piecewise-linear fashion:

$$\rho(s) = A_n e^{-k_n s}, \quad (32)$$

for $s \in I_n$, $I_n = [s_n, s_{n+1}]$, where the partitioning and sizes of the intervals I_n , i.e. the set of numbers $\{s_j\}$, can be chosen at will to reflect the desired precision in describing $\rho(s)$. By requiring continuity of $\rho(s)$ and a normalization condition $\rho(0) = 1$, the constants A_n can be determined as a function of k_n :

$$A_n = \exp\left(-\sum_{j=0}^{n-1} \Delta_j (k_j - k_n)\right), \quad (33)$$

where $\Delta_j = s_{j+1} - s_j$ is the size of the j -th interval. In order to determine the constants k_n , the FFA uses restricted expectation values defined by

$$\langle\langle X \rangle\rangle_n(\lambda) = \frac{\partial \ln \mathcal{Z}_n(\lambda)}{\partial \lambda}, \quad (34)$$

where the restricted partition function is

$$\mathcal{Z}_n(\lambda) = \int \mathcal{D}\phi e^{-S_R[\phi] + \lambda S_I[\phi]} \theta_n(S_I[\phi]), \quad (35)$$

with $\theta_n(x) = 1$ for $x \in I_n$ and 0 otherwise.

With the above piecewise-linear parametrization of $\rho(s)$, the restricted partition function and expectation values can be computed in closed form. It turns out that

$$Y_n(\lambda) \equiv \frac{\langle\langle X \rangle\rangle_n(\lambda) - D_{n-1}}{\Delta_n} - \frac{1}{2} = h((\lambda - k_n)\Delta_n), \quad (36)$$

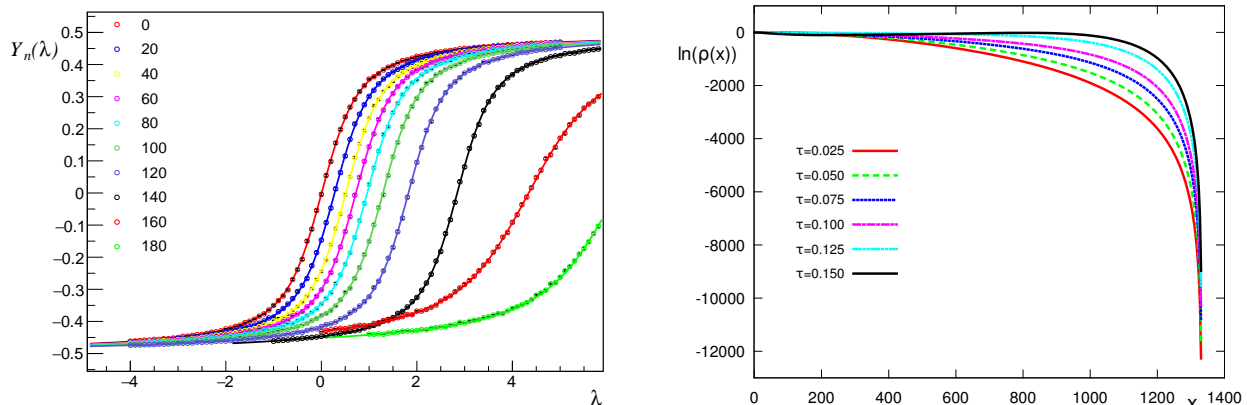


Figure 3: (Left) $Y_n(\lambda)$ as a function of λ for several discretizations n . (Right) Density of states for several values of the nearest-neighbor coupling τ . Both plots correspond to the SU(3) spin model of Ref. [44].

where $D_{n-1} = \sum_{j=0}^{n-1} \Delta_j$ and

$$h(x) = \frac{1}{1 - e^{-x}} - \frac{1}{x} - \frac{1}{2}. \quad (37)$$

These equations encode a crucial aspect of the method: once the intervals I_n are chosen (such that the Δ_n are fixed constants), each of the functions $Y_n(\lambda)$ is entirely determined by the single parameter k_n and must follow the shape dictated by $h(x)$. Thus, the function $Y_n(\lambda)$ is a kind of response function in which the source parameter λ is coupled to the imaginary part of the action S_I to constrain the value of k_n for each n . If the one-parameter fit to $h(x)$ is unsatisfactory, that signals a poor choice of the discretization $\{s_j\}$, such that a more refined mesh is likely needed. An example of the typical shape of $Y_n(\lambda)$ is shown in the left panel of Fig. 3 for several values of n for the SU(3) spin model of Ref. [44].

Once the k_n are known, one may reconstruct $\rho(s)$ and calculate the full partition function as a Fourier transformation via Eq. (30)). This last step will be sensitive to the large oscillations due to the $\cos(s)$ factor. As an example, the density of states obtained in Ref. [44] for the SU(3) spin model is shown in the right panel of Fig. 3, for several values of the nearest-neighbor coupling τ . The variations of $\rho(s)$ over many orders of magnitude are evident from that figure.

While we have focused here on the FFA, the LLR method [33] accomplishes exponential error suppression by calculating the slopes k_n of the distribution using a fixed-point iteration method. The latter is based on the work of Robbins and Monro [45], which guarantees that the values obtained in subsequent iterations are Gaussian-distributed around the exact answer. The above-mentioned exponential error suppression amounts to a constant relative error in the determination of the density of states over the full domain of the phase, which is crucial in order to carry out the Fourier integral in Eq. (30)).

The FFA and the LLR methods have been used to analyze several models on the lattice at finite density such as the Z_3 spin model [43], the SU(3) gauge theory with static color sources [44, 46], and two-color QCD with heavy quarks [37]. One of the most interesting advantages of DoS methods is that they are extremely parallelizable on modern computers. These methods require a large set of calculations, e.g. several independent calculations as a function of λ and n to determine k_n , but each of those is an independent run and can therefore be done in a perfectly scalable fashion. As long as the number of λ and n points does not grow exponentially with the spacetime volume (there is not indication thus far in the literature that that is the case, due largely to the smoothness and lack of sharp features in $\ln \rho(s)$), the computational cost will scale better than that of reweighting methods.

On the other hand, DoS approaches present a paradigm that is quite different from conventional MC methods when it comes to calculating different observables. For observables \mathcal{O} that do not depend explicitly (and only) on the action $S[\phi]$, it will not be enough to know $\rho(s)$. In such a case, a source term $j\mathcal{O}$ would

have to be included in the action and a family of densities $\rho(s, j)$ would need to be calculated at least for small j . Once $\rho(s, j)$ is thus obtained, numerical differentiation of $\ln \mathcal{Z}[j]$ yields the desired $\langle O \rangle$ in the limit $j \rightarrow 0$. Such an approach may seem slightly cumbersome or costly, but it amounts to multiple applications of the same idea which moreover retains the full parallelizability property mentioned above.

2.4. Dual variables for bosons

Dualization is another approach involving rewriting the partition function \mathcal{Z} so as to eliminate or ameliorate the sign problem. The dual variables are a new set of variables, typically discrete, that may yield a representation of \mathcal{Z} entirely in terms of positive quantities. While the concept of duality is in itself an old one, the use of dual variables in quantum Monte Carlo calculations first appeared in the 1980's: for instance, Ref. [47] showed that the strong-coupling limit of QCD could be represented as a system of dimers. Later on, Ref. [48] used dual variables to analyze the bosonic Hubbard model. The concept was later applied to fermions as well, which we review in the next section. For pure bosonic theories at finite density, it was shown in Ref. [49] that dual variables are not just an alternative representation: they successfully solve the sign problem for both relativistic as well as nonrelativistic systems. Moreover, the dual variables can be efficiently sampled using the worm algorithm [50, 51]. Since the early 2010's, a few groups have pursued the study of several quantum field theories (from simple models to effective theories of QCD) at finite temperature and density (see e.g. [52, 53, 54, 55, 56, 57, 58, 59]).

Following the notation and steps of Ref. [16], we show how to introduce dual variables first in relativistic bosons and then in the nonrelativistic case. The lattice action for a relativistic complex valued field ϕ_x is

$$S[\phi] = \sum_x \left(\eta |\phi_x|^2 + \lambda |\phi_x|^4 - \sum_{\nu=1}^4 [e^{\mu\delta_{\nu,4}} \phi_x^* \phi_{x+\hat{\nu}} + e^{-\mu\delta_{\nu,4}} \phi_x^* \phi_{x-\hat{\nu}}] \right), \quad (38)$$

where x is a spacetime lattice point and $\hat{\nu}$ denotes a unit vector in the ν -th direction ($\nu = 4$ being the imaginary-time direction). At finite μ , the quantity in square brackets ceases to be real, which exposes the sign problem. Exponentiating the action, as one would normally do to compute the partition function, we note that

$$e^{-S} = \prod_x e^{-\eta |\phi_x|^2 - \lambda |\phi_x|^4} \prod_{x,\nu} \exp(e^{\mu\delta_{\nu,4}} \phi_x^* \phi_{x+\hat{\nu}}) \exp(e^{-\mu\delta_{\nu,4}} \phi_x^* \phi_{x+\hat{\nu}}). \quad (39)$$

At each spacetime-Lorentz point x, ν , the offending term becomes a factor that can be rewritten by expanding each of the exponentials in a Taylor series as

$$\prod_{x,\nu} \exp(e^{\mu\delta_{\nu,4}} \phi_x^* \phi_{x+\hat{\nu}}) \exp(e^{-\mu\delta_{\nu,4}} \phi_x^* \phi_{x+\hat{\nu}}) = \sum_{\{n,\bar{n}\}} \mathcal{N}_{n,\bar{n}} \prod_x e^{\mu(n_{x,4} - \bar{n}_{x,4})} \phi_x^{*\sum_{\nu}(n_{x,\nu} + \bar{n}_{x-\hat{\nu},\nu})} \phi_x^{\sum_{\nu}(\bar{n}_{x,\nu} + n_{x-\hat{\nu},\nu})}, \quad (40)$$

where $\mathcal{N}_{n,\bar{n}} = \prod_{x,\nu} 1/(n_{x,\nu}! \bar{n}_{x,\nu}!)$ and the sum $\sum_{\{n,\bar{n}\}}$ denotes a sum over all configurations of the Taylor indices $n_{x,\nu} \geq 0$ and $\bar{n}_{x,\nu} \geq 0$. Using the above and the polar form $\phi_x = r_x e^{i\theta_x}$, we obtain for the partition function

$$\mathcal{Z} = \sum_{\{n,\bar{n}\}} \mathcal{N}_{n,\bar{n}} \prod_x e^{\mu(n_{x,4} - \bar{n}_{x,4})} R[n, \bar{n}, x] T[n, \bar{n}, x], \quad (41)$$

where

$$R[n, \bar{n}, x] = \int_0^\infty dr_x r_x^{1 + \sum_{\nu}(n_{x,\nu} + n_{x-\hat{\nu},\nu} + \bar{n}_{x,\nu} + \bar{n}_{x-\hat{\nu},\nu})} e^{-\eta r_x^2 - \lambda r_x^4}, \quad (42)$$

which is a non-negative, local function of the index configuration $\{n, \bar{n}\}$ (note also that the exponent of r_x is strictly positive), and

$$T[n, \bar{n}, x] = \int_{-\pi}^{\pi} \frac{d\theta_x}{2\pi} e^{-i\theta_x \sum_{\nu}(n_{x,\nu} - \bar{n}_{x,\nu} - n_{x-\hat{\nu},\nu} + \bar{n}_{x-\hat{\nu},\nu})}, \quad (43)$$

which results in Kronecker delta functions for each x imposing constraints on the configurations. In principle, the job is done at this point: we have shown that there is a discrete-field representation of the partition

function as a sum over positive quantities. It is useful, however, to take a few more steps towards simplifying the calculation, specifically towards implementing the constraints imposed by the function $T[n, \bar{n}, x]$. To that end, one parameterizes the sum and difference of n and \bar{n} via two new ‘dual’ variables k, ℓ defined via

$$n_{x,\nu} - \bar{n}_{x,\nu} \equiv k_{x,\nu} \quad \text{and} \quad n_{x,\nu} + \bar{n}_{x,\nu} \equiv |k_{x,\nu}| + 2\ell_{x,\nu}, \quad (44)$$

which take values over all integers and all non-negative integers, respectively. We finally obtain

$$\mathcal{Z} = \sum_{k,\ell} \mathcal{N}_{|k|+\ell,\ell} \prod_x W(s_x) e^{\mu \sum_x k_{x,4}} \prod_x \delta(\nabla_\nu k_{x,\nu}), \quad (45)$$

where

$$W(n) = \int_0^\infty dr r^{n+1} e^{-\eta r^2 - \lambda r^4}, \quad (46)$$

$$s_x = \sum_\nu [|k_{x,\nu}| + |k_{x-\hat{\nu},\nu}| + 2(\ell_{x,\nu} + \ell_{x-\hat{\nu},\nu})], \quad \text{and} \quad \nabla_\nu k_{x,\nu} \equiv \sum_\nu [k_{x,\nu} - k_{x-\hat{\nu},\nu}]. \quad (47)$$

The constraint $\nabla_\nu k_{x,\nu} = 0$ enforces that the field $k_{x,\nu}$ be solenoidal, such that the flux of $k_{x,\nu}$ is conserved.

Pure gauge theories can also be written in terms of dual variables and, as above, results in a new representation for the partition function in terms of purely positive terms. This approach yielded the first real and positive dualization of *abelian* gauge theories with a so-called θ term [60], which is a term in the action coupled to a topological charge (see Refs. [61, 62] for updates on that work). Because that term is necessarily complex, it results in a sign problem in conventional path integral representations. The current challenge for this approach is the extension to *non-abelian* gauge theories and the inclusion of fermions (see however next section).

The case of nonrelativistic bosons can also be addressed with dual variables with some modifications with respect to the relativistic case. We show some of steps of that derivation here as a pedagogical example; they closely follow the relativistic case. As we will show in more detail in Sec. 5, the problem appears in nonrelativistic bosons not because of the chemical potential but because of the asymmetry in the time derivative: there are only particles and no antiparticles. (The physical source of the problem is thus the same as in the relativistic case: the breaking of time-reversal invariance.) Starting with the lattice action for the complex valued field ϕ_x in 3+1 dimensions (although this example can be easily generalized to $d+1$ dimensions), we have

$$S = \sum_x \left(\lambda |\phi_x|^4 + \phi_x^* \phi_x - e^{\tau\mu} \phi_x^* \phi_{x+\hat{4}} - \frac{1}{2} \sum_{k=1}^3 [\phi_x^* \phi_{x+\hat{k}} + \phi_x^* \phi_{x-\hat{k}} - 2\phi_x^* \phi_x] \right), \quad (48)$$

Then,

$$e^{-S} = \prod_x e^{-4|\phi_x|^2 - \lambda |\phi_x|^4} \prod_x \exp(e^{\tau\mu} \phi_x^* \phi_{x+\hat{4}}) \prod_{x,k} \exp(\phi_x^* \phi_{x+\hat{k}}/2) \exp(\phi_x^* \phi_{x-\hat{k}}/2), \quad (49)$$

where we now expand the exponentials of the derivative terms in a power series, such that

$$\begin{aligned} & \prod_x \exp(e^{\tau\mu} \phi_x^* \phi_{x+\hat{4}}) \prod_{x,k} \exp(\phi_x^* \phi_{x+\hat{k}}/2) \exp(\phi_x^* \phi_{x-\hat{k}}/2) \\ &= \sum_{\{n,m,\bar{m}\}} \mathcal{N}_{n,m,\bar{m}} e^{\tau\mu n_x} \phi_x^{*n_x + \sum_k (m_{x,k} + \bar{m}_{x,k})} \phi_x^{n_{x-\hat{4}} + \sum_k (m_{x-\hat{k},k} + \bar{m}_{x+\hat{k},k})}, \end{aligned} \quad (50)$$

where $\mathcal{N}_{n,m,\bar{m}} = \prod_x 1/n_x! \prod_{x,k} 1/(2^{m_{x,k} + \bar{m}_{x,k}} m_{x,k}! \bar{m}_{x,k}!)$, and n_x is a site variable, whereas $m_{x,k}$ and $\bar{m}_{x,k}$ are link variables in the spatial directions. As in the previous example, one may now write the fields in terms of their polar representation $\phi_x = r_x e^{i\theta_x}$ to obtain constraints for the integer fields n, m, \bar{m} and eventually arrive at a sum of positive definite terms for \mathcal{Z} . Explicitly,

$$\mathcal{Z} = \sum_{n,m,\bar{m}} \mathcal{N}_{n,m,\bar{m}} \prod_x e^{\tau\mu n_x} R[n, m, \bar{m}, x] T[n, m, \bar{m}, x], \quad (51)$$

where

$$R[n, m, \bar{m}, x] = \int_0^\infty dr_x r_x^{1+n_x+n_{x-\hat{4}}+\sum_k(m_{x,k}+\bar{m}_{x,k}+m_{x-\hat{k},k}+\bar{m}_{x+\hat{k},k})} e^{-4r_x^2-\lambda r_x^4}, \quad (52)$$

which is a non-negative, local function of the index configuration $\{n, m, \bar{m}\}$ (also, as before, the exponent of r_x is strictly positive), and

$$T[n, m, \bar{m}, x] = \int_{-\pi}^{\pi} \frac{d\theta_x}{2\pi} e^{-i\theta_x[n_x-n_{x-\hat{4}}-\sum_k(m_{x,k}+\bar{m}_{x,k}-m_{x-\hat{k},k}-\bar{m}_{x+\hat{k},k})]}, \quad (53)$$

which results in Kronecker delta functions that impose constraints on the configurations.

It is then clear that the dual-variable formulation avoids the sign problem for nonrelativistic bosons, as first noted in Ref. [49]. It is worth noting, however, that other cases such as coupling to angular momentum, are not obviously solvable with this technique.

While this method completely solves the sign problem in the cases shown above (and some others, e.g. bosons with non-abelian spin-orbit coupling), the calculation of specific observables acquires a new degree of complexity due to the dramatic change of variables. This is merely an algebraic inconvenience but, in practice, the change from the original fields ϕ to the discrete fields n, m, \bar{m} implies that any operator expression in the ϕ language needs to be re-derived (e.g. by inserting sources in the original action or using the parameters of the theory).

In this section we have focused on exact alternative representations of scalar bosons. However, such representations have also been found for gauge fields [63, 64] which are valid also away from the strong coupling limit.

2.5. Dual variables for fermions and fermion bags

One of the first uses of dual variables for fermions in Monte Carlo calculations was unrelated to the sign problem: it was found in Ref. [47] that QCD in the strong-coupling limit could be represented as a system of dimers, which inspired multiple studies [65, 66, 67, 68, 69, 70]. However, dual variables by themselves do not necessarily avoid the fermion sign problem. As first described in Ref. [71], in what is now known as the ‘meron cluster’ approach, one must sum analytically over configurations in a given cluster (where the type of configuration cluster must be cleverly identified) and then stochastically over clusters. When the clusters are properly chosen, they contain configurations that may vary in sign but such that the overall contribution of a cluster is of constant sign across clusters.

The fermion bag approach of Refs. [72, 73] (extended to continuous time in Ref. [74]; see also Refs. [75, 76, 77, 78]) extends the meron cluster approach to a larger class of theories. Rather than following those derivations (based on Grassmann numbers), here we connect with them from a different perspective. We begin by re-writing the partition function as

$$\mathcal{Z} = \text{Tr} \left[e^{-\beta(\hat{H}-\mu\hat{N})} \right] = \text{Tr} \left[\left(e^{-\tau(\hat{H}-\mu\hat{N})} \right)^{N_\tau} \right], \quad (54)$$

where $\beta = \tau N_\tau$. Using a Suzuki-Trotter decomposition, we may approximate

$$e^{-\tau(\hat{H}-\mu\hat{N})} \simeq e^{-\tau(\hat{T}-\mu\hat{N})} e^{-\tau\hat{V}}, \quad (55)$$

where \hat{T} is the kinetic energy and \hat{V} the interaction. As an example, we specialize to the case where $\hat{V} = -U \sum_x \hat{n}_\uparrow(x) \hat{n}_\downarrow(x)$, and then we have

$$e^{-\tau\hat{V}} = \prod_x e^{\tau U \hat{n}_\uparrow(x) \hat{n}_\downarrow(x)} = \prod_x (1 + B \hat{n}_\uparrow(x) \hat{n}_\downarrow(x)) = \sum_{m_x=0,1} B^{\sum_x m_x} \prod_x (\hat{n}_\uparrow(x) \hat{n}_\downarrow(x))^{m_x}, \quad (56)$$

where $B = e^{\tau U} - 1$. We may use the above at each point in imaginary time by inserting this expression into Eq. (55) to obtain

$$e^{-\beta(\hat{H}-\mu\hat{N})} = \prod_{t=1}^{N_\tau} \hat{\mathcal{T}}_t \prod_x (1 + B \hat{n}_\uparrow(x) \hat{n}_\downarrow(x))_t = \sum_{m_{x,t}=0,1} B^{\sum_{x,t} m_{x,t}} \prod_{t=1}^{N_\tau} \left[\hat{\mathcal{T}}_t \prod_x (\hat{n}_\uparrow(x) \hat{n}_\downarrow(x))_t^{m_{x,t}} \right], \quad (57)$$

where $\hat{\mathcal{T}}_t \equiv e^{-\tau(\hat{T}-\mu\hat{N})}$ and we note that the product over the time slices actually factorizes across flavors as

$$\prod_{t=1}^{N_\tau} \left[\hat{\mathcal{T}}_t^\uparrow \prod_x \hat{n}_\uparrow(x)_t^{m_{x,t}} \right] \prod_{t=1}^{N_\tau} \left[\hat{\mathcal{T}}_t^\downarrow \prod_x \hat{n}_\downarrow(x)_t^{m_{x,t}} \right]. \quad (58)$$

Below we will show the following trace-determinant identity

$$\text{Tr} \prod_{t=1}^{N_\tau} \left[\hat{\mathcal{T}}_t^\uparrow \prod_x \hat{n}_\uparrow(x)_t^{m_{x,t}} \right] = \det W_\uparrow[\{m\}], \quad (59)$$

where $W_s[\{m\}]$ is the free fermion matrix for spin s in which the rows and columns x_0, t_0 for which $m_{x_0, t_0} = 1$ are dropped (see below for details on the form of $W_s[\{m\}]$). Using the above in the definition of \mathcal{Z} yields

$$\mathcal{Z} = \sum_{m_{x,t}=0,1} B^{\sum_{x,t} m_{x,t}} \det W_\uparrow[\{m\}] \det W_\downarrow[\{m\}], \quad (60)$$

where we finally have completely re-written the full partition function as a sum over configurations of the monomer field $m_{x,t}$.

For unpolarized nonrelativistic systems, $W_s[\{m\}]$ is real and takes on the same value for $s = \uparrow, \downarrow$, such that there is no sign problem, as long as $B \geq 0$, i.e. for attractive interactions. Thus far, the same conditions apply for the auxiliary field formulation of the problem: repulsive interactions ($B < 0$) or polarization ($W_\uparrow[\{m\}] \neq W_\downarrow[\{m\}]$) would lead to a sign problem. This formulation, however, lends itself to an interpretation of the sum in terms of clusters known as fermion bags, which are disjoint regions \mathcal{B}_i of the discrete field $m_{x,t}$ within which $m_{x,t} = 0$ (see Fig. 4). As the corresponding interaction vertices (i.e. insertions of U) are thus absent in $W_s[\{m\}]$, fermions are free to move about inside the bag. Using that property, Ref. [72] argued that, while the contributions to a given fermion bag configuration may vary in sign, the overall contribution of each bag to the full partition function is actually positive. Thus, if one is able to add up the terms within each bag, then it is possible to use Metropolis-based importance sampling to sum over all possible fermion bag configurations.

The right-hand side of Eq. (59) can also be calculated using Wick's theorem, if interpreted as the expectation value of a time-dependent operator in a noninteracting system. In that weak-coupling interpretation, it is possible to show that

$$\text{Tr} \prod_{t=1}^{N_\tau} \left[\hat{\mathcal{T}}_t^\uparrow \prod_x \hat{n}_\uparrow(x)_t^{m_{x,t}} \right] = \det M_\uparrow \det G_\uparrow[\{m\}], \quad (61)$$

where M_\uparrow is the noninteracting spacetime fermion matrix and $G_\uparrow[\{m\}]$ is a propagator matrix whose size depends on the monomer configuration $m_{x,t}$ and which contains noninteracting propagators connecting the monomer sites where $m_{x,t} = 1$. As explained in Ref. [73], the equality between Eqs. (59) and (61) represents a duality relation between strong coupling and weak coupling; in the former case, a large number of monomers appear and Eq. (59) is easier to calculate than Eq. (61), which becomes easier at weak coupling.

In combination with the hopping expansion (which amounts to expanding the exponential of the kinetic energy rather than the potential energy), one arrives at other useful sign-problem-free representations of fermionic partition functions. One such example is well-known and is the case of nonrelativistic fermions in 1D with two-body interactions [79]. Another more recently discovered case is that of nonrelativistic fermions in 1D with four-body interactions, shown and used in Refs. [80, 81, 82], where also a fermion-bag type idea is used to sum over configuration clusters. Interestingly, baryons at strong coupling can also be described by bags where three quarks propagate coherently as a single free fermion (i.e. a baryon) inside bags, while the complementary domain displays quark- and di-quark-type excitations [83]. Other relevant examples can be found in Refs. [66, 84, 85].

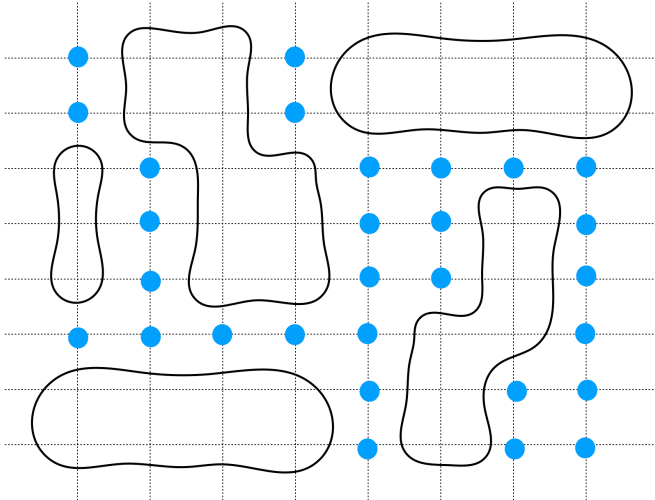


Figure 4: Fermion bag interpretation of the dual-variable approach to many-fermion systems. The blue dots represent the points on the spacetime lattice for which the discrete field acquires values $m_{x,t} = 1$. The regions enclosed by continuous black lines represent the fermion bags, within which $m_{x,t} = 0$ and where fermions move freely. This picture is not general but meant only as an illustration. The true shape of the allowed bag configurations will depend on the specific form of the Hamiltonian; in particular, the form of the kinetic energy operator is crucial in determining whether such a bag decomposition is possible.

Proof of trace-determinant identity. For completeness, we outline the proof of the trace-determinant identity Eq. (59) used above. We have not seen this way to approach the proof anywhere else, and since we find it particularly clear, we include it here. First we quote the auxiliary identity

$$\text{Tr} \left[\prod_{k=1}^N e^{\hat{B}_k} e^{\hat{A}_k} \right] = \det \begin{pmatrix} 1 & 0 & 0 & 0 & \cdots & e^{B_N} \\ -e^{A_1} & 1 & 0 & 0 & \cdots & 0 \\ 0 & -e^{B_1} & 1 & \ddots & 0 & 0 \\ \vdots & \cdots & \ddots & \ddots & \vdots & \\ 0 & 0 & -e^{A_{N-1}} & 1 & 0 & \\ 0 & 0 & 0 & -e^{B_{N-1}} & 1 & 0 \\ 0 & 0 & 0 & \cdots & -e^{A_N} & 1 \end{pmatrix}, \quad (62)$$

which is a reformulation of a well-known identity in the operator formulation of quantum Monte Carlo (see e.g. [86]). Here, the left-hand side trace is over Fock space, the entries of the Fermi matrix on the right-hand side are themselves matrices (i.e. the above is shown in block form), and $\hat{A}_k = \sum_{i,j} [A_k]_{ij} \hat{c}_i^\dagger \hat{c}_j$ and $\hat{B}_k = \sum_{i,j} [B_k]_{ij} \hat{c}_i^\dagger \hat{c}_j$ are (generally non-commuting) one-body operators. For our purposes, k represents a particular time slice, $\hat{B}_k = j_{x,k} \hat{n}_{x,k}$, such that $[e^{B_k}]_{x,x'} = \delta_{x,x'} e^{j_{x,k}}$, and \hat{A}_k encodes the kinetic energy, i.e. it is actually a k -independent operator. Our focus is on the B_k factors.

The crucial step in proving Eq. (59) is in differentiating both sides of Eq. (62) with respect to $j_{x,k}$ in as many points $\{x, k\}$ as needed (namely the points where $m_{x,k} = 1$; recall each point appears only once in the matrix) to match the desired insertions of $\hat{n}(x)$ at the desired time slices k . To carry out the differentiations on the right-hand side, we first use the Laplace cofactor expansion of the determinant and set the corresponding $j_{x,k}$ to zero once the derivative is taken. Once all the desired derivatives are applied, what remains is the corresponding cofactor determinant. The latter is the determinant of the matrix on the right-hand side of Eq. (62) where the rows and columns of a given e^{B_k} containing the differentiated points $\{x, k\}$ are simply dropped, and the sources j in any remaining terms are set to zero; that prescription defines the square matrix $W_s[\{m\}]$, whose number of rows (and columns) is reduced from the original matrix by the number of non-zero monomers. Note that there will, typically, be more than one spatial point x affected within a given temporal block e^{B_k} ; similarly, any temporal block not affected by the derivatives will turn into an identity matrix once the sources are set to zero. Note also that any overall signs are unimportant because they cancel against the corresponding expression for the other fermion species.

2.6. Majorana fermions

In Ref. [87] a fermion representation was introduced that does not display a sign problem for a broad class of systems. Those developments were precipitated in part by the work of Huffman and Chadracharan of Ref. [78]. In this representation, conventional fermionic operators $\hat{\psi}(\mathbf{x})$ are written in terms of two species of Majorana fermions $\hat{\gamma}_{1,2}(\mathbf{x})$ via

$$\hat{\psi}(\mathbf{x}) = \frac{1}{2}(\hat{\gamma}_1(\mathbf{x}) + i\hat{\gamma}_2(\mathbf{x})), \quad (63)$$

$$\hat{\psi}^\dagger(\mathbf{x}) = \frac{1}{2}(\hat{\gamma}_1(\mathbf{x}) - i\hat{\gamma}_2(\mathbf{x})). \quad (64)$$

Using this representation along with a HS transformation with an auxiliary field ϕ , it is possible to integrate out the fermionic degrees of freedom such that the partition function then takes the form

$$\mathcal{Z} = \int \mathcal{D}\phi W_1[\phi] W_2[\phi], \quad (65)$$

where

$$W_a[\phi] = +\sqrt{\det M_a[\phi]}, \quad (66)$$

and $M_a[\phi]$ is the Fermi matrix characterizing the dynamics of the Majorana fermions of type a in the external auxiliary field ϕ . Under conditions of time-reversal invariance for the Majorana fermions, it is possible to show that $W_1[\phi] = W_2[\phi]^*$, such that

$$W_1[\phi] W_2[\phi] = |W_1[\phi]|^2 \geq 0, \quad (67)$$

and therefore the sign problem is completely eliminated.

A characterization of the classes of sign problems that are solved by this technique can be found in Refs. [88, 89] (see Ref. [90] for a general and more recent approach to such a characterization, based on semigroups). In particular, it is worth noting that the sign problem in fully polarized (or spinless) fermions is solved by this technique. Various applications were explored in Refs. [91, 92, 93, 94, 95] and the connection with conventional methods into a unifying principle for sign-problem free calculations, under certain symmetry conditions, was developed in Ref. [96] and Ref. [24]. It should be stressed that, rather than a method or an algorithm, the Majorana representation is a way to discover systems that do not have a sign problem (and for which it is not otherwise obvious that this is the case in conventional fermion formulations). Once that property is established, conventional algorithms can be used to carry out the calculation.

2.7. Imaginary asymmetry

Fermions at finite polarization or mass imbalance present a sign problem because although the determinant in Eq. (11) factorizes and the factors are real, they will not typically be equal for all values of the HS field. A trick to overcome that problem, commonly used in relativistic physics [97, 98, 99, 100] (although its origin can be traced back to condensed matter [101]), is to make the asymmetry imaginary. For instance, if there are two spin flavors with corresponding chemical potentials $\mu_{\uparrow,\downarrow} = \mu \pm \delta\mu$, then taking $\delta\mu \rightarrow i\delta\mu_R$, where $\delta\mu_R$ is real, such that $\delta\mu$ is purely imaginary, makes the fermion determinants complex conjugates of one another and their product is real and positive, i.e.

$$\det M_\uparrow \det M_\downarrow \rightarrow |\det M_\uparrow|^2, \quad (68)$$

when $\delta\mu \rightarrow i\delta\mu_R$. Below, we will refer to imaginary asymmetry methods in general by the abbreviation ‘‘iHMC’’. In relativistic physics, the equivalent of the above is the introduction of a finite chemical potential that breaks the particle-antiparticle symmetry of the vacuum (thus inducing a finite density of particles or antiparticles, breaking time-reversal invariance and creating a sign problem).

Naturally, a caveat of this approach is that one must return to the real asymmetry axis (see left panel of Fig. 5), which usually involves a fit to data and some form of analytic continuation and thus some degree of

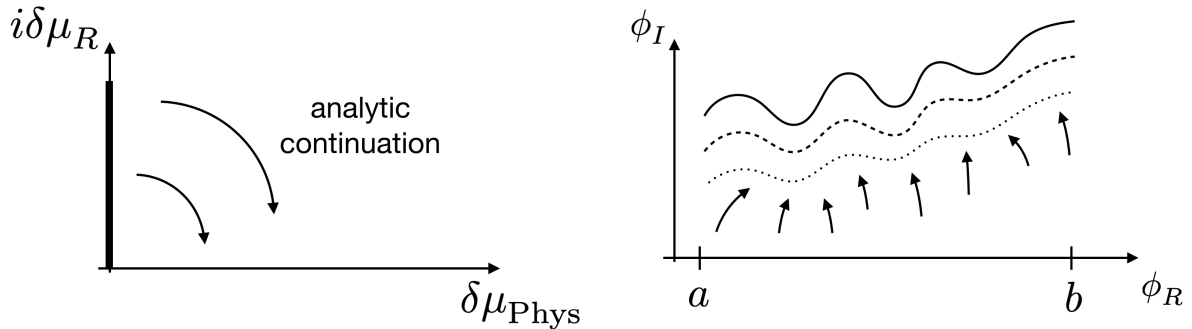


Figure 5: (Left) Approaches based on imaginary chemical potential asymmetry, as parametrized by $i\delta\mu_R$, where $\delta\mu_R$ is real, avoid the sign problem (see text) but the results must then be analytically continued to the physical axis where the asymmetry is real. (Right) Approaches based on deformed contour or Lefschetz thimbles aim to minimize the phase oscillations by numerically modifying the domain of integration of the path integral, allowing the field to acquire an imaginary part.

uncontrolled approximations. The fact that investigations on the imaginary asymmetry axis are done in an entirely nonperturbative way are certainly an attractive feature. From a practical standpoint, the idea has actually seen some important successes in lattice QCD [102, 103, 104] (where the chemical potential must be made entirely imaginary to avoid the sign problem; see left panel of Fig. 6) as well as in nonrelativistic physics, where it has been applied to chemical potential as well as mass asymmetries [105, 106, 107, 108, 109]; see center and right panels of Fig. 6. Other interesting applications, such as imaginary angular velocity, coupled to angular momentum, remain unexplored.

It should be pointed out that, for small asymmetries, one can avoid the problem of analytic continuation completely by performing a Taylor expansion in the asymmetry (around vanishing asymmetry, of course). Such an approach, advocated in Ref. [110] and used in Ref. [111] for QCD at finite chemical potential, can be very efficient (to the extent that the static response functions that result from the Taylor expansion can be calculated in a statistically controlled manner). The effort on the QCD side has been pushed to sixth order in the baryon chemical potential by the Bielefeld-BNL-CCNU collaboration, as shown in Ref. [112].

2.8. Lefschetz thimbles

In the presence of a phase problem, i.e. when the action $S[\phi]$ is complex, it may be possible to deform the contour of integration from the real line $\phi \in (-\infty, \infty)$ into the complex plane (see right panel of Fig. 5) in such a way as to make the phase of the action constant, or approximately so. Such a contour deformation changes neither the theory nor the observables, as the integrand in the path integral of any theory of interest will be an analytic function of ϕ . If such a contour can be determined either a priori or dynamically during a calculation, the sign problem could potentially be solved or at least tamed. As a Monte Carlo method, the idea can be traced back to the work of Ref. [113] where the so-called shifted contour auxiliary-field Monte Carlo method was put forward for electronic systems (see also Ref. [114, 115]). More recently, contour deformation and Lefschetz thimbles have re-emerged as a method in quantum field theory [116, 117, 118, 119, 120, 121, 122, 123, 124, 125, 126, 127, 128, 129, 130].

As in complex Langevin (which will be explored in the remainder of this review), the idea behind Lefschetz-thimbles approaches involves complexifying the field: $\phi \rightarrow \phi_R + i\phi_I$. One is interested in finding, in such a complexified configuration space, the stationary points for which $\delta S/\delta\phi = 0$, as those points feature reduced phase oscillations for $\exp(-i\text{Im}S[\phi])$. Such an approach is of course the generalization of the saddle-point (or critical point) method of evaluating complex integrals and the higher-dimensional version is often

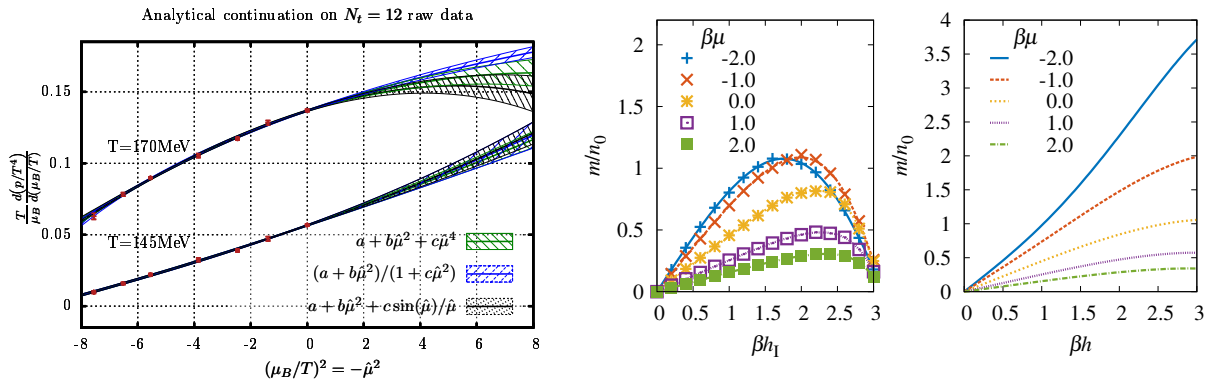


Figure 6: (Left) Results of analytic continuation from imaginary chemical potential in QCD, from Ref. [104]. (Middle and Right) Results for the magnetization equation of state after analytic continuation from imaginary chemical asymmetry h_I in non-relativistic 1D fermions, from Ref. [107].

referred to as Picard-Lefschetz theory. The corresponding deformed, high-dimensional integration contours of steepest descent are called Lefschetz thimbles.

In practice, the locations of such (stable) points of steepest descent are found by evolving the field along a fictitious time t (unrelated to the imaginary time τ) according to the holomorphic gradient flow equation

$$\frac{d\phi_R}{dt} = -\text{Re} \left[\frac{\delta S}{\delta \phi} \right], \quad (69)$$

$$\frac{d\phi_I}{dt} = +\text{Im} \left[\frac{\delta S}{\delta \phi} \right], \quad (70)$$

$$(71)$$

which, as we shall see below, is remarkably similar to the CL equations (see also Ref. [131] for a particularly lucid side-by-side discussion of CL versus Lefschetz thimbles approaches).

The crucial advantages of deforming the path integral to capture, effectively, a set of mean-field configurations and the corresponding fluctuations, are that $\text{Im}S[\phi]$ is locally constant and the real part, which determines the weight $\exp(-\text{Re}S[\phi])$, is maximally localized around the saddle point. In other words: Lefschetz thimbles are the best locations to carry out stochastic evaluations of path integrals. While the constant- $\text{Im}S[\phi]$ property is crucial, the method does not rely on finding the precise location of the critical points. Rather, it is based on finding a useful deformation which may or may not be close to the stationary phase contours attached to the critical points (wherever those may be), but where the variations in $\text{Im}S[\phi]$ are small [132]. Those ideas were crucial for the application of Refs. [133, 134] where they were used to calculate the properties of a low-dimensional field theory in real time. Furthermore, Ref. [135] found that, even if the holomorphic gradient flow of Eq. (69) is used to push the deformation very close to the thimbles (which is naively the ideal situation), then the high barriers separating the thimbles would make the sampling very challenging in practice.

One of the difficulties of deforming a contour in a functional integral is the calculation of the associated Jacobian factor [136]. While that is a computational issue that is difficult but tractable, a more serious challenge lies in accounting for all the possible thimbles. The latter is often referred to as a ‘global’ sign problem, as opposed to the ‘residual’ sign problem coming from the remaining curvature (i.e. variations in the imaginary part of the Jacobian across the thimble). In that regard, it is useful to note that (for a fixed set of input parameters), only a subset of thimbles contribute to the partition function. The global sign problem depends on the subset and the relative weights of each thimble, both of which are difficult to determine in practice. However, the holomorphic flow bypasses that complication. It is then possible to track the global and the residual sign problems on the deformed surface by measuring the average phase.

3. The Langevin method for real and complex variables

Stochastic quantization as a method for treating Euclidean field theories has been around since Parisi and Wu first proposed the connection between the Euclidean field theories and statistical systems coupled to a heat bath [137]. It is now well-established as a successful tool for treating quantum many-body systems with a real Euclidean action [138]. This section examines the method for systems without a sign problem (referred to from here on as “real Langevin”) and its extension to systems with complex actions as a possible circumvention of the sign problem (“complex Langevin” or CL, the focus of this review). We present a pedagogical example to illustrate the real and complex Langevin methods using a simple toy model, and discuss some of the challenges that arise in using the complex Langevin method along with proposed solutions to those problems.

3.1. Complex Langevin: origins and modern re-emergence

Shortly after the introduction of the concept of real stochastic quantization, it was realized that the approach could be extended to the case of complex actions. Loosely speaking, using a Langevin equation rather than an importance sampling approach eliminates the restriction to real and positive semidefinite measures. This is due to the ability of the probability measure used in a Langevin method to be complexified – at least formally. In 1983 such a strategy was discussed independently by Klauder [139, 140] and Parisi [141] as an alternative to existing Monte Carlo methods and marked the first investigations of how the complex Langevin equation can be used to address the complex phase problem.

The elegant form of the approach as well as the potential to circumvent the sign problem drew considerable interest in the years after the initial proposals. Following the first successful numerical application for the quantum Hall effect by Klauder [142], the method was employed in many studies, albeit with mixed success. Unfortunately, the convergence of the method cannot be guaranteed a priori and even if convergence is achieved, spurious solutions with biased expectation values might be found. This is connected to subtle mathematical issues that arise in the case of complex weight and the structure of the associated complex Fokker-Planck equation. As a consequence, the initial flurry of interest stalled and progress on these matters slowed down over the years. However, studies have investigated the applicability of CL to a set of toy problems [143] and interestingly the method has also spread to simulations of polymeric fluids [144, 145] and to reaction simulations in the context of physical chemistry [146, 147] as a way to include beyond mean-field corrections.

As recently as the mid 2000s to early 2010s, the CL approach re-emerged as a method of interest in relativistic physics, particularly in QCD. In this new era, early applications to relativistic physics examined non-equilibrium QFT, which can provide insights into high-energy physics, particularly heavy ion collisions. Due to the non-perturbative nature of these non-equilibrium systems, standard approximation techniques fail. Lattice simulations provide a potential avenue for exploration, but these non-equilibrium systems do not lend themselves to a Euclidean treatment, and a Minkowski formulation suffers from a sign problem. In 2005, Berges and Stamatescu demonstrated the viability of CL to treat non-equilibrium QFT using first-principles simulations [148]. Later work built on these results to examine how CL could lead to breakthroughs in our understanding of QCD plasmas in heavy-ion collisions, early thermalization, and other open questions in quantum field theory [149].

In 2008, Aarts and Stamatescu demonstrated that CL could be applied to models of finite density QCD that exhibit a sign problem [150]. Shortly after that, Aarts demonstrated that CL could be used to circumvent the sign problem in the relativistic Bose gas with finite chemical potential [151, 152]. This began a resurgence of interest in this method in the field of finite density Lattice QCD (LQCD), in which non-perturbative calculations of strongly interacting matter with finite baryon chemical potential are inhibited by the sign problem. This renewed interest led to work in the next few years on optimization of the method to prevent runaways and improve stability, using stochastic reweighting, gauge fixing, and adaptive step size algorithms [153, 154, 155].

The successes of the method, and advances made in treating instabilities and singularities in the fermion determinant, have generated interest in applying CL to non-relativistic systems, particularly many-fermion systems, in which sign problems arise frequently. Work with the CL method in the context of non-relativistic

systems is just beginning, but is already showing great promise. Discussion of these recent applications to relativistic and non-relativistic physical systems can be found in Secs. 4 and 5.

Despite the formal challenges of CL, it should be pointed out that, at least in principle, the existence of a well-defined probability measure on a complexified field space is guaranteed under certain conditions (often referred to as Weingarten’s theorem [156]). However, the challenge lies in constructing such a measure, which has been investigated by Salcedo and others [157, 158, 159, 160, 161, 162, 163, 164]. While this is a very attractive area of research, we will not pursue it further in this review.

3.2. Stochastic quantization: path integrals and the Langevin process

The main ingredient of the CL method is the concept of *stochastic quantization*. The idea was introduced in the seminal 1981 paper of Parisi and Wu [137] and a few years later summarized nicely in the famous review article by Damgaard and Hüffel [138]¹. Notably, stochastic quantization has played an important role both theoretically as well as computationally; in particular, it has been used extensively in field theory (see e.g. Ref. [166]) and condensed matter (see e.g. Ref. [167]), and is the precursor of the hybrid Monte Carlo algorithm [168, 169], which has been the workhorse of LQCD for decades. In the following we present a brief introduction to stochastic quantization in order to lay out the foundation for later considerations.

For a quantum field theory of a real field ϕ governed by a real action $S[\phi]$, stochastic quantization provides an intuitive way to understand path integrals of the form

$$\mathcal{Z} = \int \mathcal{D}\phi e^{-S[\phi]}. \quad (72)$$

As a first step, we introduce a purely fictitious time variable t , which represents the direction of the stochastic evolution. This fictitious time evolution is then governed by a stochastic differential equation, namely the Langevin equation:

$$\frac{d\phi}{dt} = -\frac{\delta S[\phi]}{\delta\phi} + \tilde{\eta}. \quad (73)$$

The first term on the right hand side is called the drift term, also sometimes referred to as the classical flow as it constitutes the deterministic part of the time-propagation of the fields. The second term on the left hand encodes the random nature of the equation and is given by a white-noise with zero autocorrelation, i.e. $\tilde{\eta} \sim \delta(t - t')$.

For practical purposes it is convenient to rewrite this equation in a discrete form which can be done by integrating both sides over the time interval Δt . This leads to the discrete Langevin equation

$$\Delta\phi = K[\phi]\Delta t + \eta, \quad (74)$$

where η is typically chosen to be a Gaussian random variable with $\langle\eta\rangle = 0$ and $\langle\eta^2\rangle = 2\Delta t$. The angle brackets denote an average over η . This random process will produce configurations ϕ that follow a certain probability distribution. The key ingredient of stochastic quantization is the realization that the equilibrium distribution (if it exists) of the $d + 1$ dimensional random process in Eq. (74) corresponds to the probability measure in the d -dimensional path integral Eq. (72). The extra dimension is simply the fictitious time t .

It is instructive to consider the above stochastic differential equation without the noise term. In that case, Eq. (73) reduces to an ordinary differential equation and its form is nothing but that of a gradient descent. Starting out at a random (non-pathological) state, this implies that the solution will converge to a stationary point of the action, which is the “mean-field” or classical solution. The simple interpretation of the noise term is that it represents quantum fluctuations around this classical solution. In order to reproduce the correct physics, we have to “add the correct amount of fluctuations” which is set by the Fluctuation-Dissipation theorem. Thus, stochastic quantization can be viewed as a very explicit form of quantization.

¹See also Ref. [165] for a more formal introduction to stochastic quantization

The random process results in a sequence of time-dependent configurations $\phi_\eta(t)$ distributed according to a time-dependent probability measure $P[\phi, t]$. The expectation value of a given observable $\mathcal{O}[\phi]$ is then given by

$$\langle \mathcal{O}[\phi_\eta(t)] \rangle = \int \mathcal{D}\phi P[\phi, t] \mathcal{O}[\phi]. \quad (75)$$

To establish the validity of such a Langevin average, we need to investigate the temporal behavior of the expectation value and show that the time-dependent probability distribution depends on $S[\phi]$ in the way dictated by Eq. (72), at least at large enough t . Such a property will justify the use of temporal averages along the Langevin evolution to estimate the true expectation values of the theory. An instructive discussion can be found in [170], which we will follow closely.

As a first step, we take the fictitious-time derivative of the expectation value

$$\frac{d \langle \mathcal{O}[\phi_\eta(t)] \rangle}{dt} = \int \mathcal{D}\phi \frac{dP[\phi, t]}{dt} \mathcal{O}[\phi]. \quad (76)$$

Note, that only the probability distribution carries a fictitious-time dependence. Alternatively, we may perform the same fictitious-time derivative by expanding the observable to second order in its ϕ dependence

$$d\mathcal{O}[\phi] = \frac{\delta\mathcal{O}[\phi]}{\delta\phi} d\phi + \frac{1}{2} \frac{\delta^2\mathcal{O}[\phi]}{\delta\phi^2} (d\phi)^2. \quad (77)$$

According to Eq. (74) we may write

$$d\phi = -\frac{\delta S[\phi]}{\delta\phi} dt + dw, \quad (78)$$

where dw is the so-called *Wiener increment* with the property

$$\langle dw^2 \rangle = \int_t^{t+dt} d\tau \int_t^{t+dt} d\tau' \langle \eta(\tau)\eta(\tau') \rangle = 2 dt, \quad (79)$$

and vanishing mean $\langle dw \rangle = 0$. Substituting in Eq. (77) and using the properties of dw yields

$$\langle d\mathcal{O}[\phi] \rangle = \left\langle -\frac{\delta\mathcal{O}[\phi]}{\delta\phi} \frac{\delta S[\phi]}{\delta\phi} + \frac{\delta^2\mathcal{O}[\phi]}{\delta\phi^2} \right\rangle dt, \quad (80)$$

which allows us to write

$$\frac{d \langle \mathcal{O}[\phi_\eta(t)] \rangle}{dt} = \left\langle -\frac{\delta\mathcal{O}[\phi]}{\delta\phi} \frac{\delta S[\phi]}{\delta\phi} + \frac{\delta^2\mathcal{O}[\phi]}{\delta\phi^2} \right\rangle \equiv \langle LO \rangle, \quad (81)$$

where we defined the so-called Langevin operator

$$L_r = \int d\tau d^d x \left(\frac{\delta}{\delta\phi} + K[\phi] \right) \frac{\delta}{\delta\phi}, \quad (82)$$

with the drift $K[\phi] = -\frac{\delta S[\phi]}{\delta\phi}$, according to Eq. (74). We may again write this as an integral over configurations

$$\frac{d \langle \mathcal{O}[\phi_\eta(t)] \rangle}{dt} = \int \mathcal{D}\phi \left(-\frac{\delta\mathcal{O}[\phi]}{\delta\phi} \frac{\delta S[\phi]}{\delta\phi} + \frac{\delta^2\mathcal{O}[\phi]}{\delta\phi^2} \right) P[\phi, t] \quad (83)$$

$$= \int \mathcal{D}\phi \mathcal{O}[\phi] \left(\frac{\delta}{\delta\phi} \frac{\delta S[\phi]}{\delta\phi} + \frac{\delta^2}{\delta\phi^2} \right) P[\phi, t]. \quad (84)$$

where the second line results from partial integration. Here we made the important assumption that the probability vanishes at the boundaries (or decays fast enough if the integration region is non-compact). These assumptions are in fact crucial and will be discussed in more detail below.

Comparing the above equation with Eq. (76) yields the Fokker-Planck (FP) equation:

$$\frac{d}{dt}P[\phi, t] = L_r^T P[\phi, t], \quad (85)$$

with the formal adjoint of the above Langevin operator

$$L_r^T \equiv \int d\tau d^d x \frac{\delta}{\delta\phi} \left(\frac{\delta}{\delta\phi} - K[\phi] \right), \quad (86)$$

which is also referred to as the FP operator or FP Hamiltonian. To show that the stationary solution of this equation is indeed our desired probability distribution we perform similarity transformation

$$\tilde{P}[\phi, t] = e^{S[\phi]/2} P[\phi, t], \quad (87)$$

to rewrite the FP equation

$$\frac{d}{dt}\tilde{P}[\phi, t] = \tilde{L}_r^T \tilde{P}[\phi, t], \quad (88)$$

with

$$\tilde{L}_r^T = e^{S[\phi]/2} L_r^T e^{-S[\phi]/2} = \int d\tau d^d x \left(-\frac{\delta}{\delta\phi} + \frac{1}{2}K[\phi] \right) \left(\frac{\delta}{\delta\phi} + \frac{1}{2}K[\phi] \right). \quad (89)$$

This last equation reveals that, with a real action $S[\phi]$, our modified FP Hamiltonian is a self-adjoint and positive semidefinite operator, with a unique FP ground state $\psi_0 = e^{-S[\phi]/2}$ and vanishing FP energy $E_0 = 0$. We can therefore project our probability over the complete set of eigenfunctions and non-negative eigenvalues of \tilde{L}_r^T , and see that our probability collapses to the ground state in the long time limit:

$$\tilde{P}[\phi, t] = \sum_{n=0}^{\infty} a_n \psi_n e^{-E_n t} \xrightarrow{t \rightarrow \infty} a_0 e^{-S[\phi]/2}. \quad (90)$$

Upon performing the back-transformation according to Eq. (87) we obtain

$$\lim_{t \rightarrow \infty} P[\phi, t] \sim e^{-S[\phi]}, \quad (91)$$

which shows that the Langevin equation produces field configurations distributed according to the Boltzmann weight $e^{-S[\phi]}$ in the limit of large fictitious time ².

The above justifies the use of temporal averages to estimate equilibrium expectation values. In fact, expectation values are obtained in practice by integrating over a time T :

$$\langle \mathcal{O} \rangle \approx \frac{1}{T} \int_{t_{\text{th}}}^{t_{\text{th}}+T} dt \mathcal{O}[\phi_\eta(t)], \quad (92)$$

where t_{th} reflects the equilibration time that is needed to approach the stationary probability distribution.

3.3. A practical guide to real Langevin

The above procedure is a well-established method for real-valued fields ϕ on a real manifold \mathcal{M} . In the following, we connect the concept with conventional Monte Carlo approaches based on Markov chains and highlight the similarities of these approaches in a practical way.

Generally, we are interested in expectation values of a given (Euclidean) field theory of the form of Eq. (75):

$$\langle \mathcal{O} \rangle = \frac{1}{Z} \int \mathcal{D}\phi \mathcal{O}[\phi] e^{-S[\phi]} \equiv \int \mathcal{D}\phi \mathcal{O}[\phi] P[\phi]. \quad (93)$$

²We have assumed here that the spectrum of \tilde{L}_r^T is discrete, which may not be true in practice. This assumption can be relaxed but it is important that the $E_0 = 0$ eigenvalue be non-degenerate.

Typically, the evaluation of such high-dimensional path integrals is achieved by stochastic sampling, i.e. by producing a sequence of random states ϕ (interchangeably called samples or configurations). However, rather than producing a random state from scratch at every step (which might be expensive), new states are obtained by changing or *updating* an existing one. This can be written in the generic form

$$\phi_{n+1} = F[\phi_n], \quad (94)$$

where the sample ϕ may be any representation of a physical state³. If the next state is only dependent on the current one and not on any previous states the process is called “memoryless” and the sequence of random samples represents a so-called “Markov chain”. This is the basis of the vast majority of most conventional Monte Carlo methods (often dubbed Markov-Chain Monte Carlo (MCMC) methods).

The Langevin method can be understood as such an approach, as we can see by recasting Eq. (74) into the form of Eq. (94):

$$\phi_{n+1} = \phi_n - \left. \frac{\delta S[\phi]}{\delta \phi} \right|_{\phi=\phi_n} \Delta t + \sqrt{2\Delta t} \eta. \quad (95)$$

By virtue of the discussion in the previous section, we know that in the long-time limit the samples $\{\phi_n\}$ follow the desired probability distribution $P[\phi]$ from Eq. (93). Therefore, the strategy to evaluate the random sequence is identical to the one in regular Monte Carlo approaches: after starting out from a randomly produced configuration, we let the sampling process equilibrate for a certain thermalization time (typically a few multiples of the autocorrelation time – see below) before we start to collect samples. An unbiased estimator of the expectation value with a total number of samples N is then given by

$$\langle \mathcal{O} \rangle \approx \frac{1}{N} \sum_{i=1}^N \mathcal{O}[\phi_i], \quad (96)$$

and the statistical uncertainty (i.e., the variance of the mean) is estimated by

$$\sigma_L = \sigma \sqrt{\frac{1 + 2\tau_a}{N}}. \quad (97)$$

Here, σ denotes the standard deviation of the set of values $\{\mathcal{O}[\phi_i]\}$ and τ_a is the integrated autocorrelation time, which reflects the (statistical) dependence of samples over their Langevin-time history⁴. From this expression we can also deduce that the number of samples is proportional to the elapsed Langevin time and the same conclusion holds: a longer Langevin evolution will result in better statistics and hence a smaller error bar.

It is important to note that the statistical uncertainty is not the only source of error, as we have introduced a systematic bias through the discretization of the Langevin equation in Eq. (74). Results must then be extrapolated to the limit of $\Delta t \rightarrow 0$ ⁵. The discretization of the Langevin equation presented above, which corresponds to Euler integration, leads to a linear dependence on the integration step Δt . Higher-order integrators can be designed if the noise term is appropriately accounted for, as investigated within RL in Refs. [172, 173, 174] and later extended to the complex case in Ref. [175]. Within the studied model, these extensions showed great success in reducing computational cost at equal systematic bias as well as to bring finite-step dependence below the statistical uncertainty. It is noted, however, that the majority of stochastic quantization studies still rely on the linear discretization as it is often sufficient to obtain useful results at modest computational effort.

³In fact, finding suitable and efficient updates is a crucial part in devising any useful Monte Carlo method.

⁴For any Markov chain method, estimation of τ_a might be a challenging task depending on the number of accessible samples. Techniques such as bootstrap and jackknife can be used to obtain a reliable error estimate that considers the statistical dependence of the samples. An educational summary can be found in Ref. [171].

⁵Notably, the hybrid Monte Carlo algorithm, mentioned above as a close cousin of RL, avoids this extrapolation in fictitious time by using Metropolis accept/reject steps. This property, however, does not imply that hybrid Monte Carlo can operate at arbitrarily large step sizes.

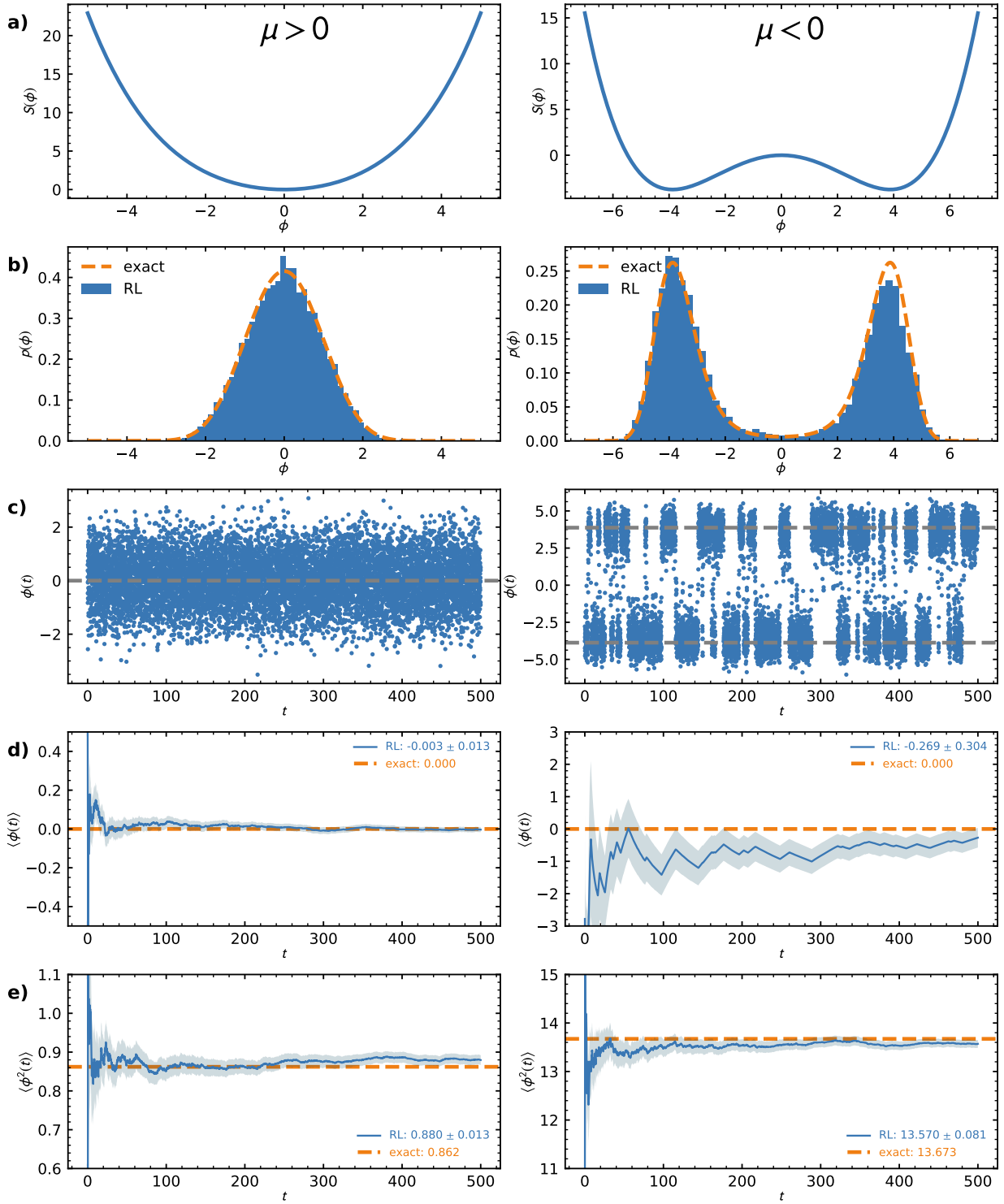


Figure 7: (a) Action as a function of the real variable ϕ . (b) Probability distribution $e^{-S[\phi]}$ (dashed lines) along with the sampled histogram (bins). (c) Measured values of ϕ as a function of Langevin time. (d) Running average of $\langle \phi \rangle$ compared to the exact solution (orange dashed line) (e) Running average of $\langle \phi^2 \rangle$ compared to the exact solution (orange dashed line).

3.3.1. Toy problem I: a pedagogical example of real Langevin

In order to illustrate the RL method in a concrete numerical setting, we consider a simple integral as a toy problem for a 0 + 0-dimensional field theory (i.e., the field ϕ depends neither on space nor time). Note that here we are not interested in a detailed study of the specific model at hand but rather aim to investigate the behavior of the RL method in a straightforward case. Of course it is highly inefficient to use RL for the solution of this simple problem, however, the section serves as a basic example of an application of the method. Furthermore, conclusions that generalize to more involved problems can be drawn by these simple considerations.

In this case, we consider the action

$$S(\phi) = \frac{\mu}{2}\phi^2 + \frac{\lambda}{4!}\phi^4, \quad (98)$$

with real couplings μ and λ . In the spirit of a real field theory, we will keep λ positive and thus end up with two distinct scenarios: one in which $\mu > 0$ (the single well anharmonic potential) and one in which $\mu < 0$ (the double well potential).

We readily derive the discrete Langevin equation for our toy-problem, according to Eq. (95):

$$\phi_{n+1} = \phi_n - \left(\mu\phi_n + \frac{\lambda}{6}\phi_n^3 \right) \Delta t + \sqrt{2\Delta t} \eta, \quad (99)$$

where η denotes a standard Gaussian white noise. In principle, this is everything needed to calculate expectation values of the form Eq. (96).

In Fig. 7, a detailed analysis of two simulations at fixed $\lambda = 0.4$ and $\mu = \pm 1$ is presented (left and right columns, respectively). The second row from the top shows the histograms of the sampled field values, which should follow the distribution $e^{-S[\phi]}$ (exact solution shown with dashed lines) in the limit of large Langevin time $t \rightarrow \infty$. While in the single-well system (left column) this is the case to a good approximation, it is apparent that the double-well scenario still suffers from a slight asymmetry. This can occur when the random process gets “stuck” in an area of configuration space and does not easily move to another high probability area of configuration space (i.e. the other well).

This behavior can be further elucidated by the measured field values as a function of t [row (c)]: on the left we see white noise centered around the expected value of 0 while on the right we observe several correlated plateaus, corresponding to either the negative or the positive well. Ultimately, this behavior leads to a signal-to-noise issue in the calculation of the expectation value $\langle \phi \rangle$, reflected by large statistical uncertainties for the double well case [right column of row (d)]. Due to the symmetry of the problem, however, the running average for $\langle \phi^2 \rangle$ converges to the exact value relatively smoothly in both cases. Thus, by investigating one observable no profound statements can be made about a different one. While the autocorrelation of observable A may be small and its statistical errors under control, observable B could display erratic behavior and suffer from extremely slow convergence.

By tuning the parameters of the model, one could even study the extreme case where the two wells are separated by a barrier that cannot be surmounted by the random walk (signaling a breakdown of ergodicity, a topic that we will return to below). In such a situation, the expectation value $\langle \phi \rangle$ would indicate that the discrete symmetry is broken, which certainly is not a physical result for our model. This reflects the problem of meta-stability of any Markov chain method, which is often very hard to detect *a priori*. Generally, one needs to address this issue carefully in real simulations, for example by sweeping numerical parameters in a systematic manner.

Finally, by inspecting the Langevin equation in Eq. (99) it becomes apparent that the autocorrelation time between samples τ_a should be inversely proportional to the Langevin time step Δt , i.e., statistically independent samples will be more expensive as the integration step decreases. On the other hand, a coarser integration step will yield a larger systematic error and thus a balance must be found where both the computational effort as well as the precision are within reasonable bounds. This behavior is illustrated in Fig. 8, where we show the dependence for $\langle \phi^2 \rangle$ as well as τ_a on the integration stepsize Δt . Indeed, we observe a systematic linear behavior of $\langle \phi^2 \rangle$, which is expected due to the order of the Langevin equation

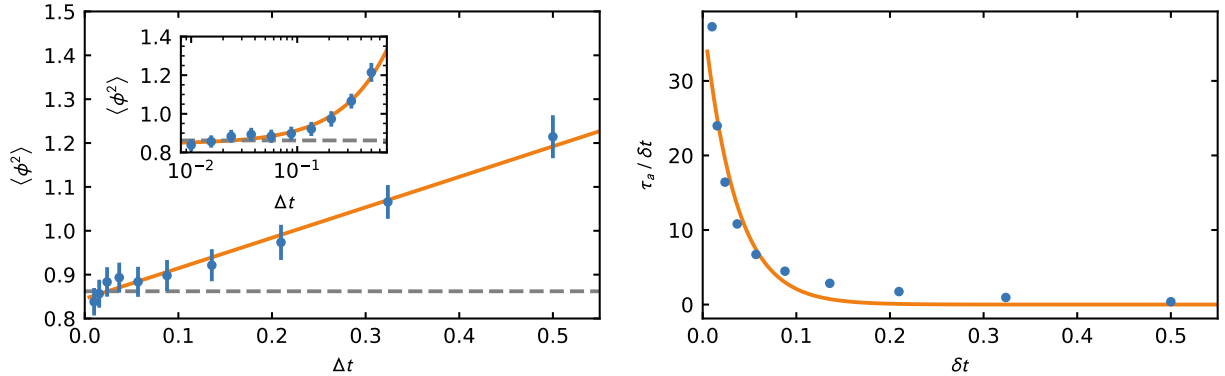


Figure 8: Real Langevin results for the simulation parameters $\mu = 1$, $\lambda = 0.4$ and a total Langevin-time of 10^3 . (Left) Symbols reflect RL results for $\langle \phi^2 \rangle$ along with the statistical errorbars as a function of integration time step Δt . The dashed line represents a linear extrapolation to the limit $\Delta t \rightarrow 0$ (horizontal dashed line). (Inset) Same data on a semi-log scale. (Right) Integrated autocorrelation time of ϕ^2 in units of the time step as a function of Δt .

(see discussion in the previous section). Further, also the integrated autocorrelation τ_a shows the expected behavior: it increases as the integration step approaches 0.

3.4. A practical guide to complex Langevin

Thus far we have seen that the concept of stochastic quantization works well, given that the action $S[\phi]$ is real, i.e. when there is no sign problem. But what about the much more general and interesting case of complex-valued actions? In that case, the probability distribution in Eq. (75) becomes a *complex* distribution

$$\rho[\phi] = \frac{e^{-S[\phi]}}{\mathcal{Z}}, \quad (100)$$

while the field ϕ is still a real quantity. With such an action, a single step in the Langevin process according to Eq. (95) would result in an imaginary component for ϕ . At least from a practical perspective, as remarked by Parisi, “nothing forbids to write a Langevin equation also for complex actions” [137]. Formal aspects aside (we return to those below), the idea is that one may perform calculations by extending the real stochastic process described above to a complex one. For a theory governed by a complex action $S[\phi]$, CL extends the target manifold of the field $\phi(x)$ to the complex plane by setting

$$\phi \rightarrow \phi_R + i\phi_I, \quad (101)$$

and analytically extending the domain of the action functional:

$$S[\phi] \rightarrow S[\phi_R + i\phi_I]. \quad (102)$$

Naturally, a necessary condition for this extension to be valid is that $S[\phi]$ must be a holomorphic function of ϕ .

The two Langevin methods – real and complexified – are compared side-by-side in Fig. 9. With such an extension, the CL method proceeds very much in the same way as the real Langevin method, but now with a double system of coupled stochastic differential equations:

$$\Delta\phi_R = K_R\Delta t + \eta_R(t), \quad (103)$$

$$\Delta\phi_I = K_I\Delta t + \eta_I(t), \quad (104)$$

	Real Langevin	Complex Langevin
Fields	ϕ	$\phi_R + i\phi_I$
Action	$S[\phi]$	$S[\phi_R + i\phi_I]$
Langevin step	$\Delta\phi = K\Delta t + \eta(t)$	$\Delta\phi_R = K_R\Delta t + \eta_R(t)$ $\Delta\phi_I = K_I\Delta t + \eta_I(t)$
Drift	$K = -\frac{\delta S}{\delta\phi}$	$K_R = -\text{Re} \left[\frac{\delta S[\phi]}{\delta\phi} \right]$ $K_I = -\text{Im} \left[\frac{\delta S[\phi]}{\delta\phi} \right]$
Noise	$\langle\eta^2\rangle = 2\Delta t$	$\langle\eta_R^2\rangle = 2N_R\Delta t$ $\langle\eta_I^2\rangle = 2N_I\Delta t$ $N_R - N_I = 1$
	$\langle\eta\rangle = 0$	$\langle\eta_R\rangle = \langle\eta_I\rangle = 0$

Figure 9: The Langevin method with real-valued fields versus complex-valued fields

where the real and imaginary drift functions K_R and K_I are found by taking the real and imaginary parts of the functional derivative of the complex action:

$$K_R = -\text{Re} \left[\frac{\delta S[\phi]}{\delta\phi} \right], \quad (105)$$

$$K_I = -\text{Im} \left[\frac{\delta S[\phi]}{\delta\phi} \right]. \quad (106)$$

The real and imaginary noise obey the properties shown in Fig. 9. It is important to note that, while the amplitudes of the real and imaginary noise terms are related, the two Wiener processes are completely independent. In practice, the imaginary noise is usually set to zero, which satisfies the constraints shown in Fig. 9 and it has been found to have the best numerical properties [176]. Finally, it should be pointed out that, beyond the complexification of each real degree of freedom, the above (coupled) Langevin processes are themselves real. We return to the justification for CL and related challenges after giving an illustrative example.

3.4.1. Toy problem II: a pedagogical example of complex Langevin

In order to see the CL machinery at work we build on the toy-problem in Sec. 3.3.1. Indeed, from a computational standpoint, CL is largely just the Langevin process of stochastic quantization with complex variables.

The most natural route towards a complex field theory would of course be to consider complex valued couplings μ and λ in Eq. (98), which in fact has been considered before, see e.g. [170]. However, this would amount to solving a different theory as the couplings necessarily take on different values. Alternatively, we may rewrite the above problem with a suitable Hubbard-Stratonovich transformation which merely amounts to an alternative representation of the same physical scenario. Moreover, this is very much in the spirit of real-world problems, where a HS-transform is often used to integrate out fermionic degrees of freedom. To

achieve this, we insert a suitable factor of 1 into the partition function in terms of an auxiliary variable σ :

$$\mathcal{Z} = \int_{-\infty}^{\infty} d\phi e^{-S(\phi)} \quad (107)$$

$$= \sqrt{\frac{\lambda}{24\pi}} \int_{-\infty}^{\infty} d\sigma \exp\left(-\frac{\lambda}{24}\sigma^2\right) \int_{-\infty}^{\infty} d\phi \exp\left[-\left(\frac{\mu}{2}\phi^2 + \frac{\lambda}{24}\phi^4\right)\right]. \quad (108)$$

A shift $\sigma \rightarrow \sigma + i\phi^2$ allows us to write

$$\mathcal{Z} = \sqrt{\frac{\lambda}{24\pi}} \int_{-\infty}^{\infty} d\sigma \int_{-\infty}^{\infty} d\phi \exp\left[-\left(\phi^2\left(\frac{\mu}{2} + \frac{i\lambda\sigma}{12}\right) + \frac{\lambda}{24}\sigma^2\right)\right], \quad (109)$$

and subsequently to integrate out the dependence on the old field ϕ (note that this is only possible in the case $\text{Re}[\mu] > 0$). Ultimately we obtain the ‘‘bosonized’’ version

$$\mathcal{Z} = \int_{-\infty}^{\infty} d\sigma \exp\left[-\left(\frac{\lambda}{24}\sigma^2 - \frac{1}{2}\log\frac{\lambda}{12\mu + 2i\lambda\sigma}\right)\right] \equiv \int_{-\infty}^{\infty} d\sigma e^{-S_B(\sigma)}, \quad (110)$$

where we defined the ‘‘bosonized action’’

$$S_B(\sigma) = \frac{\lambda}{24}\sigma^2 - \frac{1}{2}\log\frac{\lambda}{12\mu + 2i\lambda\sigma}, \quad (111)$$

which is, by construction, a complex quantity. According to the discussion in the previous section we can still evaluate expectation values stochastically by using the complex Langevin equation

$$\sigma_R^{n+1} = \sigma_R^n - \Delta t \text{Re}\left[\frac{\lambda}{12}\sigma^n + i\frac{\lambda}{12\mu + 2i\lambda\sigma^n}\right] + \eta, \quad (112)$$

$$\sigma_I^{n+1} = \sigma_I^n - \Delta t \text{Im}\left[\frac{\lambda}{12}\sigma^n + i\frac{\lambda}{12\mu + 2i\lambda\sigma^n}\right]. \quad (113)$$

Specifically, we write for the second moment of the initial field ϕ in terms of the new field σ :

$$\langle\phi^2\rangle = \left\langle\frac{6}{6\mu + i\lambda\sigma}\right\rangle_{\sigma}, \quad (114)$$

where the subscript σ denotes averaging over different realizations of σ .

From this point on, we proceed exactly as in the real case, with the exception that we now have to deal with a complex variable σ . The qualitative dependence of the numerical results on the integration step size Δt should still be the same. This is indeed the case, as apparent from the lower left panel of Fig. 10, where we show CL results for the model given by Eq. (98) with parameters $\mu = 1.0$ and $\lambda = 0.4$. We observe that the CL correctly reproduces the exact result. Interestingly the CL values show a much milder dependence on the integration step, which is likely a consequence of the specific representation and in any way should not to be interpreted as a general result.

It is instructive to investigate the sampled configurations by looking at the complex weight according to Eq. (110). This is shown in the upper left panel of Fig. 10 where it becomes clear that the Langevin process now samples a complex quantity which is necessary to represent the correct answer. The coloring highlights the sampled configurations of σ corresponding to regions with $\text{Re}[\sigma] > 0$ and $\text{Re}[\sigma] < 0$. These two sets are connected through a point in configuration space which corresponds to a stationary point in the ‘‘classical flow’’, i.e. the vanishing of the drift terms in Eq. (112). (The entire flow diagram is shown on the right panel of Fig. 10). The attractive fixed point (marked by the lower green dot) pulls the field towards the connection point, while the noise induces fluctuations around that point, which occur mainly in the real component, as we have chosen to use only real noise in Eq. (112) (such that the only way the

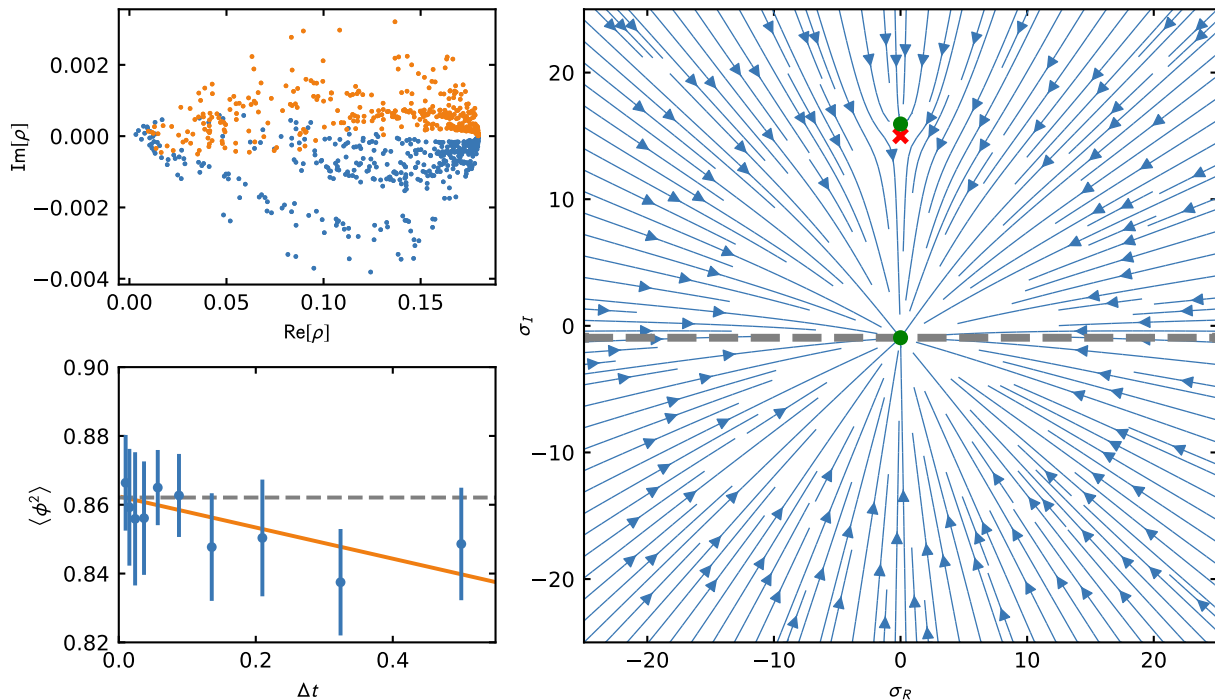


Figure 10: CL analysis for the action Eq. (98) with $\mu = 1.0$ and $\lambda = 0.4$, corresponding to the single well potential. (Upper left) Imaginary vs. real part of the complex weight in Eq. (110). Samples with $\text{Re}[\sigma] > 0$ and $\text{Re}[\sigma] < 0$ are shown in orange and blue symbols respectively. (Lower left) Integration step dependence of the second moment $\langle \phi^2 \rangle$ as obtained with CL (symbols). The solid line represents a linear fit to the data in order to extrapolate to $\Delta t \rightarrow 0$ and the dashed line shows the exact result. (Right) Classical flow diagram with attractive fixed points (green dots) and the pole associated with the branch point of the action (red cross). The gray dashed line represents the domain of the equilibrium probability distribution.

imaginary part can change is through the complex part of the drift). Thus, the imaginary component stays approximately constant during the Langevin evolution.

The situation might change drastically if poles are encountered inside the domain of the distribution, which could lead to a breakdown of ergodicity, due in turn to a breakdown of holomorphicity of the action stated above (see also the discussion below). In the model considered here, we can find a pole at the point $\sigma = 6\frac{\mu}{\lambda}$, which corresponds to the branch-point of the action (marked by the red cross). At first glance this looks very dangerous as there is also an attractive stationary point (upper green dot) right next to the pole which would suggest faulty behavior. However, the imaginary part of the drift points away from the pole and even if a trajectory approaches this area of configuration space, fluctuations (in the real direction) will kick the process back into a stable trajectory that decays towards the attractive fixed point below. In equilibrium, the distribution will thus be confined to the gray dashed line far away from the pole, ensuring correct behavior (i.e. it is approximately shifted from the real axis by a constant offset). In fact, the existence of such an attractive fixed point is a necessary condition for the existence of an equilibrium distribution of the Langevin process [177, 178]. Luckily, this appears to be the case for systems of physical interest.

3.5. Formal aspects and justification

The CL process defines a random walk in a complexified manifold, such that for a given configuration $\phi = \phi_R + i\phi_I$ there is a well-defined probability $P[\phi_R, \phi_I, t]$ at time t . For a given observable \mathcal{O} , there will be an expectation value

$$\langle \mathcal{O} \rangle_{P(t)} \equiv \int \mathcal{D}\phi_R \mathcal{D}\phi_I P[\phi_R, \phi_I, t] \mathcal{O}[\phi_R + i\phi_I]. \quad (115)$$

By virtue of the CL process, the real probability $P[\phi_R, \phi_I, t]$ obeys the FP equation:

$$\frac{\partial P}{\partial t} = L^T P, \quad (116)$$

where

$$L^T = \int d\tau d^d x \left\{ \frac{\delta}{\delta \phi_R} \left[N_R \frac{\delta}{\delta \phi_R} - K_R \right] + \frac{\delta}{\delta \phi_I} \left[N_I \frac{\delta}{\delta \phi_I} - K_I \right] \right\}. \quad (117)$$

It is not obvious *a priori* whether this process would reproduce the desired expectation values of the physical observables, i.e. whether $\langle \mathcal{O} \rangle_{P(t)}$ actually corresponds to the physical expectation value of the theory, at least in the large- t limit. In fact, it is not even clear that the process would converge and if it does, whether it converges to the correct answer. Indeed, following the steps outlined above for the case of real Langevin, one finds that the resulting FP Hamiltonian is neither self-adjoint nor positive semidefinite, such that the proof of convergence to the desired probability distribution is spoiled.

The fundamental question underlying the validity of the CL approach is the relation between the CL distribution $P[\phi_R, \phi_I, t]$ and the desired complex distribution $\rho[\phi]$ in Eq. (100). The latter defines the physics of interest and is a fixed point of its own FP equation

$$\frac{\partial \rho}{\partial t} = L_0^T \rho, \quad (118)$$

where

$$L_0^T = \int d\tau d^d x \frac{\delta}{\delta \phi_R} \left[\frac{\delta}{\delta \phi_R} + \frac{\delta S}{\delta \phi_R} \right], \quad (119)$$

which is obtained by temporal differentiation of

$$\langle \mathcal{O} \rangle_{\rho(t)} \equiv \int \mathcal{D}\phi_R \rho[\phi_R, t] \mathcal{O}[\phi_R]. \quad (120)$$

Again, the absence of boundary terms at infinity when integrating by parts was assumed. More specifically, the crucial question is whether

$$\langle \mathcal{O} \rangle_{P(t)} = \langle \mathcal{O} \rangle_{\rho(t)}, \quad (121)$$

holds.

In Refs. [176, 179] it was shown how the desired relationship Eq. (121) can be proven for holomorphic observables, as long as the action and the associated drift are holomorphic functions of ϕ . The proof relies on analyzing the behavior of

$$F(t, \tau) = \int \mathcal{D}\phi_R \mathcal{D}\phi_I P[\phi_R, \phi_I, t - \tau] \mathcal{O}[\phi_R + i\phi_I, \tau], \quad (122)$$

where $0 \leq \tau \leq t$. The function $F(t, \tau)$ interpolates between the two expectation values of interest:

$$F(t, 0) = \langle \mathcal{O} \rangle_{P(t)}, \quad F(t, t) = \langle \mathcal{O} \rangle_{\rho(t)}. \quad (123)$$

where we have assumed that the initial conditions are chosen as

$$P(\phi_R, \phi_I, 0) = \rho[\phi_R, 0] \delta(\phi_I - \phi_{I,0}). \quad (124)$$

We find that

$$F(t, 0) = \int \mathcal{D}\phi_R \mathcal{D}\phi_I P[\phi_R, \phi_I, t] \mathcal{O}[\phi_R + i\phi_I, 0] = \langle \mathcal{O} \rangle_{P(t)}, \quad (125)$$

while, using the initial conditions of Eq. (124),

$$F(t, t) = \int \mathcal{D}\phi_R \mathcal{D}\phi_I P[\phi_R, \phi_I, 0] \mathcal{O}[\phi_R + i\phi_I, t] = \int \mathcal{D}\phi_R \rho[\phi_R, 0] \mathcal{O}[\phi_R + i\phi_{I,0}, t] = \langle \mathcal{O} \rangle_{\rho(t)}, \quad (126)$$

where we have used Eq. (118) to shift the Langevin evolution operator from \mathcal{O} to ρ by transposition (which involves integration by parts).

If $F(t, \tau)$ is independent of τ , then Eq. (121) holds, and the Langevin method is formally shown to be valid for complex-valued variables, i.e. to converge to the correct physical answers (assuming it converges). Naturally, this statement assumes that the expectation values in Eq. (121) agree at $t = 0$, which can be ensured by choosing the initial condition of the Langevin process as above. The τ derivative of $F(t, \tau)$ involves an integration by parts:

$$\frac{\partial}{\partial \tau} F(t, \tau) = \int \mathcal{D}\phi_R \mathcal{D}\phi_I \{ P[\phi_R, \phi_I, t - \tau] L \mathcal{O}[\phi_R + i\phi_I, \tau] - L^T P[\phi_R, \phi_I, t - \tau] \mathcal{O}[\phi_R + i\phi_I, \tau] \}, \quad (127)$$

where L is the Langevin operator and L^T its adjoint. If integration by parts is carried out and – importantly – the boundary terms are zero, then $\frac{\partial}{\partial \tau} F(t, \tau) = 0$. If the decay of

$$P[\phi_R, \phi_I, t - \tau] \mathcal{O}[\phi_R + i\phi_I, \tau], \quad (128)$$

and its derivatives is not fast enough to ensure that the boundary terms will vanish, then it cannot be guaranteed that the expectation values of the quantities of interest obtained via a Langevin process will converge to the correct values [176, 179].

While the condition of fast decay was recognized in [176, 179], the precise rate was not immediately clear. In Ref. [180], the above arguments were reviewed by considering a finite step-size in Langevin time. It was then found that the above integration by parts is valid if the probability distribution of the drift term falls off faster than any power at large drift magnitude. In practice, it is very difficult to establish the behavior of Eq. (127), but it is perfectly possible to study the probability distribution of the drift and establish whether the decay is exponential.

3.6. Challenges

The challenges faced by the CL method can be roughly divided into two kinds: mathematical and practical, which naturally have some overlap. In this subsection we attempt to summarize the current understanding of these issues.

3.6.1. Mathematical aspects: convergence, correctness, boundary terms, and ergodicity

- *Convergence* – Without a doubt, the biggest challenge for CL is the lack of general mathematical proofs, the previous section notwithstanding. More specifically, as pointed out most recently in Ref. [178], it remains unknown whether the Langevin operators defined above as L , L_0 , L^T , L_0^T properly define unique stochastic processes, although in practice this is not typically an issue. Crucially, it remains unknown under what conditions the positive measure $P[\phi_R, \phi_I, t]$ converges to an equilibrium measure, although (again) there is substantial numerical evidence that such an equilibrium measure exists in many cases of interest.
- *Correctness* – The above issues aside, CL has been shown to fail in certain cases (due either to failure to converge or convergence to the wrong answer), but also appears to work in scenarios that lie outside the holomorphic-action regime mentioned above. In cases of failure, the behavior has been traced back to insufficient *decay at infinity*, or to a breakdown of ergodicity due to *poles in the action* (which should be expected in fermionic systems as the fermion determinant will vanish at specific points, thus leading to meromorphic drifts).
 - *Boundaries at infinity* – The behavior of boundaries at infinity is a relevant question for models in relativistic and non-relativistic physics. In particular, for gauge theories the complexification of the link variables leads to non-compact groups, e.g. $SU(3)$ becomes $SL(3, \mathbb{C})$. As we explain in Sec. 5, a similar effect is seen in nonrelativistic physics when using compact HS transformations. In either case, merely assuming that the derivative of $F(t, \tau)$ in Eq. (127) vanishes is a bad idea. For that to happen, the solutions to the FP equation must fall off sufficiently quickly

along non-compact directions in the (complexified) space of field configurations (see in particular Refs. [181, 182] for a recent and insightful discussion of an exactly solvable case). That property is very difficult to determine *a priori*, but can be checked *a posteriori* following the arguments of Ref. [180]. Case studies show that in many cases, while the solutions fall off faster than exponentially in the real directions, the decay in the imaginary directions may be insufficient [176]. Such an insufficient decay at infinity can also lead to the so-called excursion problem, which we discuss below.

- *Poles and ergodicity* – For fermionic actions where poles appear naturally, the results for the holomorphic case can be used, provided that a region around the poles is cut out [177]. That procedure is justified as long as the probability measure vanishes around those poles sufficiently fast; in other words, one has to address the boundaries around the poles alongside those at infinity mentioned above. A detailed study of incorrect convergence due to poles in the drift function showed that the location of these poles, the decay of the drift function, and the behavior of the observables in the region near the poles all played a role in whether the method would return correct results [177, 180].

As mentioned above, a re-examination of the conditions for correctness in Refs. [183, 180] revealed that failure of CL that in some cases has been attributed to the excursion and singular drift problems are actually due to the drift function falling off too slowly.

It was argued in Ref. [124], using a semiclassical analysis, that when more than one saddle point in the complex plane contributes to the ensemble averages, the CL method can lead to incorrect answers due to the different complex phases associated with each saddle point. The interference of these complex phases is an essential in phenomena such as the Silver Blaze phenomenon and real-time dynamics.

3.6.2. Practical aspects: numerical instabilities, gauge cooling, dynamic stabilization, and regulators

On the practical side, several strategies have been identified to tackle specific issues.

- *Instabilities* – One of the issues recognized early on (in fact, since the 1980s; see e.g. [184, 185]) is the appearance of instabilities in the form of runaway trajectories along the CL evolution. These can become very frequent so as to completely spoil a calculation performed at fixed step size. In Ref. [154], the need for adaptive step size integration of the complex Langevin equations was identified. It was found that such an approach provides a full solution to the problem of instabilities and has thus become the standard for CL calculations.
- *Boundaries at infinity* – A separate but crucial issue for correctness, mentioned above, is that of insufficient decay at infinity. In practice, it can lead to uncontrolled excursions of the CL process into the complex plane, making calculations unstable. To that end, a few practical solutions have been explored which have, in some cases been mathematically well justified.
 - *Gauge cooling* [186, 187, 188, 189, 190] is one example of such practical solutions which, though necessary, is often not sufficient. It remains, however, the best understood approach from a mathematical perspective [189]: In contrast to the next two items, gauge cooling is a mathematically exact procedure. The idea is that at each Langevin step, one can make a gauge transformation (in the extended non-compact group, say $SL(3, \mathbb{C})$) to keep the link variables close to the compact subgroup $SU(3)$.
 - *Dynamic stabilization* [191, 192, 193, 194] was developed to further aid with the excursion problem. The essential idea of this approach is to add a term to the Langevin drift K in the schematic form

$$K \rightarrow -DS + i\alpha_{DS}M, \quad (129)$$

where $-DS$ is the standard CL drift, α_{DS} is a control parameter, and M acts only in the non- $SU(3)$ directions and grows rapidly with the distance from the $SU(3)$ manifold. The above

modification to the Langevin evolution cannot be derived from the action but it vanishes in the continuum limit and prevents large excursions into the complex plane.

- *Regulators* or modified actions, first appeared in a nonrelativistic application, namely Ref. [195]. They were also discussed more recently in Ref. [182] and the idea is similar to dynamic stabilization, except that the resulting modifications on the Langevin equations are directly derived from the action. In both of those works, the modification consisted of adding a term of the form $\xi\phi^2$, with the prescription that one should examine the behavior of the CL results in the limit $\xi \rightarrow 0$. While the advantages of such a practical solution were clear, it is by no means a full solution and in many cases – especially at strong coupling or low temperatures – it is not possible to make ξ small and obtain a converging calculation.
- Quantum field theories can be cast in terms of differential equations rather than path integrals; this is called the Schwinger action principle. A specific set of differential equations resulting from this principle is the Schwinger-Dyson equations, and these involve variations with respect to the source fields. Of the many solutions to this set of differential equations, only one at most corresponds to the Feynman path integral. It appears that the CL method is able to converge to multiple stationary distributions, and while at most one of those distributions corresponds to the desired distribution, it has been shown that these stationary distributions of the complex Langevin equation satisfy the Schwinger-Dyson equations [149, 196].

The initial conditions appear to play a role in this behavior: CL converges to certain solutions of the Schwinger-Dyson equation with one set of initial conditions and to another with a different set, and for certain conditions CL does not converge at all [197, 198]. The role of the Schwinger-Dyson equations in the presence of zeros of the complex density ρ was analyzed in detail in Ref. [199]. Further study of the convergence of CL to incorrect solutions must be an integral part of the understanding and application of this method to systems with complex actions.

4. Applications in relativistic physics: non-equilibrium QFT and finite density QCD

After interest in applying CL to relativistic physics expanded with a series of papers on finite density QCD in the mid-2000s (see Refs. [148, 149, 150, 151, 152, 200]), much work has gone into the testing of the methodology, its capabilities, and its limitations. While CL has successfully circumvented the sign problem in a few key areas, it suffers from some of the problems discussed previously in Sec. 3. As a result, recent emphasis has been on determining regions of applicability and adjusting the method in order to prevent “excursions” of the Langevin evolution into the complex plane and ensure convergence to the correct solution.

While the aim of this review is to focus on applications of CL to nonrelativistic quantum many-body problems, in this section we provide a very brief summary of selected applications to relativistic field theories. For more on the use of CL in relativistic physics, we refer the reader to Refs. [178, 200].

4.1. QCD-inspired toy models

In Lattice QCD, the main promise of CL is its potential to explore regions of the QCD phase diagram which are currently inaccessible due to a sign problem. Historically, the emphasis has been on the region of non-zero quark chemical potential, which suffers from a complex phase problem, but also to real-time dynamics [201, 202, 203] and the coupling to a topological charge (see Ref. [178]) are also of great interest. While the CL method has not yet been able to produce detailed solutions in this region (some attempts notwithstanding, see below), a number of simpler models have been successfully studied. We mention here just a few of those cases.

- *XY model* – Results using CL in the three-dimensional XY model at non-zero chemical potential [155] turn out to be very promising for the ordered phase, but fail to reproduce known answers for the disordered (high-temperature) phase. The XY model is useful for testing CL because the sign problem can be circumvented in other ways, for example using dual variables in a world-line formulation.

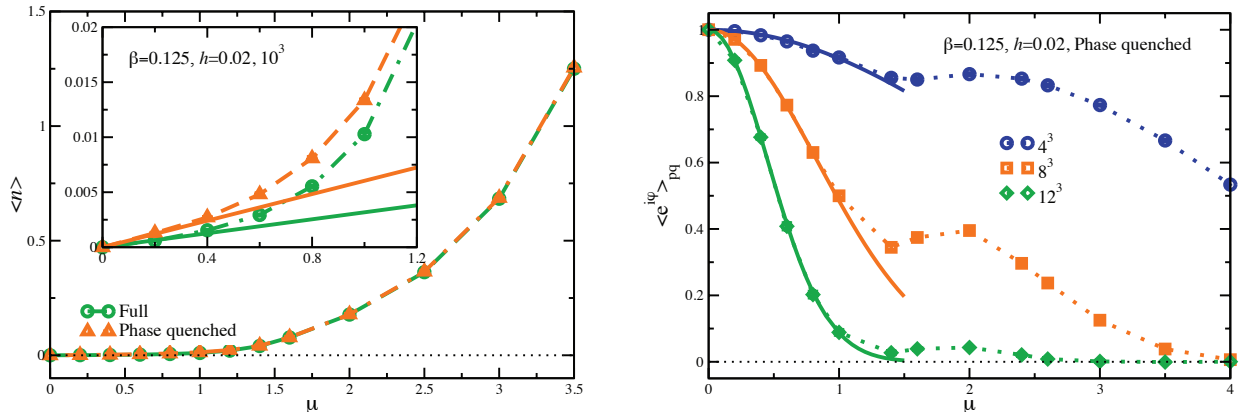


Figure 11: (Left) SU(3) spin-model in the full and the phase-quenched theory as a function of μ . The inset shows a close-up of the small μ region. The lines are the predicted linear dependence for small μ in excellent agreement with the CL results. (Right) Average phase factor as a function of μ for the SU(3) model, highlighting the severeness of the sign problem that the CL is able to solve. See Ref. [175].

Moreover, the model is very sensitive to instabilities in the algorithm - just as heavy-dense QCD is. The instabilities in the algorithm can be eliminated by the addition of adaptive stepsize to the Langevin evolution, which had been shown to work in the three-dimensional XY model at non-zero chemical potential and in the heavy-dense limit of QCD (HQCD) [154]. Adaptive step size prevents the CL trajectory from changing by too large a value, thereby diverting from the real axis and into the complex plane. Another way to improve the convergence of CL in the XY model is by dynamic stabilization, which forces the Langevin trajectory to remain near the real axis by means of unitary transformations [193]. These transformations modify the drift function to prevent large excursions in the imaginary direction [178, 192].

- *SU(3) spin model* – The three-dimensional SU(3) spin model is an effective Polyakov loop model for QCD at nonzero temperature and density. It suffers from a sign problem at nonzero chemical potential and typically reweighting or the phase-quenched approximation are used to study its behavior. Complex Langevin was used to successfully address this model, originally in Ref. [204] and more recently in Refs. [175, 205] with remarkable accuracy across a phase transition, with particular emphasis on the justification of the approach. Results are shown in Fig. 11 along with the average phase factor in the phase-quenched theory, which deteriorates quickly with increasing system size. The success of CL within this model underlines its ability to solve severe sign problems.
- *Random matrix theory* – Random matrix theory (RMT) models of finite density QCD are another way to study the accessibility of CL to outstanding problems in QCD. Such models can be constructed with complex fermion determinants and feature finite density phase transitions, where many problems with CL can arise. Some recent work on one of these models suggests that with suitably designed reweighting methods, CL is able to fully reproduce the known analytical solution to the model at the finite phase transition [206].
- *Polyakov loop model* – Attempts to control and stabilize the Langevin evolution on these toy models for QCD have led to breakthroughs in methodology. One - already discussed above - is dynamic stabilization, which modifies the drift term of the Langevin equation in order to control fluctuations that might lead the simulation into the complex plane. Another, gauge cooling [186, 187, 207], has allowed for a successful simulation of a QCD-like gauge model, namely the Polyakov loop model, at finite density.

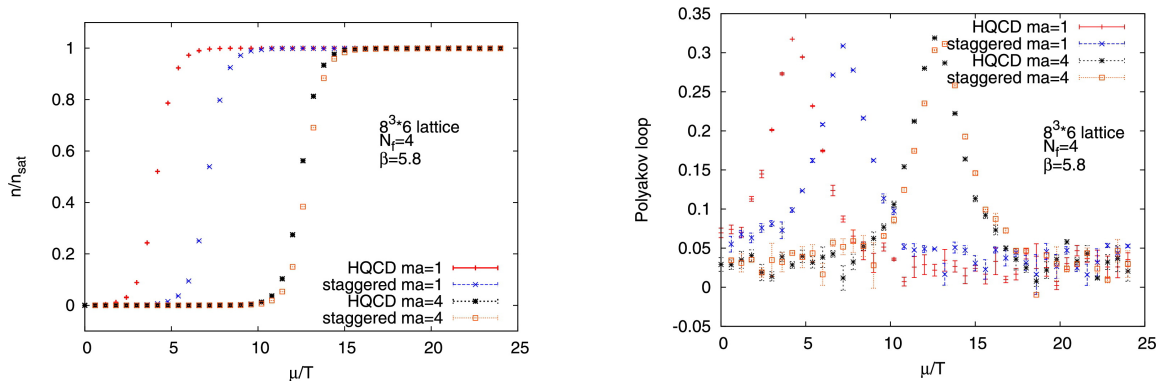


Figure 12: Comparison of the average quark densities (left) and the Polyakov loop (right) as obtained from HQCD and a CL study of full QCD with staggered fermions, see Ref. [208].

4.2. 3 + 1 dimensional QCD at finite chemical potential

One of the early attempts to calculate the properties of full QCD at finite chemical potential is the work of Ref. [208]. Later on, the results of Ref. [209] suggested CL with gauge cooling produces trustworthy solutions for 3 + 1 dimensional QCD at zero temperature and finite chemical potential. Work on this same system using a combination of adaptive stepsize and gauge cooling to prevent runaways in the complex plane for weak coupling showed promise. In fact, the results share some important physical traits with the system. However, known results were not accurately recovered. To be more specific, the observation of the transition from hadronic to nuclear matter (at $\mu \approx m_N/3$) is visible, as is evidence of saturation at large chemical potential [210]. The zero chemical potential limit disagreed with known results, but to a very small degree. With larger lattices and lower coupling, the known results are still not accurately recovered. This has been traced back to the fact that these calculations suffer from the appearance of zeroes in the fermion determinant in this regime [211] (see also [212, 213]).

Another way to treat the singular drift problem is to deform the fermion matrix in order to avoid zeroes in the determinant and therefore poles in the complex plane that might cause the solution to diverge. This solution can also be combined with gauge cooling to prevent the excursion problem, and recent work combining these two adaptations to a CL evolution of 3 + 1 dimensional QCD at low temperature and finite density indeed looks promising [190, 214].

4.3. Low-dimensional QCD at non-zero chemical potential

The CL approach has been applied to low-dimensional toy models for the matter sector of QCD [215, 216] and it has now also been shown to be effective in low-dimensional QCD calculations. To be more specific, in 0 + 1 dimensional QCD, the quark density and chiral condensate have been computed using CL, with gauge cooling used to prevent the simulation from deviating in the imaginary direction [217]. Simulations in 1 + 1 dimensional QCD have also correctly calculated the chiral condensate in the thermodynamic limit [218]. In recent years, work on combining reweighting techniques with CL have expanded the range of applications of the method to previously inaccessible parameter space in QCD, allowing for greater ranges of values for the mass, temperature, and chemical potential in 1 + 1-dimensional QCD [219, 220].

4.4. Ongoing work in QCD

There are still open areas of exploration in this field of CL studies of QCD. Much of that work is being done using RMT models, which share relevant properties of QCD [221]. These models can capture some of the physics of certain limits of QCD, and applications of the CL method to these systems can help elucidate

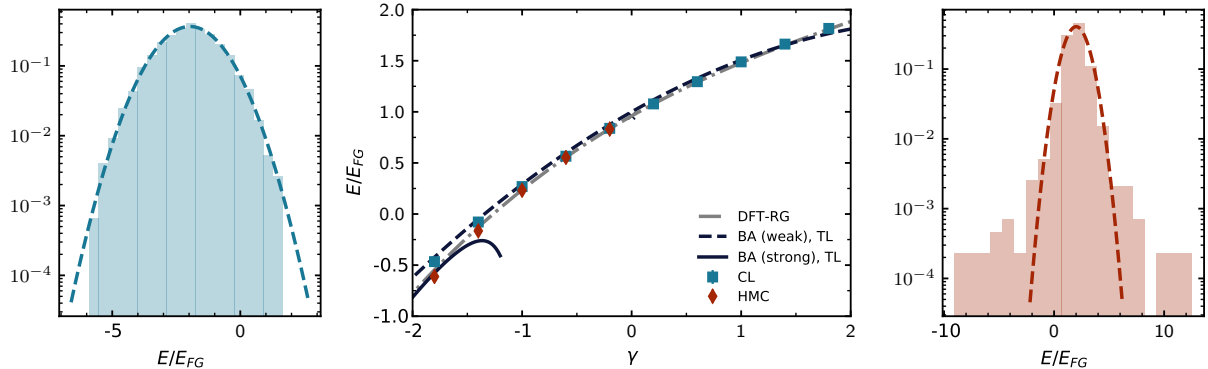


Figure 13: (Left) Log-histogram for sampled ground-state energies at strong attractive coupling $\gamma = -3.0$. Perfect gaussian behavior is observed (dashed line). (Center) Ground-state energy of $N = 5 + 5$ fermions as a function of the dimensionless coupling γ . The CL results (blue squares) are compared to HMC results (red diamonds) as well as to the Bethe-Ansatz solutions for strong and weak coupling (solid and dashed lines, respectively) and results obtained by a DFT-RG approach [226] (dashed-dotted line). (Right) Log-histogram for sampled ground-state energies at strong repulsive coupling $\gamma = 3.0$. Heavy tails of the distributions (as compared to a Gaussian, dashed line) spoil the correctness criterion.

where problems can arise in the method and how to control and correct for these problems. When applied to chiral RMT at nonzero chemical potential, CL produces results which agree with analytical results at large quark mass - although not for small quark mass [222]. Similarly, it has been able to compute the QCD phase diagram in the heavy quark limit on the entire temperature-chemical potential plane [223, 224, 225].

5. Applications in nonrelativistic matter: ultracold atomic gases

In contrast to the relativistic case, applications of CL to nonrelativistic matter remain largely in their infancy (notwithstanding notable work such as Ref. [143]). As described below, there have been attempts to characterize bosons as well as fermions in a variety of situations, but as of this writing only one calculation has been successfully carried out for a strongly coupled fermionic system in 3D at finite temperature. Nonrelativistic systems have difficulties of their own in the form of phase transitions and strongly coupled regimes, but they do not feature quintessential (and technically challenging) QCD elements such as non-abelian gauge fields. Nevertheless, as we shall see, some of the challenges faced by CL calculations are universal, as are the ideas to tackle them and the tools to diagnose them (see Sec. 3).

Among the vast array of nonrelativistic systems that remain to be explored, some pressing candidates remain across different areas, such as the repulsive 2D Hubbard model, the polarized electron gas, spin-isospin polarized nuclei, and neutron and nuclear matter, to name a few. We hope that the growing applications outlined in this section will lead to further work in those areas.

5.1. Nonrelativistic bosons

One of the pioneering applications of CL to nonrelativistic systems in the modern era (roughly within the last decade) concerned the study of a bosonic quantum field theory in a rotating frame [227]. The number density and condensate fraction with no rotation computed via CL was found to agree with mean-field calculations, and when rotation was introduced, the CL results showed quantized circulation for high condensate fraction. This is consistent with vortex formation in rotating superfluids, a phenomenon which has been directly observed using rotating ultracold bosonic atoms. The results for the circulation using CL do not agree with mean-field calculations for small condensate fraction, as expected due to the breakdown of mean-field theory to describe a system with strong quantum fluctuations. Aside from this brief exploration, the application of CL to circumvent the sign problem in systems of nonrelativistic systems, in particular bosons, remained scarce.

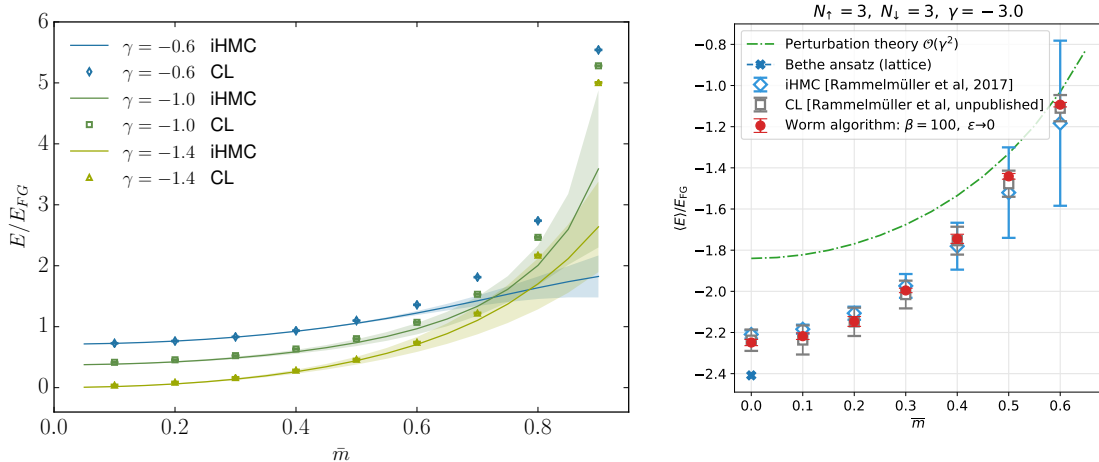


Figure 14: (Left) Comparison of iHMC and CL as a function of relative mass-imbalance \bar{m} for $N_{\uparrow} + N_{\downarrow} = 5 + 5$ particles at fixed interaction strengths γ . (Right) Ground-state energy of $N = 3 + 3$ fermions as a function of \bar{m} as obtained with the Worm algorithm [229] in comparison with CL results as well as iHMC values and perturbation theory. The plot is taken from Ref. [229].

5.2. Nonrelativistic fermions in one dimension

One-dimensional (1D) Fermi gases have drawn considerable interest in the past, when exact solutions for various models have been derived by the use of the so-called Bethe ansatz (see e.g., Ref. [228] for an extensive review). The availability of these exact solutions, paired with a relatively modest computational cost, make these systems excellent benchmark scenarios for any newly devised method, such as the CL approach for nonrelativistic quantum matter. Moreover, 1D systems have become accessible in experiments in recent years, which provides yet another motivation to study these exotic and intrinsically strongly interacting systems.

It is worthwhile to note here that in the special case of 1D it is often possible to re-write relativistic and nonrelativistic models using dual variables, in a way that avoids sign problem. One would be able to compute quantities by conventional Monte Carlo methods. While this is an option in 1D, those approaches do not generalize to higher dimensions, in contrast to the CL method. In fact, the dimensionality of the problem is mainly a question of computational effort and all insights gained on the numerical behavior of CL simulations carry over to higher dimensions.

In this section, we will review recent advances that have been made in applying CL to one-dimensional fermionic systems that suffer from a sign problem. Specifically, we will discuss systems at zero temperature featuring attractive and repulsive interactions, finite spin-polarization as well as asymmetry in the masses of the fermions in Sec. 5.2.1. Furthermore, we recall results obtained at finite temperature in Sec. 5.2.2 where repulsively interacting fermions are shown as well as systems at asymmetric chemical potential.

5.2.1. 1D fermions in the ground state

In the following, we will consider a systems of $N = N_{\uparrow} + N_{\downarrow}$ fermions at fixed linear lattices of N_x sites, which corresponds to working in the canonical ensemble. The physics in 1D is set by the dimensionless interaction parameter $\gamma = g/n$ where g is the bare interaction and n is the linear particle density.

Balanced systems. As a first benchmark of the CL method in the ground state, the spin- and mass-balanced Fermi gas was investigated in Ref. [109]. A comparison to various other methods is shown in Fig. 13, where generally good agreement is apparent across the entire range of interactions shown. While the CL results shown are at $N = 5 + 5$ particles and a finite lattice of $N_x = 40$, the curves for the Bethe ansatz expansions (strong [230] and weak [231] coupling) correspond to the thermodynamic limit (TL) of taking

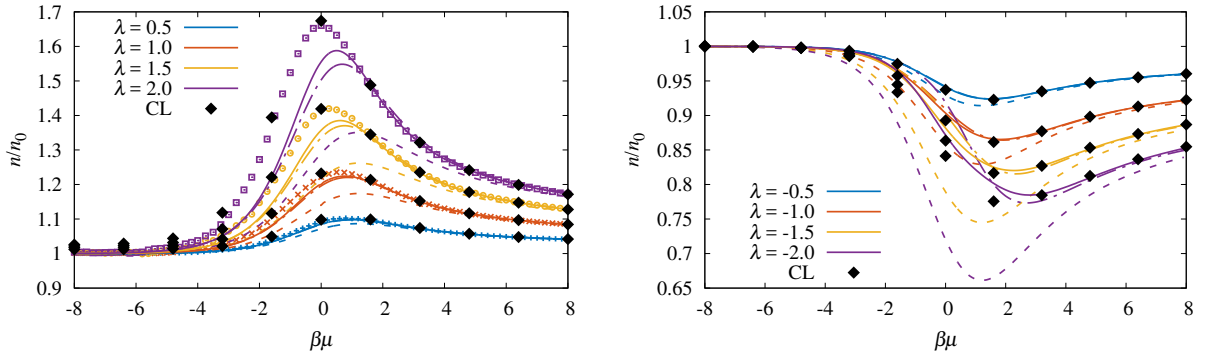


Figure 15: Density n of the attractive (left) and repulsive (right) unpolarized Fermi gas in units of the density of the noninteracting system n_0 , as shown for the dimensionless interaction strengths $\lambda = 0.5, 1.0, 1.5, 2.0$ (attractive), and $\lambda = -0.5, -1.0, -1.5, -2.0$ (repulsive). The NLO (dashed line), N2LO (dash-dotted line), and N3LO (solid line) results of perturbation theory are displayed for each coupling and are compared with HMC results (see Ref. [233]) in the attractive case. For both plots, the black diamonds show CL results (RL for the attractive case), regulated with $\xi = 0.1$ as described in the main text. Results were computed on a spatial lattice of $N_x = 80$ for CL and HMC, and of $N_x = 100$ for perturbation theory. The statistical uncertainty of the CL results is estimated to be on the order of the size of the symbols, or less, as supported by the smoothness of those results.

particle number and volume to infinity at constant density. The agreement on the repulsive sides indicates sufficiently large box sizes. On the attractive side agreement is observed, however, larger spatial lattices are needed as is suggested by the slight discrepancy between CL and the volume-extrapolated HMC values of Ref. [232], as well as results obtained by a DFT-RG approach in Ref. [226]. Another possible source of systematic bias is the finite (adaptive) integration step of $\Delta t = 0.01$, which was used throughout this study. Although the Δt dependence was checked in Ref. [109], where it was found that Δt was sufficiently small (within the statistical uncertainty), the influence of Δt could vary in other areas of parameter space, in particular with varying coupling strength.

While the agreement among the methods looks excellent, a closer look reveals interesting technical subtleties. During stochastic calculations it is instrumental to study histograms of all measured quantities to ensure correct behavior. As can be appreciated in the outer panels of Fig. 13, two distinct behaviors were observed in different regimes: the strongly attractive case ($\gamma = -3.0$) displays well behaved, localized distributions; the strongly repulsive case ($\gamma = 3.0$), on the other hand, exhibits a large amount of outliers with respect to an assumed Gaussian. The existence of so-called “fat tails” renders the simulation problematic as this violates the conditions for correct behavior and thus undermines the validity of the CL approach. Therefore, it was conjectured that the CL values are possibly faulty in this parameter regime, which was later confirmed by a different few-body method [229] based on dual variables and the worm algorithm. A more precise understanding of the behavior at strong repulsive interaction, and eventually its resolution, would be very useful.

Mass-imbalanced Fermi-Fermi mixtures. Mixtures of different fermion species, i.e. where the constituents have unequal masses, are challenging to address theoretically. While many 1D models are integrable via the Bethe ansatz, there is no such solution in the mass-imbalanced case. Nevertheless, these systems are of great interest as there are a number of experimental realizations available for these mixtures. The CL method can be straightforwardly extended to cover fermion systems with unequal masses by the use of spin dependent dispersion relations, i.e. a spin-dependent mass m_σ . To quantify the mass asymmetry between two species, the dimensionless relative mass-imbalance is introduced

$$\bar{m} = \frac{m_\uparrow - m_\downarrow}{m_\uparrow + m_\downarrow}, \quad (130)$$

which is restricted to the interval $[0, 1]$. While the use of spin-dependent dispersion relations is unproblematic from a conceptual viewpoint, there might arise numerical difficulties due to a separation of scales. Thus,

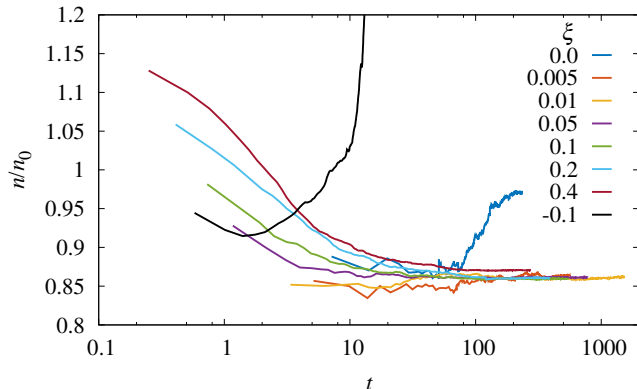


Figure 16: The normalized density n/n_0 , where n_0 is the noninteracting result, for $\lambda = -1.0$ and $\beta\mu = 1.6$, as a function of the Langevin time t for several values for the regulating parameter ξ [see Eq. (132)]. The result was computed on a spatial lattice of $N_x = 80$ and a temporal lattice of $N_\tau = 160$. For a choice of $\xi = 0$, where the regulating term is removed, CL tends toward an incorrect value for the density. When $\xi \simeq 0.1$, the additional term provides a restoring force and the stochastic process converges to a different value consistent with perturbation theory. For $\xi < 0$, the solution diverges, as expected, for a given ξ .

one may use different parameterizations of the mass imbalance depending on the specific implementation of the algorithm.

In Ref. [109] the mass-imbalanced few-body problem was studied and the average mass was fixed to $m_0 = 1$. In this way, a comparison is made possible to results obtained with the iHMC method (imaginary asymmetry – introduced in Sec. 2.7). A comparison is shown in the left panel of Fig. 14 for fixed values of the interaction strength γ . Excellent agreement of CL and iHMC is reported across a wide range of mass imbalances. Starting at $\bar{m} \sim 0.6$ the iHMC results start to deviate as a consequence of the instability of the analytic continuation. The CL results, on the other hand, remain smooth and precise up to high mass imbalances. The agreement between these different methods provides confidence that the CL method is suitable to study this problem. Recently, a worldline algorithm was adapted to study mass-imbalanced few-body systems without a sign-problem [229, 234] in 1D and its results have been compared to the CL values obtained in [109] (shown in the right panel of Fig. 14). On the attractive side, excellent agreement is observed for all mass imbalances, which further validates the CL method in this setting. A comparison on the repulsive side, however, revealed that the CL values deviate from the worldline results, which is connected to the occurrence of heavy tails mentioned above and in Ref. [109]. It remains to be shown whether mass-imbalanced Fermi mixtures with repulsive interactions in the ground state are accessible with CL.

5.2.2. 1D fermions at finite temperature

Repulsive interactions. One of the first attempts to use CL for nonrelativistic fermions was Ref. [195], where the thermodynamics of a repulsive 1D Fermi gas was calculated using that method as well third-order lattice perturbation theory (see Fig. 15). The density and pressure were computed for a range of couplings and temperatures. The calculations were also compared with prior hybrid Monte Carlo results for attractive interactions, where there is no sign problem and the convergence of the perturbative expansion could be assessed. On the repulsive side, CL was found to agree with the third-order perturbative expansion at weak coupling and away from the virial region (where the fugacity is small), beyond which perturbation theory was expected to break down.

That same work explored for the first time the use of a regulator to avoid uncontrolled excursions of the auxiliary field into the complex plane, as we explain next. In those calculations, the excursions into the complex plane were highly problematic because the dependence of the action and the drift on the auxiliary field σ involved hyperbolic functions. The HS transformation used in that work depends on $\sin \sigma$, and the complexification $\sigma \rightarrow \sigma_R + i\sigma_I$ results in

$$\sin \sigma = \sin(\sigma_R) \cosh(\sigma_I) + i \cos(\sigma_R) \sinh(\sigma_I). \quad (131)$$

As a consequence, a growing magnitude of σ_I amounted to increasing the fermion-fermion coupling at an exponential rate. In such a situation, the calculation would either stall or result in a converged but incorrect answer. This exponential growth is similar to the problem found in gauge theories, as the complexified link

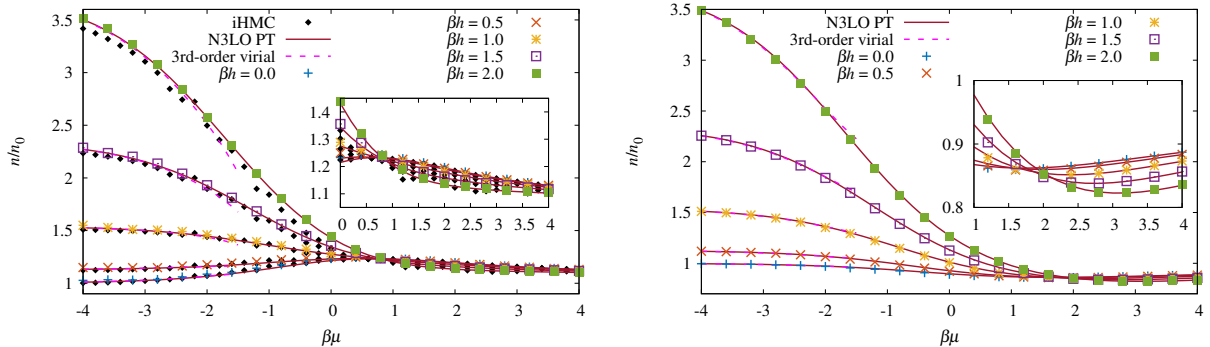


Figure 17: Density equation of state $n = n_{\uparrow} + n_{\downarrow}$ normalized by the non-interacting, unpolarized counterpart n_0 , for attractive (left) and repulsive (right) interactions of strength $\lambda = \pm 1$. Insets: Zoom in on the region $\beta\mu > 0$ (left) and $\beta\mu > 1$ (right). In all cases, the CL results are shown with colored symbols, iHMC results (from Ref. [107]) appear with black diamonds, perturbative results at third order are shown with solid lines, and virial expansion results appear as dashed lines.

variables representing the gauge field become unbounded in the same fashion in those theories. For lattice calculations of gauge theories, Refs. [192, 193] tackled the problem of large excursions by so-called dynamic stabilization (see Sec. 3.6). Following a similar idea, Ref. [195] added a regulating term to the CL dynamics controlled by a parameter ξ , such that the new CL equations became

$$\Delta\sigma_R = -\text{Re} \left[\frac{\delta S[\sigma]}{\delta\sigma} \right] \Delta t - 2\xi\sigma_R\Delta t + \eta\sqrt{\Delta t}, \quad (132)$$

$$\Delta\sigma_I = -\text{Im} \left[\frac{\delta S[\sigma]}{\delta\sigma} \right] \Delta t - 2\xi\sigma_I\Delta t. \quad (133)$$

The new term in the action can be understood as a harmonic oscillator trapping potential, i.e. a restoring force that prevents the field from running away. That modification introduces a systematic effect that needs to be studied for each quantity of interest as a function of ξ as $\xi \rightarrow 0$. Fig. 16 shows the running average of the density as a function of the Langevin time t for several values of ξ in the neighborhood of 0. As is evident in that figure, there is a sizable window of small values of ξ where CL converges.

Spin-polarized systems. Encouraged by the success of CL in calculating 1D systems with repulsive interactions, the follow-up study of Ref. [235], extended the results of Ref. [195] to the spin-polarized case by introducing a non-vanishing asymmetry $\beta h = \beta(\mu_{\uparrow} - \mu_{\downarrow})/2$. Such an asymmetry leads to a sign problem for the case of attractive interactions and to a phase problem for repulsive interactions. As mentioned above, such a sign or phase problem can be avoided in 1D using specific methods which, unfortunately, do not generalize to higher dimensions. In the study of Ref. [235], the density and magnetization equations of state were calculated and compared with perturbation theory, imaginary polarization approaches, and the virial expansion. A sample of those results is reproduced in Fig. 17.

5.3. Nonrelativistic fermions in three dimensions: the polarized unitary Fermi gas

One of the most studied many-body systems in recent years is the so-called unitary Fermi gas (UFG). Due to a diverging s -wave scattering length, the microscopic information about the interaction between the spin-up and -down particles is lost and all observed quantities can be written as universal functions of the fermion density and temperature (as these are the only scales left at our disposal). Its intricate behavior is linked to various many-body phenomena, and moreover it is realized to an excellent precision in numerous cold atoms experiments, having led to a plethora of precise measurements of its unique behavior.

For $SU(2)$ symmetric fermions, i.e. for equal numbers of spin-up and -down particles, it is possible – albeit challenging – to study the UFG with conventional Monte Carlo approaches. Past stochastic studies of the UFG have been conducted using methods such as hybrid Monte Carlo (HMC) [236, 237, 238] and

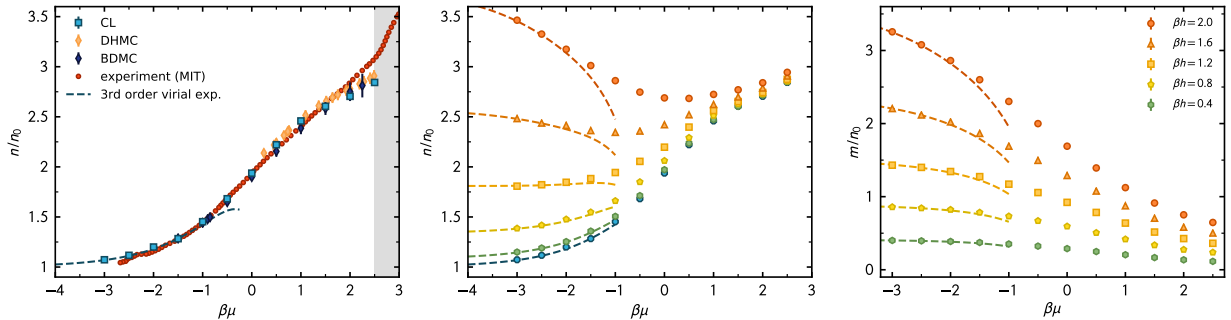


Figure 18: (Left) Density in units of the non-interacting density as a function of the dimensionless parameter $\beta\mu$ for the balanced Fermi gas. Additionally, comparison to theoretical values (BDMC [243], DHMC [236]) and experimental values from the MIT group [243] are shown. (Center) Density in units of the non-interacting density as a function of $\beta\mu$ for the polarized Fermi gas, compared to the third order virial expansion at high temperatures. (Right) Magnetization in units of the non-interacting density as a function of $\beta\mu$ compared to the 3rd order virial expansion at high temperatures.

auxiliary field methods (AFQMC) on the lattice [239, 240, 241] as well as various flavors of diagrammatic Monte Carlo methods [242, 243] in the continuum.

By introducing a finite chemical potential asymmetry the $SU(2)$ symmetry is broken, creating a sign problem. To address that issue, the CL method was applied to the spin-polarized unitary Fermi gas for the first time in Ref. [244], finding excellent agreement with available benchmark results. In the left panel of Fig. 18, the density equation of state is shown for a balanced gas in comparison to previously obtained results from DHMC [236] and bold diagrammatic Monte Carlo (BDMC) [243] studies, as well as experimental values from the MIT group [243]. Across a wide range of $\beta\mu$ values, excellent agreement was reported down to low temperatures. In the vicinity of the phase transition to superfluidity, however, the CL results, along with all other theoretical values, start to deviate from the experimental values, which is attributed to finite lattice effects and can, in principle, be mitigated by extending the box sizes beyond $N_x = 11$.

In the central and right panels of Fig. 18 the density and magnetic EOS are shown, respectively. It is important to note here that these system can be dealt with by essentially the same computational effort as in the spin-balanced case, whereas a re-weighting approach would suffer from an exponential increase in computational effort. As can be appreciated from the figure, excellent agreement with the virial expansion (see e.g. [245]) is achieved at high temperatures, which gives confidence on the reliability of the CL results in that regime. Moving towards lower temperatures, the virial expansion is expected to break down, whereas the CL results continue to evolve smoothly across the entire parameter range studied.

While the virial expansion allows for a validation of CL results at high temperatures, no benchmark is available in the literature at finite spin polarization. As a way to perform an internal consistency check, Ref. [244] exploited one of the Maxwell relations known from statistical mechanics. More specifically, the equality in cross derivatives of \mathcal{Z} with respect to βh and $\beta\mu$, i.e.

$$\left(\frac{\partial n}{\partial(\beta h)}\right)_{\beta\mu} = \left(\frac{\partial m}{\partial(\beta\mu)}\right)_{\beta h}, \quad (134)$$

should be satisfied for all parameter values. The two different derivatives are shown as red and blue symbols in Fig. 19. While the agreement was suggested already in the EOS for the virial regime, the excellent agreement across almost all values of $\beta\mu$ and βh is a non-trivial verification and provides another argument for the validity of the CL calculation. We emphasize that these data points were obtained by completely independent calculations, i.e. no prior information entered this cross check.

6. Summary and Outlook

In this report we have discussed the origin and methods to address the sign problem as it appears across a wide range of systems in relativistic and nonrelativistic quantum many-body physics. We have proposed

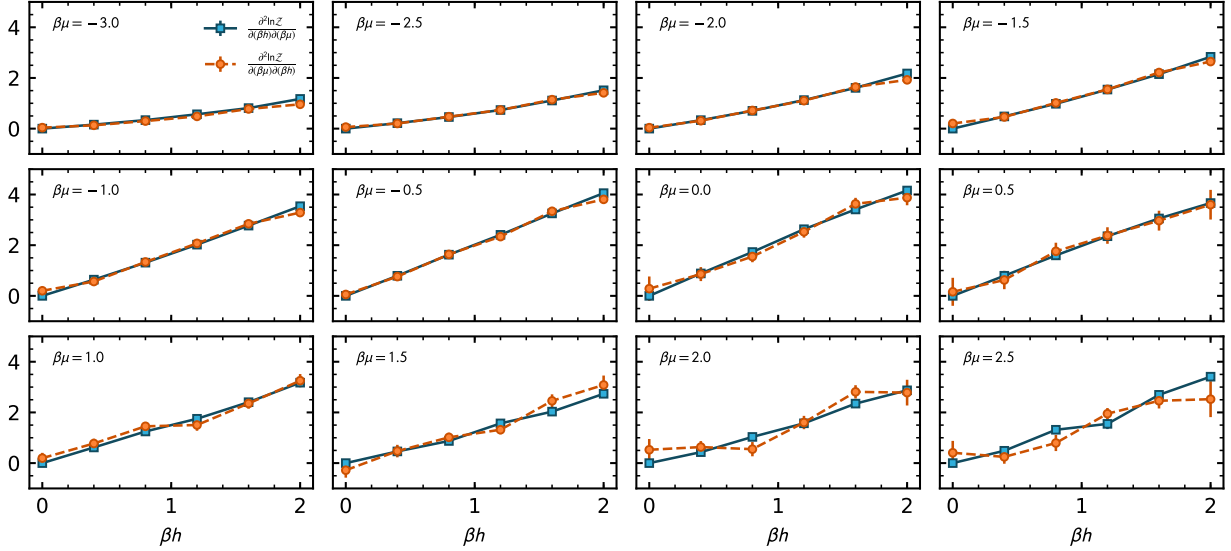


Figure 19: Second derivatives of $\ln \mathcal{Z}$ to verify Maxwell relations as a function of βh . Every plot corresponds to a fixed value of $\beta\mu$. The lines are guides to the eye.

a broad classification of the various methods into *new-variables*, *statistical*, and *complex-plane* approaches. After a brief overview of each of those categories, we focused on the complex form of stochastic quantization, namely CL.

Complex Langevin first appeared in the 80s as a natural generalization of stochastic quantization for cases with a complex action. Operationally, stochastic quantization does not require a probability to be defined (there is no Metropolis accept/reject step), which made field complexification (itself needed in the presence of a sign or complex phase problem) look more like a feature than a bug. From the mathematical standpoint, however, the challenges seemed daunting. It took decades for the community to begin to understand the properties and behavior of CL, to clarify the origin of its problems and limitations, and to propose solutions. Some of that progress was enabled by advances in hardware, as modern personal computers are powerful enough to run small but useful quantum field theory calculations with little wait; that was certainly not the case in the 80s, nor in the 90s when initial explorations of this method were underway.

As computer power continues to grow, and given the overall progress made during the last decade, there is good reason for optimism. Furthermore, there are now several groups and international collaborations around the world applying CL methods to many systems, which generate a wider range of situations than ever before from which insight can be gained. The most remarkable step forward, in the latest chapter in the history of CL, is the derivation of conditions for correctness and how they relate to behavior at the boundaries of the integration region (at infinity and at zeros of the complex weight). This new understanding has spawned new practical solutions such as gauge cooling, dynamic stabilization, and modified actions (regulators), which have enabled more applications than previously thought possible. Continued studies of CL will help illuminate when the method is reliable and when it is not. A more detailed understanding of the structure of the problems in CL might help develop new methods to ameliorate or solve those problems.

Acknowledgements

We are especially grateful to G. Aarts, F. Attanasio, G. Basar, S. Chandrasekharan, P. de Forcrand, C. Gattringer, E. Huffman, K. Langfeld, and E. Seiler for their extremely useful comments on earlier versions of this manuscript. We would also like to acknowledge G. Aarts, C. Gattringer, C. Ratti, and H. Singh for kindly allowing us to reproduce their figures.

This material is based upon work supported by the National Science Foundation under Grant No. PHY1452635 (Computational Physics Program). C.E.B. acknowledges support from the United States Department of Energy through the Computational Science Graduate Fellowship (DOE CSGF) under grant number DE-FG02-97ER25308. J.B. acknowledges support by the DFG under grant BR 4005/4-1 (Heisenberg program). J.B. and F.E. acknowledge support by the DFG grant BR 4005/5-1. J.B. and L.R. acknowledge support by HIC for FAIR within the LOEWE program of the State of Hesse.

References

References

- [1] H. A. Bethe, E. E. Salpeter, *Quantum Mechanics of One- and Two-Electron Atoms* (1957).
- [2] P. A. M. Dirac, Proceedings of the Royal Society of London. Series A, Containing Papers of a Mathematical and Physical Character 123 (1929).
- [3] B. R. Barrett, P. Navratil, J. P. Vary, *Ab initio no core shell model*, Progress in Particle and Nuclear Physics 69 (2013) 131 .
- [4] C. W. Johnson, W. E. Ormand, K. S. McElvain, H. Shan, *BIGSTICK: A flexible configuration-interaction shell-model code* (2018), [1801.08432](https://arxiv.org/abs/1801.08432).
- [5] R. J. Bartlett, M. Musiał, *Coupled-cluster theory in quantum chemistry*, Rev. Mod. Phys. 79 (2007) 291.
- [6] G. Hagen, T. Papenbrock, M. Hjorth-Jensen, D. J. Dean, *Coupled-cluster computations of atomic nuclei*, Rept. Prog. Phys. 77 (2014) 096302, [1312.7872](https://arxiv.org/abs/1312.7872).
- [7] C. P. Burgess, *Introduction to Effective Field Theory*, Ann. Rev. Nucl. Part. Sci. 57 (2007) 329, [hep-th/0701053](https://arxiv.org/abs/hep-th/0701053).
- [8] E. Epelbaum, H.-W. Hammer, U.-G. Meißner, *Modern theory of nuclear forces*, Rev. Mod. Phys. 81 (2009) 1773.
- [9] R. Machleidt, D. R. Entem, *Chiral effective field theory and nuclear forces*, Phys. Rept. 503 (2011) 1, [1105.2919](https://arxiv.org/abs/1105.2919).
- [10] R. Shankar, *Effective field theory in condensed matter physics*, in: *Conceptual foundations of quantum field theory. Proceedings, Symposium and Workshop, Boston, USA, March 1-3, 1996* (1996), pp. 47–55, [cond-mat/9703210](https://arxiv.org/abs/cond-mat/9703210).
- [11] A. M. J. Schakel, *Boulevard of Broken Symmetries* (WORLD SCIENTIFIC, 2008), <https://www.worldscientific.com/doi/pdf/10.1142/6826>.
- [12] N. Metropolis, A. W. Rosenbluth, M. N. Rosenbluth, A. H. Teller, E. Teller, *Equation of State Calculations by Fast Computing Machines*, The Journal of Chemical Physics 21 (1953) 1087.
- [13] E. Y. Loh, J. E. Gubernatis, R. T. Scalettar, S. R. White, D. J. Scalapino, R. L. Sugar, *Sign problem in the numerical simulation of many-electron systems*, Phys. Rev. B 41 (1990) 9301.
- [14] S. Koonin, D. Dean, K. Langanke, *Shell model Monte Carlo methods*, Phys. Rept. 278 (1997) 1 .
- [15] Y. Alhassid, *The shell model Monte Carlo approach to level densities: recent developments and perspectives*, Eur. Phys. J. A51 (2015) 171, [1601.00107](https://arxiv.org/abs/1601.00107).
- [16] C. Gatteringer, K. Langfeld, *Approaches to the sign problem in lattice field theory*, Int. J. Mod. Phys. A 31 (2016) 1643007, [1603.09517](https://arxiv.org/abs/1603.09517).
- [17] L. Bongiovanni, *Numerical methods for the sign problem in Lattice Field Theory*, Ph.D. thesis, Swansea U. (2015), [1603.06458](https://arxiv.org/abs/1603.06458).
- [18] G. Aarts, *Introductory lectures on lattice QCD at nonzero baryon number*, J. Phys. Conf. Ser. 706 (2016) 022004, [1512.05145](https://arxiv.org/abs/1512.05145).
- [19] A. M. Ferrenberg, R. H. Swendsen, *New Monte Carlo technique for studying phase transitions*, Phys. Rev. Lett. 61 (1988) 2635.
- [20] J. E. Hirsch, *Discrete Hubbard-Stratonovich transformation for fermion lattice models*, Phys. Rev. B 28 (1983) 4059.
- [21] D. Lee, *Ground state energy at unitarity*, Phys. Rev. C 78 (2008) 024001.
- [22] G. G. Batrouni, P. de Forcrand, *Fermion sign problem: Decoupling transformation and simulation algorithm*, Phys. Rev. B 48 (1993) 589.
- [23] C. Wu, S.-C. Zhang, *Sufficient condition for absence of the sign problem in the fermionic quantum Monte Carlo algorithm*, Phys. Rev. B 71 (2005) 155115.
- [24] Z.-X. Li, H. Yao, *Sign-Problem-Free Fermionic Quantum Monte Carlo: Developments and Applications*, Ann. Rev. Condensed Matter Phys. 10 (2019) 337, [1805.08219](https://arxiv.org/abs/1805.08219).
- [25] G. G. Batrouni, R. T. Scalettar, *Anomalous decouplings and the fermion sign problem*, Phys. Rev. B 42 (1990) 2282.
- [26] F. F. Assaad, M. Imada, D. J. Scalapino, *Charge and spin structures of a $d_{x^2-y^2}$ superconductor in the proximity of an antiferromagnetic Mott insulator*, Phys. Rev. B 56 (1997) 15001.
- [27] Y. Motome, M. Imada, *A Quantum Monte Carlo Method and Its Applications to Multi-Orbital Hubbard Models*, J. Phys. Soc. Jpn. 66 (1997) 1872.
- [28] T. Sato, F. F. Assaad, T. Grover, *Quantum Monte Carlo Simulation of Frustrated Kondo Lattice Models*, Phys. Rev. Lett. 120 (2018) 107201.
- [29] S. Capponi, F. F. Assaad, *Spin and charge dynamics of the ferromagnetic and antiferromagnetic two-dimensional half-filled Kondo lattice model*, Phys. Rev. B 63 (2001) 155114.
- [30] F. F. Assaad, *Quantum Monte Carlo Simulations of the Half-Filled Two-Dimensional Kondo Lattice Model*, Phys. Rev. Lett. 83 (1999) 796.

- [31] F. Wang, D. P. Landau, *Efficient, Multiple-Range Random Walk Algorithm to Calculate the Density of States*, Phys. Rev. Lett. 86 (2001) 2050.
- [32] A. Bazavov, B. A. Berg, D. Du, Y. Meurice, *Density of states and Fisher's zeros in compact $U(1)$ pure gauge theory*, Phys. Rev. D 85 (2012) 056010.
- [33] K. Langfeld, B. Lucini, A. Rago, *Density of States in Gauge Theories*, Phys. Rev. Lett. 109 (2012) 111601.
- [34] Z. Fodor, S. D. Katz, C. Schmidt, *The Density of states method at non-zero chemical potential*, JHEP 03 (2007) 121, [hep-lat/0701022](#).
- [35] K. Langfeld, B. Lucini, *Density of states approach to dense quantum systems*, Phys. Rev. D 90 (2014) 094502.
- [36] K. Langfeld, B. Lucini, A. Rago, R. Pellegrini, L. Bongiovanni, *The density of states approach for the simulation of finite density quantum field theories*, J. Phys. Conf. Ser. 631 (2015) 012063, [1503.00450](#).
- [37] K. Langfeld, J. M. Pawłowski, *Two-color QCD with heavy quarks at finite densities*, Phys. Rev. D 88 (2013) 071502.
- [38] A. Gocksch, *Simulating Lattice QCD at Finite Density*, Phys. Rev. Lett. 61 (1988) 2054.
- [39] C. Schmidt, *Lattice QCD at finite density*, PoS LAT2006 (2006) 021, [hep-lat/0610116](#).
- [40] S. Ejiri, *Existence of the critical point in finite density lattice QCD*, Phys. Rev. D 77 (2008) 014508.
- [41] S. Ejiri, *Canonical partition function and finite density phase transition in lattice QCD*, Phys. Rev. D 78 (2008) 074507.
- [42] S. Ejiri, K. Kanaya, T. Umeda, *Ab initio study of QCD thermodynamics on the lattice at zero and finite densities*, PTEP 2012 (2012) 01A104, [1205.5347](#).
- [43] C. Gattringer, P. Torek, *Density of states method for the Z_3 spin model*, Phys. Lett. B 747 (2015) 545 .
- [44] M. Giuliani, C. Gattringer, P. Torek, *Developing and testing the density of states FFA method in the $SU(3)$ spin model*, Nucl. Phys. B 913 (2016) 627 .
- [45] H. Robbins, S. Monro, *A Stochastic Approximation Method*, Ann. Math. Statist. 22 (1951) 400.
- [46] M. Giuliani, C. Gattringer, *Density of States FFA analysis of $SU(3)$ lattice gauge theory at a finite density of color sources*, Phys. Lett. B 773 (2017) 166 .
- [47] P. Rossi, U. Wolff, *Lattice QCD with fermions at strong coupling: A dimer system*, Nucl. Phys. B 248 (1984) 105 .
- [48] F. Hébert, G. G. Batrouni, H. Mabilat, *Exact duality and dual Monte Carlo simulation for the bosonic Hubbard model*, Phys. Rev. B 61 (2000) 10725.
- [49] M. G. Endres, *Method for simulating $O(N)$ lattice models at finite density*, Phys. Rev. D 75 (2007) 065012.
- [50] N. Prokof'ev, B. Svistunov, *Worm Algorithms for Classical Statistical Models*, Phys. Rev. Lett. 87 (2001) 160601.
- [51] O. F. Syljuåsen, A. W. Sandvik, *Quantum Monte Carlo with directed loops*, Phys. Rev. E 66 (2002) 046701.
- [52] D. Banerjee, S. Chandrasekharan, *Finite size effects in the presence of a chemical potential: A study in the classical nonlinear $O(2)$ sigma model*, Phys. Rev. D 81 (2010) 125007.
- [53] Y. D. Mercado, H. G. Evertz, C. Gattringer, *QCD Phase Diagram According to the Center Group*, Phys. Rev. Lett. 106 (2011) 222001.
- [54] C. Gattringer, *Flux representation of an effective Polyakov loop model for QCD thermodynamics*, Nucl. Phys. B 850 (2011) 242 .
- [55] M. Fromm, J. Langelage, S. Lottini, O. Philipsen, *The QCD deconfinement transition for heavy quarks and all baryon chemical potentials*, JHEP 01 (2012) 042, [1111.4953](#).
- [56] Y. D. Mercado, H. G. Evertz, C. Gattringer, *Worm algorithms for the 3-state Potts model with magnetic field and chemical potential*, Computer Physics Communications 183 (2012) 1920 .
- [57] Y. D. Mercado, C. Gattringer, *Monte Carlo simulation of the $SU(3)$ spin model with chemical potential in a flux representation*, Nucl. Phys. B 862 (2012) 737 .
- [58] C. Gattringer, T. Kloiber, *Lattice study of the Silver Blaze phenomenon for a charged scalar ϕ^4 field*, Nucl. Phys. B 869 (2013) 56, [1206.2954](#).
- [59] C. Gattringer, T. Kloiber, *Spectroscopy in finite density lattice field theory: An exploratory study in the relativistic Bose gas*, Phys. Lett. B 720 (2013) 210, [1212.3770](#).
- [60] C. Gattringer, T. Kloiber, M. Müller-Preussker, *Dual simulation of the two-dimensional lattice $U(1)$ gauge-Higgs model with a topological term*, Phys. Rev. D 92 (2015) 114508.
- [61] C. Gattringer, D. Göschl, T. Sulejmanpasic, *Dual simulation of the 2d $U(1)$ gauge Higgs model at topological angle $\theta = \pi$: Critical endpoint behavior*, Nucl. Phys. B 935 (2018) 344, [1807.07793](#).
- [62] T. Sulejmanpasic, C. Gattringer, *Abelian gauge theories on the lattice: θ -terms and compact gauge theory with(out) monopoles*, Nucl. Phys. B 943 (2019) 114616, [1901.02637](#).
- [63] H. Vairinhos, P. de Forcrand, *Lattice gauge theory without link variables*, JHEP 12 (2014) 038, [1409.8442](#).
- [64] H. Vairinhos, P. de Forcrand, *Integrating out lattice gauge fields*, PoS CPOD2014 (2015) 061, [1506.07007](#).
- [65] U. Wolff, *Simulating the all-order strong coupling expansion I: Ising model demo*, Nucl. Phys. B 810 (2009) 491.
- [66] U. Wolff, *Simulating the all-order hopping expansion II: Wilson fermions*, Nucl. Phys. B 814 (2009) 549.
- [67] U. Wolff, *Simulating the all-order strong coupling expansion III: $O(N)$ sigma/loop models*, Nucl. Phys. B 824 (2010) 254.
- [68] U. Wolff, *Simulating the all-order strong coupling expansion IV: $CP(N-1)$ as a loop model*, Nucl. Phys. B 832 (2010) 520.
- [69] P. de Forcrand, M. Fromm, *Nuclear Physics from Lattice QCD at Strong Coupling*, Phys. Rev. Lett. 104 (2010) 112005.
- [70] W. Unger, P. de Forcrand, *Continuous Time Monte Carlo for Lattice QCD in the Strong Coupling Limit*, J. Phys. G38 (2011) 124190, [1107.1553](#).
- [71] S. Chandrasekharan, U.-J. Wiese, *Meron-Cluster Solution of Fermion Sign Problems*, Phys. Rev. Lett. 83 (1999) 3116.
- [72] S. Chandrasekharan, *Fermion bag approach to lattice field theories*, Phys. Rev. D 82 (2010) 025007.
- [73] S. Chandrasekharan, *Fermion Bag Approach to Fermion Sign Problems*, Eur. Phys. J. A49 (2013) 90, [1304.4900](#).
- [74] E. Huffman, S. Chandrasekharan, *Fermion bag approach to Hamiltonian lattice field theories in continuous time*, Phys.

- Rev. D 96 (2017) 114502.
- [75] S. Chandrasekharan, A. Li, *Fermion bag approach to the sign problem in strongly coupled lattice QED with Wilson fermions*, JHEP 2011 (2011) 18.
 - [76] S. Chandrasekharan, A. Li, *Fermion Bags, Duality, and the Three Dimensional Massless Lattice Thirring Model*, Phys. Rev. Lett. 108 (2012) 140404.
 - [77] S. Chandrasekharan, *Solutions to sign problems in lattice Yukawa models*, Phys. Rev. D 86 (2012) 021701.
 - [78] E. F. Huffman, S. Chandrasekharan, *Solution to sign problems in half-filled spin-polarized electronic systems*, Phys. Rev. B 89 (2014) 111101.
 - [79] J. E. Hirsch, R. L. Sugar, D. J. Scalapino, R. Blankenbecler, *Monte Carlo simulations of one-dimensional fermion systems*, Phys. Rev. B 26 (1982) 5033.
 - [80] M. G. Endres, *Lattice theory for nonrelativistic fermions in one spatial dimension*, Phys. Rev. A 85 (2012) 063624.
 - [81] M. G. Endres, *Transdimensional Equivalence of Universal Constants for Fermi Gases at Unitarity*, Phys. Rev. Lett. 109 (2012) 250403.
 - [82] M. G. Endres, *Numerical study of unitary fermions in one spatial dimension*, Phys. Rev. A 87 (2013) 063617.
 - [83] C. Gatttringer, *Baryon bags in strong coupling QCD*, Phys. Rev. D 97 (2018) 074506.
 - [84] U. Wenger, *Efficient simulation of relativistic fermions via vertex models*, Phys. Rev. D 80 (2009) 071503.
 - [85] V. Ayyar, S. Chandrasekharan, J. Rantaharju, *Benchmark results in the 2D lattice Thirring model with a chemical potential*, Phys. Rev. D 97 (2018) 054501.
 - [86] J. E. Drut, A. N. Nicholson, *Lattice methods for strongly interacting many-body systems*, J. Phys. G 40 (2013) 043101, [1208.6556](#).
 - [87] Z.-X. Li, Y.-F. Jiang, H. Yao, *Solving the fermion sign problem in quantum Monte Carlo simulations by Majorana representation*, Phys. Rev. B 91 (2015) 241117.
 - [88] Z. C. Wei, C. Wu, Y. Li, S. Zhang, T. Xiang, *Majorana Positivity and the Fermion Sign Problem of Quantum Monte Carlo Simulations*, Phys. Rev. Lett. 116 (2016) 250601.
 - [89] Z.-X. Li, Y.-F. Jiang, H. Yao, *Majorana-Time-Reversal Symmetries: A Fundamental Principle for Sign-Problem-Free Quantum Monte Carlo Simulations*, Phys. Rev. Lett. 117 (2016) 267002.
 - [90] Z.-C. Wei, *Semigroup Approach to the Sign Problem in Quantum Monte Carlo Simulations* (2017), [1712.09412](#).
 - [91] Z.-X. Li, Y.-F. Jiang, H. Yao, *Fermion-sign-free Majorana-quantum-Monte-Carlo studies of quantum critical phenomena of Dirac fermions in two dimensions*, New J. Phys. 17 (2015) 085003, [1411.7383](#).
 - [92] Y.-H. Liu, L. Wang, *Quantum Monte Carlo study of mass-imbalanced Hubbard models*, Phys. Rev. B 92 (2015) 235129.
 - [93] Z.-X. Li, Y.-F. Jiang, S.-K. Jian, H. Yao, *Fermion-induced quantum critical points*, Nature Commun. 8 (2017) 314.
 - [94] S.-K. Jian, H. Yao, *Fermion-induced quantum critical points in three-dimensional Weyl semimetals*, Phys. Rev. B 96 (2017) 155112.
 - [95] T. Hayata, A. Yamamoto, *Quantum Monte Carlo simulation of a two-dimensional Majorana lattice model*, Phys. Rev. B 96 (2017) 035129.
 - [96] L. Wang, Y.-H. Liu, M. Iazzi, M. Troyer, G. Harcos, *Split Orthogonal Group: A Guiding Principle for Sign-Problem-Free Fermionic Simulations*, Phys. Rev. Lett. 115 (2015) 250601.
 - [97] P. deForcrand, O. Philipsen, *The QCD phase diagram for small densities from imaginary chemical potential*, Nucl. Phys. B 642 (2002) 290.
 - [98] P. de Forcrand, O. Philipsen, *The QCD phase diagram for three degenerate flavors and small baryon density*, Nucl. Phys. B 673 (2003) 170.
 - [99] M. D'Elia, M.-P. Lombardo, *Finite density QCD via an imaginary chemical potential*, Phys. Rev. D 67 (2003) 014505.
 - [100] M. D'Elia, M.-P. Lombardo, *QCD thermodynamics from an imaginary μ_B : Results on the four flavor lattice model*, Phys. Rev. D 70 (2004) 074509.
 - [101] E. Dagotto, A. Moreo, R. L. Sugar, D. Toussaint, *Binding of holes in the Hubbard model*, Phys. Rev. B 41 (1990) 811.
 - [102] P. de Forcrand, O. Philipsen, *Constraining the QCD Phase Diagram by Tricritical Lines at Imaginary Chemical Potential*, Phys. Rev. Lett. 105 (2010) 152001.
 - [103] P. Cea, L. Cosmai, M. D'Elia, A. Papa, F. Sanfilippo, *Critical line of two-flavor QCD at finite isospin or baryon densities from imaginary chemical potentials*, Phys. Rev. D 85 (2012) 094512.
 - [104] J. N. Guenther, R. Bellwied, S. Borsanyi, Z. Fodor, S. D. Katz, A. Pasztor, C. Ratti, K. K. Szabó, *The QCD equation of state at finite density from analytical continuation*, Nucl. Phys. A 967 (2017) 720, [1607.02493](#).
 - [105] D. Roscher, J. Braun, J.-W. Chen, J. E. Drut, *Fermi gases with imaginary mass imbalance and the sign problem in Monte Carlo calculations*, J. Phys. G 41 (2014) 055110, [1306.0798](#).
 - [106] J. Braun, J.-W. Chen, J. Deng, J. E. Drut, B. Friman, C.-T. Ma, Y.-D. Tsai, *Imaginary Polarization as a Way to Surmount the Sign Problem in Ab Initio Calculations of Spin-Imbalanced Fermi Gases*, Phys. Rev. Lett. 110 (2013) 130404.
 - [107] A. C. Loheac, J. Braun, J. E. Drut, D. Roscher, *Thermal equation of state of polarized fermions in one dimension via complex chemical potentials*, Phys. Rev. A 92 (2015) 063609.
 - [108] J. Braun, J. E. Drut, D. Roscher, *Zero-Temperature Equation of State of Mass-Imbalanced Resonant Fermi Gases*, Phys. Rev. Lett. 114 (2015) 050404.
 - [109] L. Rammelmüller, W. J. Porter, J. E. Drut, J. Braun, *Surmounting the sign problem in nonrelativistic calculations: A case study with mass-imbalanced fermions*, Phys. Rev. D 96 (2017) 094506.
 - [110] P. de Forcrand, S. Kim, O. Philipsen, *A QCD chiral critical point at small chemical potential: Is it there or not?*, PoS LATTICE2007 (2007) 178, [0711.0262](#).
 - [111] G. Endrodi, Z. Fodor, S. D. Katz, K. K. Szabo, *The QCD phase diagram at nonzero quark density*, JHEP 04 (2011) 001,

- 1102.1356.
- [112] S. Sharma, *The QCD Equation of state and critical end-point estimates at $\mathcal{O}(\mu_B^6)$* , Nucl. Phys. A 967 (2017) 728, [1704.05969](#).
- [113] N. Rom, D. Charutz, D. Neuhauser, *Shifted-contour auxiliary-field Monte Carlo: circumventing the sign difficulty for electronic-structure calculations*, Chem. Phys. Lett. 270 (1997) 382 .
- [114] E. Witten, *Analytic Continuation Of Chern-Simons Theory*, AMS/IP Stud. Adv. Math. 50 (2011) 347, [1001.2933](#).
- [115] E. Witten, *A New Look At The Path Integral Of Quantum Mechanics* (2010), [1009.6032](#).
- [116] M. Cristoforetti, F. Di Renzo, L. Scorzato, *New approach to the sign problem in quantum field theories: High density QCD on a Lefschetz thimble*, Phys. Rev. D 86 (2012) 074506.
- [117] M. Cristoforetti, F. Di Renzo, A. Mukherjee, L. Scorzato, *Monte Carlo simulations on the Lefschetz thimble: Taming the sign problem*, Phys. Rev. D 88 (2013) 051501.
- [118] A. Mukherjee, M. Cristoforetti, L. Scorzato, *Metropolis Monte Carlo integration on the Lefschetz thimble: Application to a one-plaquette model*, Phys. Rev. D 88 (2013) 051502.
- [119] H. Fujii, D. Honda, M. Kato, Y. Kikukawa, S. Komatsu, T. Sano, *Hybrid Monte Carlo on Lefschetz thimbles - A study of the residual sign problem*, JHEP 10 (2013) 147, [1309.4371](#).
- [120] M. Cristoforetti, F. Di Renzo, G. Eruzzi, A. Mukherjee, C. Schmidt, L. Scorzato, C. Torrero, *An efficient method to compute the residual phase on a Lefschetz thimble*, Phys. Rev. D 89 (2014) 114505.
- [121] T. Kanazawa, Y. Tanizaki, *Structure of Lefschetz thimbles in simple fermionic systems*, JHEP 2015 (2015) 44.
- [122] Y. Tanizaki, H. Nishimura, K. Kashiwa, *Evading the sign problem in the mean-field approximation through Lefschetz-thimble path integral*, Phys. Rev. D 91 (2015) 101701.
- [123] K. Fukushima, Y. Tanizaki, *Hamilton dynamics for Lefschetz-thimble integration akin to the complex Langevin method*, PTEP 2015 (2015) 111A01, [1507.07351](#).
- [124] T. Hayata, Y. Hidaka, Y. Tanizaki, *Complex saddle points and the sign problem in complex Langevin simulation*, Nucl. Phys. B 911 (2016) 94, [1511.02437](#).
- [125] Y. Tanizaki, Y. Hidaka, T. Hayata, *Lefschetz-thimble approach to the Silver Blaze problem of one-site fermion model*, PoS LATTICE2016 (2016) 030, [1610.00393](#).
- [126] A. Alexandru, G. m. c. Başar, P. F. Bedaque, G. W. Ridgway, N. C. Warrington, *Monte Carlo calculations of the finite density Thirring model*, Phys. Rev. D 95 (2017) 014502.
- [127] J. Nishimura, S. Shimasaki, *Unification of the complex Langevin method and the Lefschetz thimble method*, EPJ Web Conf. 175 (2018) 07018, [1710.07027](#).
- [128] M. V. Ulybyshev, S. N. Valgushev, *Path integral representation for the Hubbard model with reduced number of Lefschetz thimbles* (2017), [1712.02188](#).
- [129] S. Bluecher, J. M. Pawłowski, M. Scherzer, M. Schlosser, I.-O. Stamatescu, S. Syrkowski, F. P. G. Ziegler, *Reweighting Lefschetz Thimbles*, SciPost Phys. 5 (2018) 044, [1803.08418](#).
- [130] A. Alexandru, G. m. c. Başar, P. F. Bedaque, H. Lamm, S. Lawrence, *Finite density QED₁₊₁ near Lefschetz thimbles*, Phys. Rev. D 98 (2018) 034506.
- [131] G. Aarts, *Lefschetz thimbles and stochastic quantization: Complex actions in the complex plane*, Phys. Rev. D 88 (2013) 094501.
- [132] A. Alexandru, G. Basar, P. F. Bedaque, G. W. Ridgway, N. C. Warrington, *Sign problem and Monte Carlo calculations beyond Lefschetz thimbles*, JHEP 05 (2016) 053, [1512.08764](#).
- [133] A. Alexandru, G. m. c. Başar, P. F. Bedaque, S. Vartak, N. C. Warrington, *Monte Carlo Study of Real Time Dynamics on the Lattice*, Phys. Rev. Lett. 117 (2016) 081602.
- [134] A. Alexandru, G. m. c. Başar, P. F. Bedaque, G. Ridgway, *Schwinger-Keldysh formalism on the lattice: A faster algorithm and its application to field theory*, Phys. Rev. D 95 (2017) 114501.
- [135] A. Alexandru, G. m. c. Başar, P. F. Bedaque, N. C. Warrington, *Tempered transitions between thimbles*, Phys. Rev. D 96 (2017) 034513.
- [136] A. Alexandru, G. m. c. Başar, P. F. Bedaque, G. W. Ridgway, N. C. Warrington, *Fast estimator of Jacobians in the Monte Carlo integration on Lefschetz thimbles*, Phys. Rev. D 93 (2016) 094514.
- [137] G. Parisi, Y.-s. Wu, *Perturbation Theory Without Gauge Fixing*, Sci. Sin. 24 (1981) 483.
- [138] P. H. Damgaard, H. Hüffel, *Stochastic quantization*, Phys. Rept. 152 (1987) 227 .
- [139] J. R. Klauder, *Stochastic Quantization*, Acta Phys. Austriaca Suppl. 25 (1983) 251.
- [140] J. R. Klauder, *A Langevin approach to fermion and quantum spin correlation functions*, Journal of Physics A: Mathematical and General 16 (1983) L317.
- [141] G. Parisi, *On complex probabilities*, Phys. Lett. B 131 (1983) 393.
- [142] J. R. Klauder, *Coherent-state Langevin equations for canonical quantum systems with applications to the quantized Hall effect*, Phys. Rev. A 29 (1984) 2036.
- [143] C. Adami, S. E. Koonin, *Complex Langevin equation and the many fermion problem*, Phys. Rev. C 63 (2001) 034319, [nucl-th/0009021](#).
- [144] V. Ganesan, G. H. Fredrickson, *Field-theoretic polymer simulations*, EPL 55 (2001) 814.
- [145] G. H. Fredrickson, V. Ganesan, F. Drolet, *Field-Theoretic Computer Simulation Methods for Polymers and Complex Fluids*, Macromolecules 35 (2002) 16.
- [146] D. Hochberg, M.-P. Zorzano, F. Morn, *Complex reaction noise in a molecular quasispecies model*, Chem. Phys. Lett. 423 (2006) 54 .
- [147] O. Deloubrière, L. Frachebourg, H. Hilhorst, K. Kitahara, *Imaginary noise and parity conservation in the reaction $A+A\rightleftharpoons 0$* , Physica A: Statistical Mechanics and its Applications 308 (2002) 135 .

- [148] J. Berges, I.-O. Stamatescu, *Simulating Nonequilibrium Quantum Fields with Stochastic Quantization Techniques*, Phys. Rev. Lett. 95 (2005) 202003.
- [149] J. Berges, S. Borsányi, D. Sexty, I.-O. Stamatescu, *Lattice simulations of real-time quantum fields*, Phys. Rev. D 75 (2007) 045007.
- [150] G. Aarts, I.-O. Stamatescu, *Stochastic quantization at finite chemical potential*, JHEP 09 (2008) 018, [0807.1597](#).
- [151] G. Aarts, *Can Stochastic Quantization Evade the Sign Problem? The Relativistic Bose Gas at Finite Chemical Potential*, Phys. Rev. Lett. 102 (2009) 131601, [0810.2089](#).
- [152] G. Aarts, *Complex Langevin dynamics at finite chemical potential: mean field analysis in the relativistic Bose gas*, JHEP 2009 (2009) 052.
- [153] Jürgen Berges, Dénes Sexty, *Real-time gauge theory simulations from stochastic quantization with optimized updating*, Nucl. Phys. B 799 (2008) 306 .
- [154] G. Aarts, F. A. James, E. Seiler, I.-O. Stamatescu, *Adaptive stepsize and instabilities in complex Langevin dynamics*, Phys. Lett. B 687 (2010) 154 .
- [155] G. Aarts, F. A. James, *On the convergence of complex Langevin dynamics: the three-dimensional XY model at finite chemical potential*, JHEP 8 (2010) 20, [1005.3468](#).
- [156] D. Weingarten, *Complex Probabilities on R^N as Real Probabilities on C^N and an Application to Path Integrals*, Phys. Rev. Lett. 89 (2002) 240201.
- [157] L. L. Salcedo, *Representation of complex probabilities*, J. Math. Phys. 38 (1997) 1710, [hep-lat/9607044](#).
- [158] L. L. Salcedo, *Existence of positive representations for complex weights*, J. Phys. A 40 (2007) 9399, [0706.4359](#).
- [159] J. Wosiek, *Beyond complex Langevin equations I: two simple examples* (2015), [1511.09083](#).
- [160] J. Wosiek, *Beyond complex Langevin equations: from simple examples to positive representation of Feynman path integrals directly in the Minkowski time*, JHEP 04 (2016) 146, [1511.09114](#).
- [161] L. L. Salcedo, *Gibbs sampling of complex-valued distributions*, Phys. Rev. D 94 (2016) 074503.
- [162] E. Seiler, J. Wosiek, *Positive Representations of a Class of Complex Measures*, J. Phys. A 50 (2017) 495403, [1702.06012](#).
- [163] L. L. Salcedo, *Positive representations of complex distributions on groups*, J. Phys. A 51 (2018) 505401, [1805.01698](#).
- [164] J. Wosiek, B. Ruba, *Beyond Complex Langevin Equations: a Progress Report*, in: *36th International Symposium on Lattice Field Theory (Lattice 2018) East Lansing, MI, United States, July 22-28, 2018* (2018), [1810.11519](#).
- [165] G. Jona-Lasinio, P. K. Mitter, *On the stochastic quantization of field theory*, Comm. Math. Phys. 101 (1985) 409.
- [166] G. G. Batrouni, G. R. Katz, A. S. Kronfeld, G. P. Lepage, B. Svetitsky, K. G. Wilson, *Langevin simulations of lattice field theories*, Phys. Rev. D 32 (1985) 2736.
- [167] G. G. Batrouni, R. T. Scalettar, *Langevin simulations of a long-range electron-phonon model*, Phys. Rev. B 99 (2019) 035114.
- [168] S. Duane, A. D. Kennedy, B. J. Pendleton, D. Roweth, *Hybrid Monte Carlo*, Phys. Lett. B195 (1987) 216.
- [169] S. Gottlieb, W. Liu, D. Toussaint, R. L. Renken, R. L. Sugar, *Hybrid-molecular-dynamics algorithms for the numerical simulation of quantum chromodynamics*, Phys. Rev. D 35 (1987) 2531.
- [170] K. Okano, L. Schulke, B. Zheng, *Complex Langevin simulation*, Prog. Theor. Phys. Suppl. 111 (1993) 313.
- [171] V. Ambegaokar, M. Troyer, *Estimating errors reliably in Monte Carlo simulations of the Ehrenfest model*, Am. J. Phys. 78 (2010) 150, [0906.0943](#).
- [172] I. Drummond, S. Duane, R. Horgan, *The stochastic method for numerical simulations:: Higher order corrections*, Nucl. Phys. B 220 (1983) 119 .
- [173] A. M. Horowitz, *The second order Langevin equation and numerical simulations*, Nucl. Phys. B 280 (1987) 510.
- [174] S. Catterall, I. Drummond, R. Horgan, *Langevin algorithms for spin models*, Phys. Lett. B 254 (1991) 177.
- [175] G. Aarts, F. A. James, *Complex Langevin dynamics in the $SU(3)$ spin model at nonzero chemical potential revisited*, JHEP 2012 (2012) 118.
- [176] G. Aarts, E. Seiler, I.-O. Stamatescu, *Complex Langevin method: When can it be trusted?*, Phys. Rev. D 81 (2010) 054508.
- [177] G. Aarts, E. Seiler, D. Sexty, I.-O. Stamatescu, *Complex Langevin dynamics and zeroes of the fermion determinant*, JHEP 2017 (2017) 44.
- [178] E. Seiler, *Status of Complex Langevin*, EPJ Web Conf. 175 (2018) 01019, [1708.08254](#).
- [179] G. Aarts, F. A. James, E. Seiler, I.-O. Stamatescu, *Complex Langevin: Etiology and Diagnostics of its Main Problem*, Eur. Phys. J. C 71 (2011) 1756, [1101.3270](#).
- [180] K. Nagata, J. Nishimura, S. Shimasaki, *Argument for justification of the complex Langevin method and the condition for correct convergence*, Phys. Rev. D 94 (2016) 114515.
- [181] L. L. Salcedo, *Does the complex Langevin method give unbiased results?*, Phys. Rev. D 94 (2016) 114505.
- [182] M. Scherzer, E. Seiler, D. Sexty, I.-O. Stamatescu, *Complex Langevin and boundary terms*, Phys. Rev. D 99 (2019) 014512.
- [183] J. Nishimura, S. Shimasaki, *New insights into the problem with a singular drift term in the complex Langevin method*, Phys. Rev. D 92 (2015) 011501.
- [184] J. Ambjorn, M. Flensburg, C. Peterson, *Langevin Simulations of Configurations With Static Charges*, Phys. Lett. 159B (1985) 335.
- [185] J. Ambjorn, S. K. Yang, *Numerical Problems in Applying the Langevin Equation to Complex Effective Actions*, Phys. Lett. 165B (1985) 140.
- [186] E. Seiler, D. Sexty, I.-O. Stamatescu, *Gauge cooling in complex Langevin for QCD with heavy quarks*, Phys. Lett. B 723 (2013) 213, [1211.3709](#).
- [187] L. Bongiovanni, G. Aarts, E. Seiler, D. Sexty, I.-O. Stamatescu, *Adaptive gauge cooling for complex Langevin dynamics*,

- PoS LATTICE2013 (2014) 449, [1311.1056](#).
- [188] H. Makino, H. Suzuki, D. Takeda, *Complex Langevin method applied to the 2D SU(2) Yang-Mills theory*, Phys. Rev. D 92 (2015) 085020.
- [189] K. Nagata, J. Nishimura, S. Shimasaki, *Justification of the complex Langevin method with the gauge cooling procedure*, PTEP 2016 (2016) 013B01, [1508.02377](#).
- [190] K. Nagata, J. Nishimura, S. Shimasaki, *Gauge cooling for the singular-drift problem in the complex Langevin method - a test in Random Matrix Theory for finite density QCD*, JHEP 07 (2016) 073, [1604.07717](#).
- [191] G. Aarts, F. Attanasio, B. Jäger, D. Sexty, *Complex Langevin in Lattice QCD: dynamic stabilisation and the phase diagram*, Acta Phys. Polon. Supp. 9 (2016) 621, [1607.05642](#).
- [192] F. Attanasio, B. Jäger, *Testing dynamic stabilisation in complex Langevin simulations*, PoS LATTICE2016 (2016) 053, [1610.09298](#).
- [193] Attanasio, Felipe, Jäger, Benjamin, *Improved convergence of Complex Langevin simulations*, EPJ Web Conf. 175 (2018) 07039.
- [194] F. Attanasio, B. Jäger, *Dynamical stabilisation of complex Langevin simulations of QCD*, Eur. Phys. J. C 79 (2019) 16.
- [195] A. C. Loheac, J. E. Drut, *Third-order perturbative lattice and complex Langevin analyses of the finite-temperature equation of state of nonrelativistic fermions in one dimension*, Phys. Rev. D 95 (2017) 094502.
- [196] S.-S. Xue, *The Fokker-Planck equations in lattice gauge theories*, Phys. Lett. B 180 (1986) 275 .
- [197] G. Guralnik, C. Pehlevan, *Complex Langevin equations and Schwinger-Dyson equations*, Nucl. Phys. B 811 (2009) 519 .
- [198] L. L. Salcedo, *Spurious solutions of the complex Langevin equation*, Phys. Lett. B 305 (1993) 125.
- [199] L. L. Salcedo, E. Seiler, *Schwinger-Dyson equations and line integrals*, J. Phys. A 52 (2019) 035201, [1809.06888](#).
- [200] G. Aarts, *Complex Langevin dynamics and other approaches at finite chemical potential*, PoS LATTICE2012 (2012) 017, [1302.3028](#).
- [201] J. Berges, S. Borsanyi, D. Sexty, I. O. Stamatescu, *Lattice simulations of real-time quantum fields*, Phys. Rev. D 75 (2007) 045007, [hep-lat/0609058](#).
- [202] J. Berges, D. Sexty, *Real-time gauge theory simulations from stochastic quantization with optimized updating*, Nucl. Phys. B 799 (2008) 306, [0708.0779](#).
- [203] T. C. de Aguiar, N. F. Svaiter, G. Menezes, *Stochastic Quantization of Real-Time Thermal Field Theory*, J. Math. Phys. 51 (2010) 102304, [0908.3009](#).
- [204] F. Karsch, H. W. Wyld, *Complex Langevin Simulation of the SU(3) Spin Model with Nonzero Chemical Potential*, Phys. Rev. Lett. 55 (1985) 2242.
- [205] G. Aarts, F. A. James, J. M. Pawłowski, E. Seiler, D. Sexty, I.-O. Stamatescu, *Stability of complex Langevin dynamics in effective models*, JHEP 03 (2013) 073, [1212.5231](#).
- [206] J. Bloch, J. Glesaaen, O. Philipsen, J. Verbaarschot, S. Zafeiropoulos, *Complex Langevin simulations of a finite density matrix model for QCD*, EPJ Web Conf. 137 (2017) 07030, [1612.04621](#).
- [207] L. Bongiovanni, G. Aarts, E. Seiler, D. Sexty, *Complex Langevin dynamics for SU(3) gauge theory in the presence of a theta term*, PoS LATTICE2014 (2014) 199, [1411.0949](#).
- [208] D. Sexty, *Simulating full QCD at nonzero density using the complex Langevin equation*, Phys. Lett. B 729 (2014) 108, [1307.7748](#).
- [209] D. K. Sinclair, J. B. Kogut, *Exploring Complex-Langevin Methods for Finite-Density QCD*, PoS LATTICE2015 (2016) 153, [1510.06367](#).
- [210] D. K. Sinclair, J. B. Kogut, *Complex Langevin for Lattice QCD at $T = 0$ and $\mu \geq 0$* , PoS LATTICE2016 (2016) 026, [1611.02312](#).
- [211] D. K. Sinclair, J. B. Kogut, *Complex Langevin Simulations of QCD at Finite Density. Progress Report*, EPJ Web Conf. 175 (2018) 07031, [1710.08465](#).
- [212] D. K. Sinclair, J. B. Kogut, *Complex Langevin for Lattice QCD*, PoS LATTICE2018 (2018) 143, [1810.11880](#).
- [213] J. B. Kogut, D. K. Sinclair, *Applying Complex Langevin Simulations to Lattice QCD at Finite Density* (2019), [1903.02622](#).
- [214] K. Nagata, J. Nishimura, S. Shimasaki, *Complex Langevin simulation of QCD at finite density and low temperature using the deformation technique*, EPJ Web Conf. 175 (2018) 07017, [1710.07416](#).
- [215] J. M. Pawłowski, C. Zielinski, *Thirring model at finite density in 0+1 dimensions with stochastic quantization: Cross-check with an exact solution*, Phys. Rev. D 87 (2013) 094503, [1302.1622](#).
- [216] J. M. Pawłowski, C. Zielinski, *Thirring model at finite density in 2+1 dimensions with stochastic quantization*, Phys. Rev. D 87 (2013) 094509, [1302.2249](#).
- [217] J. Bloch, J. Mahr, S. Schmalzbauer, *Complex Langevin in low-dimensional QCD: the good and the not-so-good*, PoS LATTICE2015 (2016) 158, [1508.05252](#).
- [218] G. Aarts, K. Splittorff, *Degenerate distributions in complex Langevin dynamics: one-dimensional QCD at finite chemical potential*, JHEP 2010 (2010) 17.
- [219] J. Bloch, J. Meisinger, S. Schmalzbauer, *Reweighted complex Langevin and its application to two-dimensional QCD*, PoS LATTICE2016 (2017) 046, [1701.01298](#).
- [220] J. Bloch, *Reweighting complex Langevin trajectories*, Phys. Rev. D 95 (2017) 054509.
- [221] J. Bloch, J. Glesaaen, J. J. M. Verbaarschot, S. Zafeiropoulos, *Complex Langevin simulation of a random matrix model at nonzero chemical potential*, JHEP 3 (2018) 15, [1712.07514](#).
- [222] A. Mollgaard, K. Splittorff, *Complex Langevin Dynamics for chiral Random Matrix Theory*, Phys. Rev. D 88 (2013) 116007, [1309.4335](#).
- [223] G. Aarts, L. Bongiovanni, E. Seiler, D. Sexty, I.-O. Stamatescu, *Complex Langevin simulation for QCD-like models*, PoS

- LATTICE2013 (2014) 451, [1310.7412](#).
- [224] G. Aarts, F. Attanasio, B. Jäger, E. Seiler, D. Sexty, I.-O. Stamatescu, *Insights into the heavy dense QCD phase diagram using Complex Langevin simulations*, PoS LATTICE2015 (2016) 155, [1510.09100](#).
- [225] G. Aarts, F. Attanasio, B. Jäger, D. Sexty, *The QCD phase diagram in the limit of heavy quarks using complex Langevin dynamics*, JHEP 09 (2016) 087, [1606.05561](#).
- [226] S. Kemler, M. Pospiech, J. Braun, *Formation of self-bound states in a one-dimensional nuclear model: A renormalization group based density functional study*, J. Phys. G 44 (2017) 015101.
- [227] T. Hayata, A. Yamamoto, *Complex Langevin simulation of quantum vortices in a Bose-Einstein condensate*, Phys. Rev. A 92 (2015) 043628.
- [228] X.-W. Guan, M. T. Batchelor, C. Lee, *Fermi gases in one dimension: From Bethe ansatz to experiments*, Rev. Mod. Phys. 85 (2013) 1633.
- [229] H. Singh, S. Chandrasekharan, *Few-body physics on a spacetime lattice in the worldline approach*, Phys. Rev. D 99 (2019) 074511.
- [230] T. Iida, M. Wadati, *Exact analysis of a delta-function spin-1/2 attractive Fermi gas with arbitrary polarization*, J. Stat. Mech. Theor. Exp. 2007 (2007) P06011.
- [231] C. A. Tracy, H. Widom, *On the ground state energy of the delta-function Fermi gas*, J. Math. Phys. 57 (2016) 103301.
- [232] L. Rammelmüller, W. J. Porter, J. Braun, J. E. Drut, *Evolution from few- to many-body physics in one-dimensional Fermi systems: One- and two-body density matrices and particle-partition entanglement*, Phys. Rev. A 96 (2017) 033635.
- [233] M. D. Hoffman, P. D. Javernick, A. C. Loheac, W. J. Porter, E. R. Anderson, J. E. Drut, *Universality in one-dimensional fermions at finite temperature: Density, pressure, compressibility, and contact*, Phys. Rev. A 91 (2015) 033618.
- [234] H. Singh, *Worldline approach to few-body physics on the lattice*, PoS LATTICE2018 (2018) 158, [1812.02364](#).
- [235] A. C. Loheac, J. Braun, J. E. Drut, *Polarized fermions in one dimension: Density and polarization from complex Langevin calculations, perturbation theory, and the virial expansion*, Phys. Rev. D 98 (2018) 054507.
- [236] J. E. Drut, T. A. Lähde, G. Wlazłowski, P. Magierski, *Equation of state of the unitary Fermi gas: An update on lattice calculations*, Phys. Rev. A 85 (2012) 051601.
- [237] G. Wlazłowski, P. Magierski, J. E. Drut, A. Bulgac, K. J. Roche, *Cooper Pairing Above the Critical Temperature in a Unitary Fermi Gas*, Phys. Rev. Lett. 110 (2013) 090401.
- [238] O. Goulko, M. Wingate, *Numerical study of the unitary Fermi gas across the superfluid transition*, Phys. Rev. A 93 (2016) 053604, [1507.08230](#).
- [239] S. Jensen, C. N. Gilbreth, Y. Alhassid, *The pseudogap regime in the unitary Fermi gas*, Eur. Phys. J. ST 227 (2019) 2241, [1807.03913](#).
- [240] J. Carlson, S. Gandolfi, K. E. Schmidt, S. Zhang, *Auxiliary-field quantum Monte Carlo method for strongly paired fermions*, Phys. Rev. A 84 (2011) 061602.
- [241] D. Lee, *Ground-state energy of spin- $\frac{1}{2}$ fermions in the unitary limit*, Phys. Rev. B 73 (2006) 115112.
- [242] R. Rossi, T. Ohgoe, K. Van Houcke, F. Werner, *Resummation of Diagrammatic Series with Zero Convergence Radius for Strongly Correlated Fermions*, Phys. Rev. Lett. 121 (2018) 130405.
- [243] K. Van Houcke, F. Werner, E. Kozik, N. Prokof'ev, B. Svistunov, M. J. H. Ku, A. T. Sommer, L. W. Cheuk, A. Schirotzek, M. W. Zwierlein, *Feynman diagrams versus Fermi-gas Feynman emulator*, Nature Physics 8 (2012) 366.
- [244] L. Rammelmüller, A. C. Loheac, J. E. Drut, J. Braun, *Finite-Temperature Equation of State of Polarized Fermions at Unitarity*, Phys. Rev. Lett. 121 (2018) 173001.
- [245] X.-J. Liu, *Virial expansion for a strongly correlated Fermi system and its application to ultracold atomic Fermi gases*, Phys. Rept. 524 (2013) 37.